Final Report

The Ultimate Personal Airplane

Group 3

TU Delft

Final Report

The Ultimate Personal Airplane

by

Group 3

to obtain the degree of Bachelor of Science
at the Delft University of Technology.

	Simon De Meester	4342542
	Andries Verstraeten	4355768
	Tim van Puffelen	4178556
	Jaep Koning	4208862
	Tomas Peeters	4178386
	Thijs Plasmeijer	4365429
	Claudia Raducanu	4347560
	Victoria Stulova	4363124
	Maxime Verheijen	4386353
	Wouter de Gruijl	4377567

Project duration:	April 24, 2017 – July 7, 2017	
DSE Coaches:	Dr. ir. A. C. in ’t Veld,	TU Delft, supervisor
	Ir. Zixuan Zheng,	TU Delft
	Ir. Ana Alves Vieira,	TU Delft

TU Delft

Preface

This report is the result of the work of ten aerospace engineering students for the Design Synthesis exercise given at the aerospace faculty in Delft. The report presents the outcome of a quest for finding the ultimate personal aircraft. After weeks of blood, sweat and tears this quest has finally been brought to an end.

The authors are grateful for the opportunity to present this report to their supervisors and receive feedback on their work. The authors would like to thank Alexander in 't Veld, Zixuan Zheng and Ana Alves Vieira for their guidance during the project. Furthermore, they want to thank dr. ir. G. La Rocca and ir. J. Sinke for their input on certain subjects, which proved to be very useful.

Group 03: The Ultimate Personal Airplane
Delft, June 2017

Summary

In this report the latest and final preliminary design for the Ultimate Personal Airplane is presented. After having chosen the initial configuration during the mid-term phase of the project, a more detailed design has been made, based upon four aircraft aspects: aerodynamics, structure, stability & control and performance. Also, the design as it is now was prepared for further modifications.

In order to achieve the goal of creating an aircraft that is capable of both transporting 4 persons over 1400 km and having good aerobatic capabilities, a design option tree was made. This tree consist out of all the options that might be able to comply with the requirements. After the unfeasible and inferior options were crossed off four preliminary design models were left: conventional, canard, blended wing and wing-box, which are shown in Figures 1 to 4. Design options on the subsystems have been implemented on the same way at the preliminary design stage. These four designs were analysed based upon design complexity and adaptability, estimated purchase price and operational price, general appeal to the clients and operational restrictions. After the trade-off, the conventional configuration was chosen as the most feasible option, as it was more likely to fulfil all the requirements by the end of the design than the other options.

Another important trade-off that was performed before the in-depth design was the propulsion system choice, which included a piston engine, wankel engine, camless piston engine, turboprop engine, and a hybrid configuration. Currently only piston engines and turboprop engines are used in aircraft of similar size and performance. General aviation aircraft of the size that this model is expected to be is just on the border of typical piston models and turboprop models: it could be either a heavy piston aircraft or light turboprop. Two factors had a major role in deciding the better propulsion system option: market analysis, which indicates increasing popularity of turboprop aircraft, and power requirements, which are challenging to be met by existing piston engines. Adding the increased safety of turboprop engines, the trade-off resulted in favour of a turboprop configuration.

To proceed with the detailed design, four numerical models were generated to simulate the capabilities of the aircraft. The aerodynamic model has been made to analyse the aerodynamic properties of the design such as the airflow around the aircraft and calculate the lift and drag on the aircraft. The stability and control model made an estimation of the required tail and control surfaces. The structural model allowed the design of the wingbox, fuselage and tail, so they can withstand the highest expected loads without yielding and breaking. Finally the performance model was able to make a detailed analysis of the take-off, landing and cruise performance. In the end, all of the models were run simultaneously in

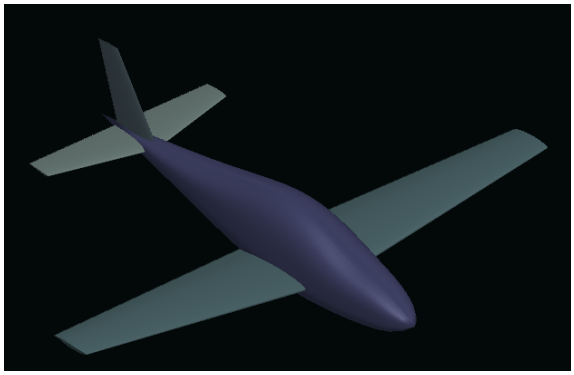

Figure 1: Isometric view of the conventional configuration

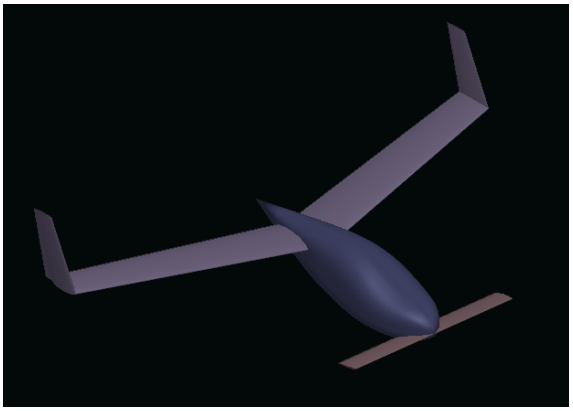

Figure 2: Isometric view of the canard configuration

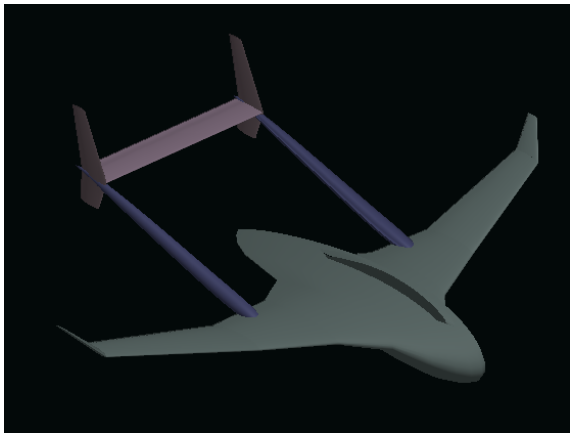

Figure 3: Isometric view of the blended wing configuration

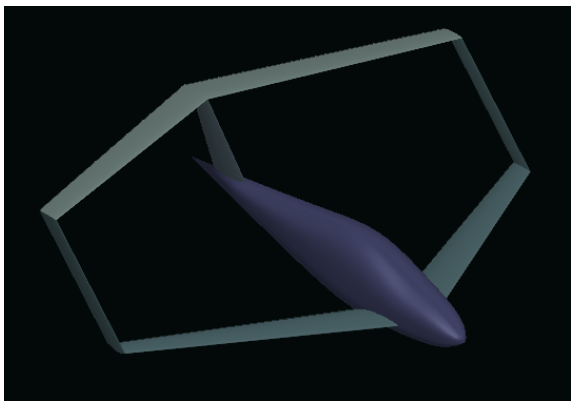

Figure 4: Isometric view of the box-wing configuration

order to analyse the resultant design.

From the aerodynamic model, a custom airfoil was created (with the aid of XFLR-5), which is focused on laminar airflow and thus produces optimal lift for the needs of the mission: decent cruise range and good aerobatic capabilities.

From the structural model, the primary material for the aircraft fuselage, wingbox and tailbox is composite sandwich with carbon laminate as the face sheet and Kevlar honeycomb as the core. The control surfaces will be made of carbon laminate only. Using sandwich allows for simplified structure, as stiffeners are not required to successfully withstand the loads. The highest loads on the wings and fuselage occur during the $+6g$ loading case, horizontal tail experiences highest load during the vertical dive, and vertical tail is loaded most during the tightest turn.

The stability and performance models verified that the resultant model is dynamically stable and can not only meet all, but outperform some of the requirements. The required sizing of the tail and control surfaces was successfully performed and analysed by the structural and aerodynamics models.

As for the miscellaneous aircraft system, it was decided that the environmental control inside the cabin will be done via pressurisation to ensure maximum level of comfort for the passengers and pilots. Ice protection is required in order to certify the aircraft for the flight in colder conditions, and it will be done via an electro-thermal system. Electricity for the aircraft systems will be provided by the means of an engine generator, supported by the battery which operates during the engine start-up and in case of generator failure. Control of the aircraft by the pilot will be done via a side stick, which is the most comfortable option considering aerobatics and cruise application. For the fuel system, a simple bladder fuel tank will be placed in the main wing, from where it will be pumped towards the engine. The landing gear is retractable to ensure the lowest possible drag, with a disk brake system. Finally, as an option, a parachute can be installed on the aircraft, so in the rare case the engine fails the probability of it resulting in a catastrophic failure is lowest. However, considering the high reliability of turboprop engines and the extra weight the parachute adds, it is optional for the customer.

The aircraft will have a conventional communication system between the pilot, avionics, air traffic control, global navigation satellite system and possibly other aircraft, so it has to be made sure that aircraft is equipped with sufficient antennae to receive and transmit the signals from and to these sources.

During the risk analysis, several additional design considerations are proposed to mitigate risks that would otherwise be deemed to high. One of them was the risk of a lightning strike, against which carbon fibre does not do much, so an additional layer of aluminium powder has to be added to the composite in later design stages. Delamination of the composite is also a severe risk, which has to be mitigated by sonic or ultrasonic inspection to detect damage. This has to be done regularly during maintenance.

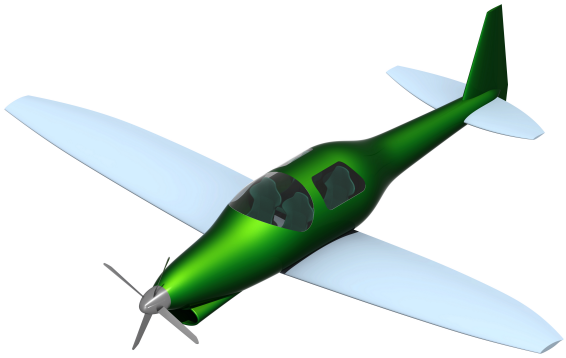

Figure 5: CATIA render of the aircraft. Isometric view.

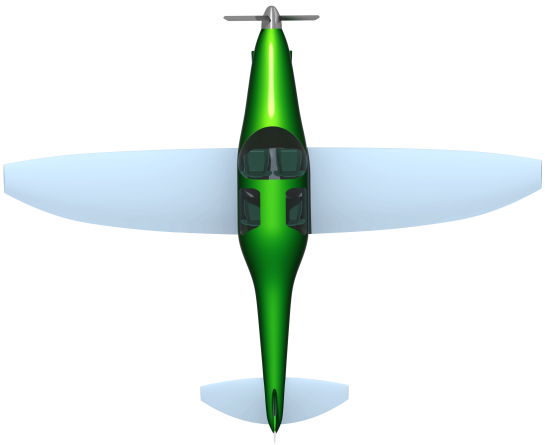

Figure 6: CATIA render of the aircraft. Top view.

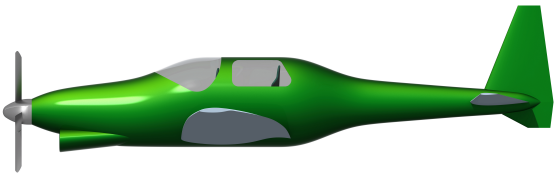

Figure 7: CATIA render of the aircraft. Side view.

Figure 8: CATIA render of the aircraft. Front view.

During the manufacturing process, making the carbon laminate of the required sizes and curvatures and assembly itself is going to be done on the assembly site. All other items like fuel systems and furniture will be purchased from other companies. For assembly, first the structural shells of the fuselage, wings and tails will be made out of carbon fibre sandwiches, then they will be filled with other items, and finally the wings and tails will be connected to the fuselage. the assembled aircraft has to be fully certified with the aid of European Aviation Safety Agency. After which it will have to be advertised by various means to attract more customers. After it is bought it will be operated and finally disposed with as much reuse of the materials as possible.

The estimated aircraft sale price is 920,000$, which includes a 15% profit margin, placing the design in a very favourable position on the market comparing to other turboprop aircraft, which are generally well over a million US dollars. The operational costs were estimated to be 229.3 $/hr, which is well within the required 400. The return of investment is dependant on the profit margin, and thus the selling price. The break-even time varies from 88 months for a 5% profit margin to 59 months for a 25% profit margin. The break-even time is 70.5 months for the 15% profit margin that is envisioned. In a worst case scenario, which was 50% less sales compared to the estimated 48 units per year and 802 sales total, resulted in a selling price of 1320000$ and a break-even time of 74.5 months.

So far, the design fulfils all of the requirements, and is relatively sustainable. Further design has to be conducted, especially with respect to the structural design of the aircraft, as the properties of composite material are significantly more complex than those of metals. The maximum take-off weight of the resultant aircraft might very well increase by the end of the design, however it is not likely to exceed the set 2000 kg, as at the moment the weight is well below it. A CATIA render of the design is shown in Figure 5, a table with specs is given in Table 1. At this point of the design all previously set requirements either are met, or are expected to be met as soon as they can be analysed.

The design has progressed far over these several weeks, however the models still have to undergo significant improvement to yield more representative results. Aerodynamics model has to include fuselage in the derivative calculations, which in turn can likely fix the stability derivative results which are

Table 1: Aircraft Specification Sheet

Parameter	Value	**Parameter**	Value
Airfoil	Custom	Material type	Sandwich
S	15.12 m^2	Laminate material	Carbon
S_h	1.68 m^2	Honeycomb material	Kevlar
S_{elev}	0.64 m^2	Skin thickness wing	2 mm
S_{ailer}	0.91 m^2	Honeycomb thickness wing	1.5 cm
S_{rud}	0.86 m^2	Skin thickness tail	1 mm
Wing span	10.54 m	Honeycomb thickness tail	1.5 cm
Aspect ratio	7.35	Skin thickness fuselage	2.1 mm
Oswald factor	0.58	Honeycomb thickness fuselage	0.5 cm
L/D_{max}	17.55	Maximum Take-Off Weight	1657.57 kg
Flap type	Slotted	Operating Empty Weight	907.01 kg
$CL_{max,TO}$	1.8	Max Payload Weight	444 kg
$CL_{max,Land}$	1.952	Mission Fuel weight	300 kg
V_{cruise}	250 kn	Max Fuel Weight	450 kg
V_{eff}	207 kn	Aerobatic Weight	1397 kg
V_{max}	299 kn	Number of seats	4
Mission range	1422 km	Engine	Ivchenko AI-450S
Ferry range	4213 km	Avionics	Garmin G1000
Rate of Climb	17.3 $m\,s^{-1}$	Climate control	Air-conditioning
Roll rate	180 $°s^{-1}$	Ice protection	Electro-thermal
Gliding range	133.7 km	Fuel tanks	Bladder,1 per wing
Take-off distance	422.3 m	Tires	Dunlop type III
Landing distance	496.8 m	Brakes	Disc
Service Ceiling	25000 ft	Ballistic Recovery System	Optional Parachute
Fuel consumption	5.7 $km\,l^{-1}$	Listing Price	920,000 $
Power	450 hp	Operating cost	229 $/hr

unrealistic. Structural model has to focus on the properties of composites, as those are much more complex comparing to more commonly used metals, which in turn might make the structure even lighter and cheaper than it is now. Performance model requires accurate flying simulation in order to produce more accurate results, as current model is based upon statistical relationships like Breguet equations. Stability & control model has to keep a careful track of all the changes made, as any changes affect the sizing of the control surfaces and therefore stability characteristics. Finally, all the models can be connected into one big model, which can react to any changes made to design parameters and produce the analysis of aircraft from the point of view of all aforementioned model. So far, the design looks really promising, and we believe that it has the potential to become a truly Ultimate Personal Airplane.

List of Symbols

Abbreviations

AFRA Aircraft Fleet Recycling Association

AOL Aircraft Operating Limitations

ATC Air Traffic Control

AWOS Automated Weather Observing System

BET Blade Element Theory

BRS Ballistic Recovery System

CF Carbon Fibre

CS-23 Certification Specification 23 for normal, utility, aerobatic and commuter aeroplanes

DAPCA Development and Procedures Costs of Aircraft

EASA European Aircraft Safety Agency

FBS Functional Breakdown Structure

FFBD Functional Flow Block Diagram

FL Flight Level

GA General Aviation

GNSS Global Navigation Satellite System

ICE Internal Combustion Engine

IFR Instrument Flight Rules

ITTC International Towing Tank Conference

LE Leading edge

LS Lower skin

MAC Mean Aerodynamic Chord

MFD Multi-function display

MFTS Master Flight Test Schedule

MOI Moment Of Inertia

MTOW Maximum Take-off Weight

O&M Operating and Maintenance

OEW Operating Empty Weight

PAPI Precision Approach Path Indicator

PFD Primary Flight Display

POH Pilots' Operating Handbook

RDT&E Research, Development, Test and Evaluation

RoC Rate of Climb

RSVM Reduced Vertical Separation Minimum

SHP Shaft Horse Power

T-VASIS T-Visual Approach Slope Indicator System

TAS True Airspeed

TBD To Be Determined

TC Type Certification

US Upper skin

VHF Very High Frequency

VLM Vortex Lattice Method

Greek symbols

$\Delta C_{l_{max}}$	Change in maximum lift coefficient	–
δ_f	Reference flap deflection	°
η_p	Propeller efficiency	–
μ_g	Ground friction coefficient	–
σ_c	Compressive Strength	Pa
σ_t	Tensile Strength	Pa
σ_y	Bending stress	Pa
$\sigma_{\text{max,LS}}$	Maximum bending stress in the lower skin	
$\sigma_{\text{max,US}}$	Maximum bending stress in the upper skin	
$\sigma_{\text{ult,CF}}$	Ultimate tensile stress of carbon fibres	
τ	Control surface effectiveness	–
τ_{max}	Maximum shear stress	
τ_{max}	Shear Strength	Pa
θ_j	Discretisation angle in the cross section	deg
θ_{app}	Approach angle	°

Parameters

$\bar{x_{ac}}$	Aerodynamic centre	/MAC
$\dot{N}_r$	Maximum allowable spin rate according to CS23	rad/s
η	Imaginary part of the eigenvalue	–
$\frac{d\epsilon}{d\alpha}$	Downwash	–
ω	Frequency	Hz
$\overline{z}$	z distance to datum line	m
$\tilde{x}$	Distance to x_{NA}	m
$\tilde{z}$	Distance to z_{NA}	m
ξ	Real part of the eigenvalue	–
ζ	Damping coefficient	–
A_{encl}	Enclosed area of a geometry	m^2
b_1	Inner location of the aileron w.r.t the root	m
b_2	Outer location of the aileron w.r.t the root	m
b_R	Rudder span	m
b_v	Vertical tail span	m
c	Mean aerodynamic chord	m
C_e	Chord length of the elevator	m
C_f	skin friction coefficient	–
C_ht	Chord length of the horizontal tail plane	m
c_p	Specific fuel consumption	$kg\,J^{-1}$
C_R	Chord length at the root of the wing	m
$C_{D\alpha}$	change in drag coefficient due to increased angle of attack	–
$C_{D_{flaps}}$	Drag coefficient with flaps out v	–
C_{D_w}	Wave drag coefficient	–
C_D	Drag coefficient	–
$C_{L\alpha_{A-h}}$	Lift coefficient of tailless aircraft differentiated w.r.t. angle of attack	–
$C_{L\alpha_h}$	Lift coefficient of the horizontal tail differentiated w.r.t. angle of attack	–
$C_{L\alpha}$	change in lift coefficient due to increased angle of attack	–
$C_{L_{\alpha_v}}$	Lift coefficient of the vertical tail differentiated w.r.t. angle of attack	–
$c_{l_{\delta_a}}$	Lift coefficient differentiated w.r.t. the aileron deflection	–
$C_{L_{A-h}}$	Lift coefficient of tailless aircraft	–
C_{L_h}	Lift coefficient of the tail	–
C_{lb}	change in rolling moment coefficient due to increased angle of sideslip	–

C_{lp}	change in rolling moment coefficient due to roll rate	–
C_{lr}	change in rolling moment coefficient due to yaw rate	–
C_L	Lift coefficient	–
$C_{m\alpha}$	change in pitching moment coefficient due to increased angle of attack	–
$C_{m\dot{\alpha}}$	change in pitching moment coefficient due to rate of increased angle of attack	–
$C_{m_{\delta_e}}$	Pitching moment differentiated w.r.t elevator deflection	–
$C_{m_{ac}}$	Moment coefficient around aerodynamic centre	–
C_{mq}	change in pitching moment coefficient due to pitch rate	–
C_{mu}	change in pitching moment coefficient due to change in airspeed	–
C_m	moment coefficient	–
C_{nb}	change in yawing moment coefficient due to increased angle of sideslip	–
C_{np}	change in yawing moment coefficient due to roll rate	–
C_{nr}	change in yawing moment coefficient due to yaw rate	–
$C_{x\alpha}$	change in X-direction force-coefficient due to increased angle of attack	–
C_{xu}	change in X-direction force-coefficient due to change in airspeed	–
C_{yb}	change in Y-direction force-coefficient due to increased angle of sideslip	–
C_{yp}	change in Y-direction force-coefficient due to roll rate	–
$C_{z\alpha}$	change in Z-direction force-coefficient due to increased angle of attack	–
$C_{z\dot{\alpha}}$	change in Z-direction force-coefficient due to rate of increased angle of attack	–
C_{zq}	change in Z-direction force-coefficient due to pitch rate	–
C_{zu}	change in Z-direction force-coefficient due to change in airspeed	–
CL_0	Highest lift coefficient at take-off	–
$CL_{max_{landing}}$	Highest lift coefficient at landing	–
$CL_{max_{TO}}$	Highest lift coefficient at take-off	–
D_A	Diameter of the fuselage segment A	m
E	Endurance	s
H	Propeller hub radius	m
h_{cruise}	Cruise altitude	ft
h_f	Flare height	ft
h_{obst}	Obstacle height	ft
i_h	Incidence angle of the horizontal tail	°
I_xy	Product moment of inertia about the xy plane	m^2
I_yy	Second moment of inertia about the y axis	m^4
I_{xx}	Second moment of inertia about the x axis	m^4

I_{xz}	Product moment of inertia about the xz plane	m^4
I_{zz}	Second moment of inertia about the z axis	m^4
L_A	Length of fuselage segment A	m
l_h	Tail arm	m
L_i	Lift of the *i*th section	N
M_{cr}	Critical Mach number	–
M_{x_i}	Moment around the x axis of the *i*th section	Nm
N_b	Number of propeller blades	–
P	Engine power	W
P	Period of the oscillation	s
Q	Torque moment	N m
q_0	Constant shear flow	N/m
q_b	Basic Shear Flow	
$q_{\max}$	Maximum shear flow	
R	Propeller radius	m
R	Range	m
R_{ferry}	Maximum ferry range	km
R_{glide}	Glide range	km
R_{MTOW}	Range at maximum take-off weight	km
Re	Reynolds number	–
$RoC_{sealevel}$	Rate of climb at sea level	$m\,s^{-1}$
S	Wing surface	m^2
$S.M.$	Stability margin	/MAC
S_h	Horizontal tail surface	m^2
S_A	Approach distance	m
S_{BR}	Braking distance	m
S_C	Climb distance	m
S_{FR}	Free-roll distance	m
S_F	Flare distance	m
S_G	Ground roll distance	m
$S_{landing}$	Landing distance	m
S_{ROT}	Rotation distance	m
S_{TO}	Take-off distance	m
S_{TR}	Transition distance	m

S_{wf}	Reference wing flap area	m^2
SFC	Specific fuel consumption	$kg\,hp^{-1}\,hr^{-1}$
T	Thrust force	N
t	Skin thickness	m
$T_{\frac{1}{2}}$	Time to reach half the amplitude	s
t_{skin}	Skin thickness	
T_{idle}	Idle thrust	N
$T_{reverse}$	Reverse thrust	N
T_{static}	Static thrust	N
V	Airspeed of wing	m/s^{-1}
V_h	Airspeed of tail	$m\,s^{-1}$
V_{BR}	Speed at the start of the braking phase	kn
V_{cruise}	Cruise speed	kn
$V_{efficient}$	Optimal speed	kn
V_{LOF}	Lift-off speed	kn
V_{max}	Maximum speed	kn
V_{S1}	Stall speed during take-off	kn
V_{SO}	Landing stall speed	kn
V_{TD}	Touchdown speed	kn
V_{VT}	Vertical tail volume coefficient	–
x_{cg}	Centre of gravity location	m
x_{ac_w}	Aerodynamic centre location of the wing	m
y_i	Spanwise distance to the *i*th section	m
M_{max}	Maximum bending moment	
Nz	Ultimate load factor	
t	Skin thickness	
V_{max}	Maximum shear force	

List of Figures

List of Tables

Contents

1

Introduction

The personal airplane market is filled with specialised aircraft which were designed with one specific mission in mind. For example, an aircraft has either good aerobatic capabilities or good long-distance travel characteristics. The goal of this design exercise is to design the Ultimate Personal Airplane that is capable of operating multiple missions relatively well. This is the fourth and final report on the design process of this Ultimate Personal Airplane. The first three reports consisted of the project plan that established the project objective and planning, the baseline report to determine the requirements and possible design solutions and the midterm report that evaluated the most promising design options and established the most promising design solution. With the decision for the final design solution the conceptual design phase was concluded and this final design report presents the preliminary design phase.

The purpose of this technical report is to conclude the exercise by arriving at a final design, evaluating this design and proposing a framework for possible further development. Aerodynamic, performance, stability & control and structural models are established in order to arrive at the final design. These models are then used in an optimisation process to establish the most optimal design, which is then presented in detail and evaluated further from technical, manufacturing & operational and economical & sustainable viewpoints. Finally a planning is proposed for possible further development of the design up to actual production and sale of the aircraft.

The report is divided into seven parts. The first part, the project preamble, deals with the process that preceded this report. It includes the project overview, presents the considered concepts and visualises the functional elements of the aircraft system in Chapters 2 to 4. Subsequently the design process is presented in Chapters 5 to 9 that discuss the design methodology, the individual models and the optimisation strategy. The third part deals with the design finalisation and includes the configuration in Chapter 15 and presents the characteristics of the design in Chapters 10 to 14. The fourth part discusses the technical analysis concerning the resource budget, system interactions and risk in Chapters 16 to 18. The analysis is continued in the field of manufacturing & operations with the manufacturing, assembly & production plan, operations & logistics and the reliability, availability, maintainability & safety analysis in Chapters 19 to 21. The analysis is finalised with an economical analysis that consists of the market analysis, a cost breakdown and the determination of the return on investment in Chapters 22 to 24. A design evaluation on compliance, feasibility and sustainability is executed in Chapters 25 and 26. The seventh and last part of the report concerns the future design process and conclusion, which proposes a future project design & development logic and Gantt chart in Chapters 27 and 28 and finally the conclusion of the project is presented in Chapter 29.

2

Project overview

2.1. Project objective

Nowadays, personal aircraft are available for many different purposes and in many different configurations. Some are focused on transport while others are used for entertainment. However, all of them are designed to fulfil a specific purpose and are usually unable to fulfil the rest of the spectrum of possible needs of a personal aircraft. Hence, the potential buyers of personal aircraft have to make a thought through decision of what they are planning to use the aircraft for and consequently have to make a trade-off. Since personal aircraft that are suitable for multiple different purposes are not yet readily available, and personal aircraft are a relatively expensive means of transport, this usually poses a difficult problem. It is likely that a solution to this problem will attract many customers.
The objective of this project is to design a multi-purpose personal aircraft that will fulfil multiple mission profiles which are desired by the customers who have multiple aims for their aircraft use. The main focus points are: relatively high cruise speed with a long range, excellent handling qualities, the capability of aerobatic manoeuvres and flight by Instrument Flight Rules (IFR).
Hence, the first part of this project dealt with defining the multiple mission profiles that the aircraft will need to perform. It should be mentioned that the mission profiles under consideration satisfy personal use only. This will exclude the commercial aviation market such as the airline or cargo industry as well as the military and aerial service or farming industry. The main market of this project stretches from light aircraft to small business jets.
For the project the following mission need statement and a project objective statement were formulated:

Mission Need Statement: The Ultimate Personal Airplane will be a small versatile aircraft that fulfils missions ranging from high range and entertainment flying to aerobatics.

Project Objective Statement: To design a small aircraft for personal use with ten students in ten weeks, that is sustainable and combines the different mission profiles of transport, aerobatic and entertainment flying for a price that is able to compete with other personal aircraft.

2.2. Requirements

In this section the mission and system requirements are presented. The first category concerns the requirements that follow from the mission that the system needs to perform, while the second category considers the requirements on the system. The requirements were established in the baseline report through a market analysis, an analysis of stakeholder needs and a requirement discovery tree. **REQ-MIS-17** has been established through comparison with a reference aircraft: the Lancair Evolution EVOT-550 [67]. The resulting design is checked for compliance with these requirements in Chapter 25.

Mission requirements

REQ-MIS-01 The aircraft shall have a maximum take-off weight (MTOW) of less than 2000 kg.

REQ-MIS-02 The aircraft shall be able to transport at least four people.

REQ-MIS-03 The aircraft shall be able to perform the basic aerobatic manoeuvres.

REQ-MIS-04 The aircraft shall be able to carry a payload of at least 444 kg.

REQ-MIS-05 The aircraft shall have a minimum range of 1400 km during IFR flight conditions.

REQ-MIS-06 The aircraft shall be able to take-off and land on grass runways.

REQ-MIS-07 (Requirement has been merged with **REQ-MIS-06**)

REQ-MIS-08 The aircraft shall have a maximum take-off distance of 500 m.

REQ-MIS-09 The aircraft shall have a maximum landing distance of 500 m.

REQ-MIS-10 The aircraft shall be able to take-off in at least 25 kn cross-wind.

REQ-MIS-11 The aircraft shall be able to land in at least 25 kn cross-wind.

REQ-MIS-12 The aircraft shall be able to cruise at a speed of at least 180 kn TAS.

REQ-MIS-13 The aircraft shall be able to cruise at 18000 ft (5485 m) during IFR flight.

REQ-MIS-14 The aircraft shall be able to sustain flight into known icing conditions.

REQ-MIS-15 The aircraft shall have a listing price lower than $1.5 million.

REQ-MIS-16 The aircraft shall have an operational cost of less than $ 400 per hour.

REQ-MIS-17 The aircraft shall have an economy cruise fuel consumption equal to or lower than 0.387 $\mathrm{l\,NM^{-1}}$.

REQ-MIS-18 The aircraft shall have a lifetime of at least 40 years.

REQ-MIS-19 The aircraft shall be recyclable according to AFRA-rules at the end of life.

The key mission requirements are: **REQ-MIS-03**, **REQ-MIS-05**, **REQ-MIS-06**, **REQ-MIS-08** and **REQ-MIS-09**. Driving mission requirements are **REQ-MIS-01**, **REQ-MIS-02**, **REQ-MIS-03**, **REQ-MIS-16**, **REQ-MIS-17**.

System requirements

REQ-SYS-01 The aircraft shall be able to sustain a negative loading of at least -3G.

REQ-SYS-02 The aircraft shall be able to sustain a positive loading of at least 6G.

REQ-SYS-03 The aircraft shall have a minimum roll rate of 180 $^\circ\,\mathrm{s^{-1}}$.

REQ-SYS-04 The aircraft shall have minimum climb rate of 15 $\mathrm{m\,s^{-1}}$.

REQ-SYS-05 The aircraft shall comply with CS-23 regulations.

REQ-SYS-06 The aircraft shall have full glass avionics.

There are no key system requirements. The driving system requirement is: **REQ-SYS-05**.

3

Considered concepts

In this chapter the concepts considered throughout the project are presented. A determination and evaluation of the options resulted in the conceptual configurations and propulsion options as presented in Section 3.1 and Section 3.2, respectively. The process then continued with an initial sizing and cost estimation of the configurations as presented in Section 3.3 and Section 3.4. Using the acquired knowledge, also through a more detailed investigation of the propulsion options, the selection process was executed as discussed in Section 3.5. The resulting design option that is developed further in this report is presented in Section 3.6.

3.1. Configurations

The configurations presented in the following section were considered in the conceptual design phase and were evaluated in order to arrive at the most suitable design option.

Conventional This design incorporates the majority of design choices commonly used in general aviation, utility and aerobatic aircraft. These designs include a fixed wing, a tail to ensure that the lateral and longitudinal stability requirements are met and conventional primary control surfaces (aileron, elevator and rudder). The large majority of aircraft ever produced feature a conventional configuration, therefore there is a large pool of reference aircraft. An example of a conventional configuration aircraft is shown in Figure 3.1.

Canard The main feature of the canard design is the location of the horizontal stabiliser which is placed in front of the main wing, in which case it is commonly referred to as a canard. The function of vertical stabiliser can be executed by the winglets, which means there is no need for using a tail. This results in the centre of gravity being shifted forward when compared to a conventional configuration, relative to the mean aerodynamic chord (MAC). A canard aircraft has a good stalling reaction when only the canard is stalled, however there is almost no possibility of stall recovery when the centre of gravity location is far aft and the main wing stalls as well. This poses restrictions on aerobatic capabilities of this design. A number of existing canard aircraft are available as reference aircraft. An example of a canard configuration aircraft is shown in Figure 3.2.

Blended wing body The blended wing body is an aircraft design that uses a gradual transition from wing to fuselage. On a conventional aircraft significant drag is created by the fuselage, while the wing-fuselage interaction decreases the lift generation efficiency. These adverse effects are severely reduced in a blended wing body design. The blended wings features consist of a very low amount of parasitic drag and a high lift over drag ratio, resulting in good cruise performance. Also, due to the high surface area a relatively low lift coefficient (C_L) is needed and thus the induced drag is reduced as well. In general aviation (GA) there are currently no blended wing body aircraft available for purchase, only prototypes have been made. An example of a canard configuration aircraft is shown in Figure 3.3.

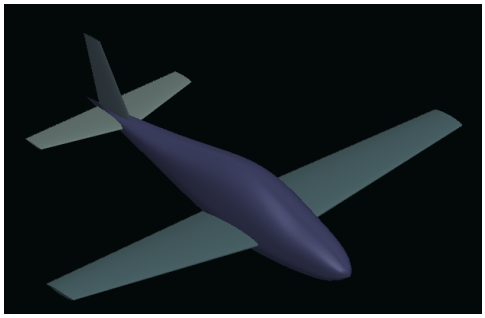

Figure 3.1: Isometric view of the conventional configuration

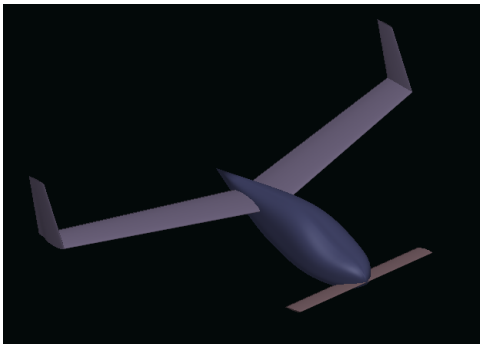

Figure 3.2: Isometric view of the canard configuration

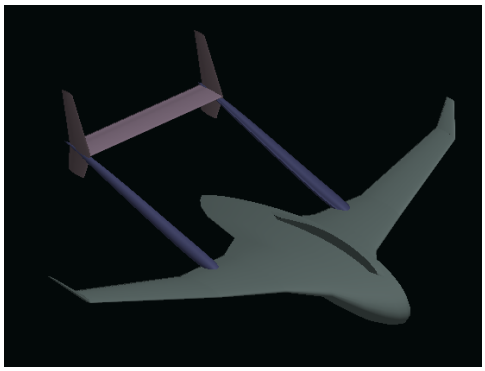

Figure 3.3: Isometric view of the blended wing configuration

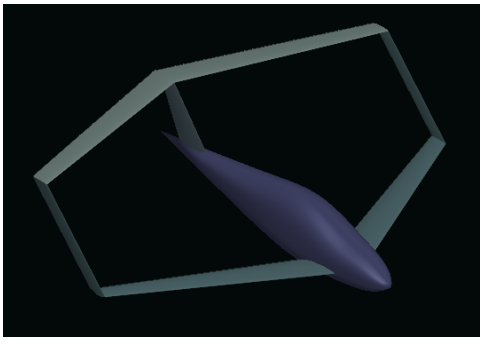

Figure 3.4: Isometric view of the box-wing configuration

Box-wing A box-wing configuration, or Prandtl plane, is an aircraft design with two wings connected to each other through vertical wings at the horizontal wing tips. Its concept has been formulated by Ludwig Prandtl as the ”best wing system”. The configuration has the theoretical capability of severely limiting the induced drag through an increased Oswald efficiency factor. This yields a relatively high lift over drag ratio, which increases cruising efficiency. No box-wing planes are currently commercially available, but numerous studies have been and are conducted and some concepts have been built but not yet flown. An example of a canard configuration aircraft is shown in Figure 3.4.

3.2. Propulsion

The following propulsion options were investigated in order to arrive at the most suitable option.

Piston engine The piston engine [55] is widely used in GA. Its simplicity and long history of use are its main strengths. Also, the fuel consumption efficiency is not related to the power setting, and hence the altitude, making it a good choice for multipurpose aircraft. The main weaknesses are a low power to mass ratio and low maximum power (in aircraft applications), especially for the diesel variants. Avgas has already been taken out of consideration due to its high fuel price and the extra pollution it causes. Therefore, commercial off-the-shelf diesel piston engines have been taken into consideration.

Camless piston engine The camless piston engine [46] is an adaptation of the piston engine where the camshaft has been removed. The valves are instead opened and closed using small pneumatic actuators. As a result the valves can be opened and closed much faster, resulting in valve opening times near that of the theoretical perfect square cam-profile. The other benefit of using these electronically controlled actuators is lots of control over the valve timings, so the valve opening characteristics can be tweaked to suit different situations. All these adaptations result in up to 45% more power and torque, while also having a fuel consumption that is reduced by up to 15% and up to 35% less emissions. As an added benefit the engine also gets smaller and lighter. The weakness of the camless piston engine lies in the fact that its not produced yet. It has been proven to run, but no commercially available vehicles

include it yet. This also means that to use this on an aircraft, an existing engine needs to be adapted into a camless one which obviously costs money and adds risk to the project. However, it might be a good consideration for future iterations of this aircraft.

Wankel engine Wankel engines [2] use a radically different way to produce power compared to piston engines. Instead of using cylinders with up and down motion (or left and right in case of a boxer engine), wankel engines use a rounded triangle rotating with an eccentric rotary motion in an elliptical housing. This means the rotor, which has the same function as a cylinder in a regular piston engine, always keeps the same direction of motion, allowing for more power out of the same displacement, as well as a far smoother engine. The key advantage of the wankel engine with respect to regular pistons is a higher power to mass (and size) ratio. Slightly higher maintenance costs are a drawback. But the major disadvantage is that wankel engines have not been produced for aircraft applications in large numbers and most of the ones that have been produced are small and low power versions to be used in ultralight aircraft. As a result a wankel engine designed originally for a car would have to be modified for aircraft use, which costs money and adds risk to the project. Additionally the engine also needs to be adjusted to run on diesel since currently no running diesel wankels are available, even though rolls-royce proved it can work [57].

Turboprop engine Turboprop engines [55] are widely used in GA. These are mostly used for larger aircraft where the power of a piston engine is not enough and a dual piston engine configuration is not preferred. Turboprop engines have a very good power to mass ratio compared to piston aircraft as they are both more powerful and lighter. However, disadvantages of the turboprop are the high acquisition cost as well as the high regular overhaul cost and increased fuel consumption. This makes the turboprop more expensive than piston engines while they have superior performance figures. Also, turboprop engines achieve their best fuel consumption efficiency at higher power setting and hence at higher altitude. This makes a turboprop a less desirable option for aerobatic and recreational missions.

Hybrid propulsion system The hybrid propulsion system [55] uses an internal combustion engine (ICE) in combination with a small electric engine and a battery pack. The electric engine aids the ICE during phases of the flight where high power is required, such as take-off and climb. Outside of these phases the ICE provides all power. As a result the highest power that the ICE needs to produce is reduced and therefore a smaller ICE can be used. The mass that is saved is then used for the electric engine and battery pack. Strengths of the hybrid are lower noise levels and engine emissions near airports due to the smaller engine and the ability to use electrical power for taxiing. A disadvantage of the hybrid is that it has not been applied to aircraft with the same performance as is needed for this project. Also, it increases complexity and thus raises maintenance costs and adds risk. Options other than batteries were considered but deemed unfeasible at the moment. Hydrogen for example has a high energy content per mass but requires a volume that is 7 times the volume of regular fuel and also requires pressurised and therefore heavy tanks. Using a piston engine has been considered as a generator for the electric engine, but the efficiency loss in this conversion made this a less feasible option. Therefore, an ICE plus small electric engine and battery pack was considered.

3.3. Initial sizing

Each of the four configuration concepts was investigated conceptually through an initial sizing process using class I and II estimations. Also, power- & wing-loading and payload-range diagrams were constructed and the stability of each concept was investigated through loading diagrams and scissor plots. The knowledge resulting from these investigations was used to make an informed decision on the configuration for which the design process would be continued.
Table 3.1 lists relevant output parameters for the four configurations. The maximum take-off mass (MTOW) and operating empty mass (OEW) are indicators of the structural efficiency of the design and made even more relevant since the driving mission requirement Item **REQ-MIS-01** states that the MTOW should be less than 2000 kg. The design payload range follows from mission requirement Item **REQ-MIS-04** and key mission requirement Item **REQ-MIS-05** that state that the aircraft should be able to carry a payload of 444 kg over a minimum range of 1400 km. The maximum range that can be achieved at minimum payload is an indication of the cruising efficiency of the design and the

fuel that can be accommodated. The required power and wing surface follow from calculations that took into consideration the required compliance with CS-23 as stated by driving system requirement Item **REQ-MIS-05**, the required climb rate as established by system requirement Item **REQ-SYS-04**, the minimum cruise speed and altitude as determined by mission requirements Item **REQ-MIS-12** and Item **REQ-MIS-13** and the maximum take-off and landing distances as given by key mission requirements Item **REQ-MIS-08** and Item **REQ-MIS-09**.

Table 3.1: Initial sizing estimations

Configuration	MTOW [kg]	OEW [kg]	Design payload range [km]	Max. range [km]	Power required [hp]	Wing surface [m^2]
Conventional	1635	997	1500	3250	442	14.4
Canard	1680	942	1500	3400	447	19.5
Blended Wing Body	1582	933	1400	3500	435	29.5
Box-wing	1752	1069	1400	3100	325	23.7

3.4. Initial cost estimation

The cost estimation was performed using the DAPCA-IV method as described by Raymer [41] with a 2012 update by the ”General Aviation Aircraft Design: Applied Methods and Procedures” book [55]. It estimates the research, development, test and evaluation (RDT&E) cost of the project and the operating & maintenance (O&M) cost. The first was used, together with a sales prediction, to establish the cost price and subsequently the listing price. The second is used to estimate the cost per operating hour of the aircraft.

The yearly sales of the aircraft were estimated to be 52, which is comparable to the sales figures of three single engine turboprop aircraft: the Pilatus PC-12, Piper PA-46-600TP M600 and Daher Socata TBM 930 which is 53 on average in 2016 [47]. This number is very optimistic at this design stage, but it deemed to be acceptable up until a deeper analysis can be made (which is done in Chapter 22 and Chapter 23). The profit margin was set to 8%. The model that was used assumes a maximum break-even time of five years, however it is expected that this will take longer to achieve for this project.

Table 3.2: Initial cost estimation

Configuration	Unit cost price	Hourly operating cost	Listing price
Conventional	$1,222,318	$170	$1,319,000
Canard	$1,047,479	$168	$1,130,000
Blended Wing Body	$1,248,650	$153	$1,399,000
Box-wing	$1,181,632	$160	$1,275,000

3.5. Selection process

The evaluations of the configurations and propulsion options yielded sufficient knowledge to make an informed choice for the most suitable design option to continue the development with. Tables 3.3 and 3.4 present the (dis)advantages of the configurations and propulsion options, respectively.

3.5.1. Configurations

First of all two of the four configuration designs were eliminated on the basis of having a better alternative available. The canard design did not seem like a better option when compared to the conventional aircraft; mostly because of its severe restrictions in aerobatic manoeuvres. Configuration possibilities are also more limited, because canard aircraft are very sensitive to centre of gravity shifts. Therefore on basis of being worse than the conventional configuration for this mission, the canard configuration was

Table 3.3: Advantages and disadvantages of the conceptual configurations

Advantages	Configuration	Disadvantages
	Conventional	
Good stall characteristics		Relatively low $\frac{L}{D}$
Good aerobatic capabilities		High trim drag
Large amount of knowledge available		
Cheaper to manufacture		
	Canard	
Two lifting surfaces		Small longitudinal tail arm of vertical stabiliser
Clean air experienced by vertical stabiliser		Risk of deep stall
Good visibility from cockpit		
Longitudinally compact		
	Blended wing body	
High cruise $\frac{L}{D}$		Economical cruise speed under 180 kn
Low MTOW		Large ailerons required to achieve roll rate
Great visibility from cockpit		Large tail required to balance c.g. shifts
High maximum range		In early stage of development
	Box-wing	
High cruise $\frac{L}{D}$		In early stage of development
Potentially highly manoeuvrable		Possibly a high damping ratio
Stiff wing-tail structure		Larger C_{D_0} because of additional surface

Table 3.4: Advantages and disadvantages of the proposed propulsion systems

Advantages	Engine type	Disadvantages
	Piston	
Low development risk		High mass
Low price		Low maximum power
	Wankel	
Relatively little vibrations		High maintenance cost
High power to mass ratio		Very low maximum power
	Camless	
Reduced emissions		High development risk
Low fuel consumption		
	Turboprop	
Readily available on the market		High price
High reliability		High fuel consumption
Low mass		High maintenance cost
	Hybrid	
Reduced noise		High development risk
Low fuel consumption		Less suitable for cruise missions
Low emissions		Increased complexity

eliminated. The second eliminated concept was the box-wing design. This time however, the reasoning was based on the development risk and appeal to the customer (from coolness and trustworthiness points of view), both having low scores. It did not have any clear advantages over other designs (the box-wing was not a winner in any trade-off criterion), so it was decided by the team to eliminate the box-wing.

The final choice was thus between the conventional configuration and the blended wing body. After discussion within the team, the blended wing body was eliminated. Reasons for this decision included the fact that the blended wing body does not perform roll manoeuvres as easily due to the large wingspan as well as the great adaptability of the conventional configuration. Therefore the design of the conventional configuration is continued as described in this report.

3.5.2. Propulsion system

When performing the propulsion system trade-off, three designs were discarded fairly fast after observing the trade-off summary. Hybrid was deemed to have too much risk while not providing enough, if any, performance benefits. The camless piston engine was deemed to take too long to develop. And lastly the wankel engine was also discarded since the only benefit it had with respect to a regular piston is the power to mass ratio, while important that did not weigh up to the equally important losses in risk and maintenance compared to the piston.

The final decision was between the piston and turboprop. The better economic choice would be the piston while the turboprop is better for performance. The market analysis identified that turboprop aircraft are selling quite well and are expected to keep doing so in the future. Also, the required performance is at the top of the piston engines available power range. For diesels it is even slightly above the maximum of 350 hp they currently have, but a diesel would be the choice when going for the piston option. This is mainly due to the fact diesels can run on the much cheaper and less polluting JET-A1 fuel. This means that, even when accounting for more powerful diesels in the future, an increase in MTOW or another parameter could render the piston option useless. This lack of power adaptability of the piston engines means the design is continued with a turboprop engine.

3.6. Resulting design option

The aircraft concept that resulted from the conceptual phase is presented here, this conceptual design will be developed further in this report. The initial design has a low wing with a balanced aspect ratio and taper ratio. A small dihedral angle has been applied in order to increase the stability of the aircraft. The tail is a conventional tail in order to have all of its surfaces blown by the turboprop engine at the front of the fuselage. Initial sizing of the tail has been done on the basis of the loading diagram and scissor plots that were generated during the initial sizing process.

3.6.1. Aircraft systems

The conceptual design for the aircraft has the engine located in tractor configuration. Having the engine in front has the benefit of reducing the noise and vibrations as the airflow it experiences is smooth, other positions would have increased noise and vibrations because the propeller moves through the wake of an airfoil or of the fuselage. The fuel will be located mainly in the wing, however it is possible that there will be a small tank that drains while inverted to allows for limited inverted flight during aerobatics. The landing gear will be attached to the wing main spar and fold into the fuselage. For the pilots visibility and passenger enjoyment the plane will have a canopy cockpit with gull wing doors. The flight control system is a mechanically linked system. The secondary flight controls are likely to be either electrically or hydro-electrically operated. For passenger comfort the cabin will be pressurised, the pressurisation will be provided by the bleed air from the turboprop engine.

3.6.2. Aerodynamics

A first order estimate of the aerodynamic characteristics for this aircraft has been made on the basis of data found in the ADSEE lecture slides [100]. For the aircraft a relatively low zero lift drag coefficient of 0.02 has been assumed because the design has a retractable gear and a streamlined fuselage. The span efficiency factor has been assumed to be rather average at 0.85. The aspect ratio is assumed to be 7.35. No specific airfoil has been selected at this point, however the initial design suggests that a 15% airfoil is a good compromise between structural mass and drag. These parameters result in a predicted $\frac{L}{D}$ ratio of 15.7. These results are promising for a general aviation aircraft, however, in this category a lot of ”boxy” aircraft are also present. The trend in most personal aircraft today is towards streamlined and sleek fuselage shapes that are designed for less drag. Therefore we aim to improve on the $\frac{L}{D}$ ratio.

4

Functional diagrams

This chapter presents the functional architecture of the aircraft system. In the development of the functional architecture, each function that the system must perform is identified and decomposed into sub-functions. The output of the process can be seen in Sections 4.1 and 4.2, in the form of the Functional Flow Block Diagram (FFBD) and the Functional Breakdown Structure (FBS).

4.1. Functional Flow Block Diagram

A functional flow block diagram (FFBD) for the designed aircraft system is presented in Figure 4.1. The top level of the diagram represents the whole aircraft life cycle: from design to disposal. Of these functions the operational function is the one that is of the most interest at this point and therefore it is broken down further, down to the third level.

4.2. Functional Breakdown Structure

Figure 4.1 presents the functional breakdown structure (FBS). Here the functions of the aircraft system are presented hierarchically using an AND tree.

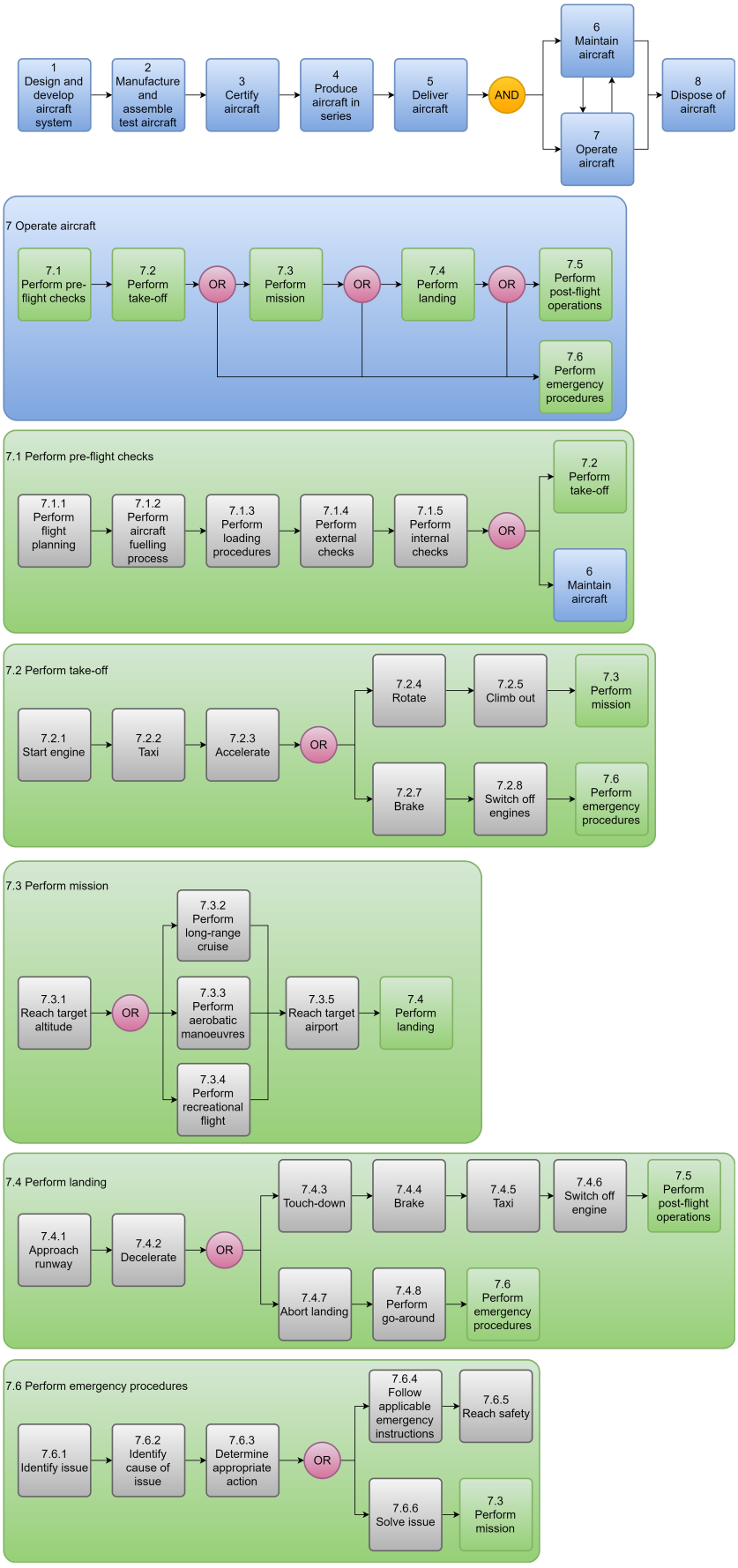

Figure 4.1: Functional flow block diagram

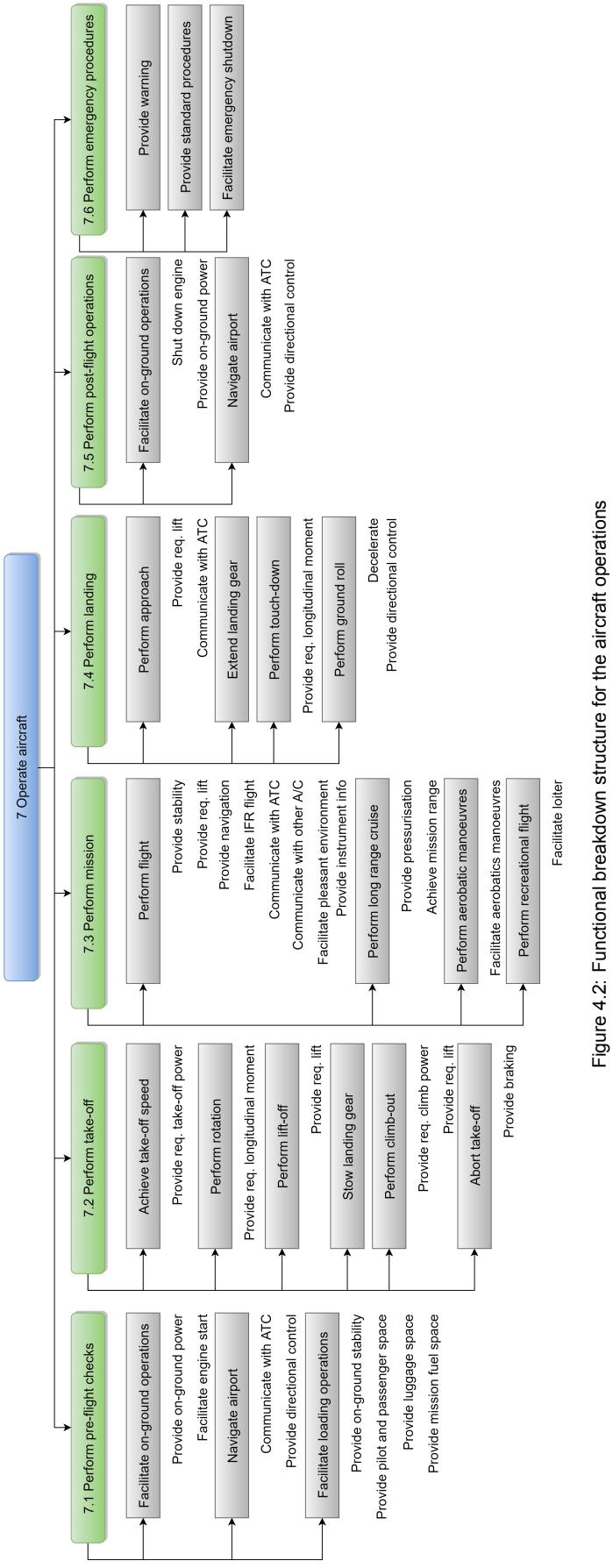

Figure 4.2: Functional breakdown structure for the aircraft operations

5

Design methodology, integration and optimisation

In this chapter the methodology of the design process during this development phase of the project is explained as well as how the design model has been integrated and optimised. The general methodology is explained in Section 5.1 and the integration and optimisation process is explained in Section 5.2.

5.1. Methodology

The target of the preliminary design phase as described in this report is to develop a reasonably accurate and detailed aircraft design. To achieve this objective four models were developed by four separate teams, each dealing with a different discipline. These four disciplines are: aerodynamics, performance, stability & control and structures. Initially the plan was devised to combine the four individual models into one big model and to develop an automated optimisation process. However, developing the models did not follow the time schedule that was setup and this left too little time to perform the combination and implement the optimisation. The precious time that was left was used to run the models separately and perform an optimisation process by manually inputting the base values and improve the values using several iterations.

The four models are described each in their own chapter: aerodynamics in Chapter 6, structures in Chapter 7, stability & control in Chapter 8 and performance in Chapter 9. For each model the applicable assumptions, the theory and model approach are presented. Also the applied verification methods are discussed, future validation efforts are proposed and the outcome is discussed shortly.

5.2. Integration & optimisation

As explained in Section 5.1, the model was supposed to be a fully integrated model, yet this turned out to cost too much time and therefore the decision was made not to do this. Integration between the parts is thus being done by manually implementing outputs from one part of the model into the next model and so on.

For optimisation a few iterations of the programs are done. Each time the outputs of the model will be used as inputs for the next iteration and adjustments in specifications will have to be made if any of the requirements are not met. The iteration process will be stopped when the iterations are deemed to have converged sufficiently and, most importantly, when all the requirements are being met. The eventual result of the entire process, the preliminary design of the aircraft, is presented in Chapters 10 to 15.

6

Aerodynamics

This chapter presents the aerodynamic model that was set up and used for the design of the aircraft. First the chapter will outline the assumptions that were made to be able to set up the model as well as the reason behind them and their possible consequences in Section 6.1. Secondly, the fundamental theory used and the model approach is presented in Section 6.2. The verification and validation process of the model is discussed and presented in Section 6.3. Finally, the outcome of the model is discussed shortly in Section 6.4.
The assumptions made are shown below.

6.1. Assumptions

AS-AERO-01 *The flow is assumed to be inviscid and irrotational*
No vortex filament that is produced dissipates and therefore either has to be a closed loop or extend into infinity. Also excludes the generation of a boundary layer on the surface of the wing.

AS-AERO-02 *For the viscous coupling the local Reynolds number and lift coefficient are assumed to be inputs for the drag*
because in Item **AS-AERO-01** no viscid effects are taken into account in the VLM a supplementary model is required for the viscous drag. In reality the pressure distribution determines the location of the transition points on an airfoil and with it the drag coefficient. The airfoil polar has been run in a 2D environment and this environment might be slightly different than the actual 3D pressure distribution. These differences are assumed to be small enough not to effect the drag coefficient significantly.

AS-AERO-03 *No flow separation is assumed to occur*
Due to the inviscid flow assumption, as given in assumption **AS-AERO-01**, no flow separation is modelled. The fuselage is designed to have a streamlined shaped, therefore this assumption is also made for the fuselage. Furthermore no separation of the empennage is modelled This limits the validity of the model to roughly 10 degrees angle of attack and 5 degrees of sideslip.

AS-AERO-04 *Apart from the defined geometry for the aircraft no other geometry is modelled*
Therefore no geometry like the earth or other aircraft is modelled. This assumption is valid as long as the separation with other objects is large enough, in that case the flow over the aircraft is undisturbed.

AS-AERO-05 *The skin friction coefficient is approximated using the ITTC-57 skin friction estimation formula*
This skin friction coefficient is used by the shipbuilding industry for nearly all their skin friction calculations. This formula describes the skin friction coefficient over a flat plate on the basis of the reynolds number of this plate. The reynolds number for this skin friction coefficient is taken as the reynolds number for the fuselage length.

6.2. Theory and model approach

For the aerodynamic model a vortex lattice method (VLM) coupled with a 2D viscous drag correction is proposed. This viscous drag is estimated using 2D drag polars generated in XFLR5 which in turn uses an implementation of XFoil and will provide the viscous drag associated with the aircraft. The VLM will provide an estimate of the induced drag caused by the lift. The viscous and induced drag are the two most important drag factors on an aircraft in subsonic flight.

Vortex lattice method The vortex lattice method is the basis of the combined model. From this model the basic lift of the aircraft can be determined. As the name implies, the model cuts up the aircraft in a set of vortices arranged in a lattice that represent the geometry of the aircraft. These vortices induce velocities on every location on the aircraft. By defining specific points where the flow must be tangential to the defined geometry it is possible to calculate the required vortex strengths. These vortex strengths then translate to forces on the aircraft. Analysing these forces can give great insight into the characteristics of the aircraft. Even more insight is provided by the viscous coupling. By looking at the forces on a small section of one of the wing surfaces of the aircraft it is possible to approximate the viscous drag of that section using the viscous model. Also, by introducing different initial conditions it is possible to determine the stability derivatives as required for the stability & control model. Because a model like this has been made industry wide in various versions it is not necessary to reinvent the wheel. This model is therefore based heavily on sources, see [1]. In the interest of brevity, the equations are not included in the report.

Viscous model The viscous model is mainly composed of interpolation of 2D drag polars generated by XFLR5 which uses an implementation of Xfoil. The interpolation is capable of interpolating between different airfoils if multiple foils are defined on a wing and dealing with the variations in Reynolds numbers and lift coefficients across the wing.

6.2.1. Wing and fuselage geometry

One of the most important aspects of a VLM is the geometric representation of the aircraft. For this implementation of the VLM a thin airfoil representation has been chosen. The result of this is that the resulting geometry of the wing represents the camberline of the chosen airfoil. The model is then defined by four airfoils that separate a half span wing in three sections. The panels that actually contain the vortices are then distributed in these three sections in both chordwise and spanwise direction in such a way that they are interpolations of the two foils that define the outer bounds of the section.
The geometry of the fuselage has been defined in a similar manner to that of the wings. Instead of the camberline the backbone of the panel creation are two half ellipses that together define a frame of the fuselage. Again the panels are then distributed between two frames.

6.2.2. Vortices

After the panel definition the vortices themselves have to be defined. A vortex in an inviscid and irrotational flow has to be either a closed loop or extend to infinity. Therefore the vortex model used in this model is the horseshoe vortex. The horseshoe vortex has a single vortex at the quarterchord point of the panel. Two trailing vortices follow from the location where this quarterchord vortex meets the edges of the panel and continue to infinity, as shown in Figure 6.1. In addition to these vortices a control point is defined as being in the middle of the panel spanwise and at threequarters chordwise. This control point is later used to define the location where the flow must be tangential to the surface of the geometry. This is identical to what is described in [1].

Induced velocity The flowfield generated from a vortex filament rotates around that vortex. This means that at any point in space it induces a velocity. This induced velocity can be calculated for the three straight parts of the vortex separately. A detailed explanation of this process can be found in [1].

Influence matrix The influence matrix is the core of the VLM. By calculating the induced velocity on the control point it is possible to calculate the velocity normal to the defined panels. Because every vortex has an influence on every control point and every control point is influenced by every panel a set of n equations with n variables can be defined. A boundary condition for these equations is

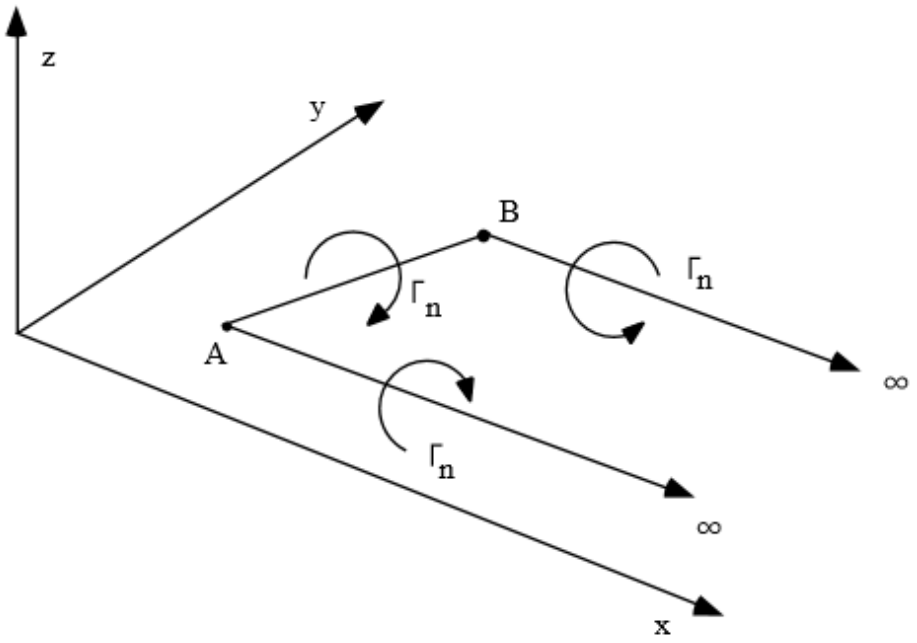

Figure 6.1: Vortex filament locations [1]

imposed such that the induced velocities to the normal of the geometry is zero, this means that the flow is parallel to the geometry as it cannot penetrate the geometry. The resulting set of equations is then supplemented with a free stream velocity vector. The resulting solution to this set of equations is then the strength of each vortex filament. With the strength of each vortex available it is possible to calculate the force that each vortex produces and the direction it is pointing to.

6.2.3. Viscous coupling

With the forces acting on the wing available it is possible to calculate the viscous drag by interpolating 2D foil data, as stated in assumption **AS-AERO-02**. Firstly, the forces over a specific span section can be transformed to a local lift coefficient. Based on the chord of the section at that location a local Reynolds number can be calculated. By using multi-dimensional interpolation on the drag polars of the foils it is possible to produce an approximation of the viscous drag at that span location. This drag is then calculated for all the wing surfaces.

Because the fuselage has no specific airfoil shape its viscous drag calculation has been done differently. The fuselage drag is based the skin friction coefficient of Equation (6.1), which is the ITTC-57 skin friction approximation as discussed in assumption **AS-AERO-05**, and the surface area of the fuselage. Lastly, the skin friction coefficient has been doubled to take into account the effect of the prop wash of the propeller blowing over the fuselage, the effect of inlet ducts and seams of access doors to the fuselage.

$$C_f = \frac{0.075}{(\log(Re) - 2)^2} \tag{6.1}$$

6.2.4. Fuselage notes

After initial testing of the model it was found that the lift and drag generated by the specified geometry of the fuselage was not delivering meaningful results. It was therefore decided that this geometry would not be included. Normally the wing geometry would terminate at the fuselage, However, to compensate for the loss of the fuselage geometry the wings now terminate halfway between the original location of the side of the fuselage and the centerplane of the aircraft. The fuselage geometry has however been maintained for the viscous drag calculation.

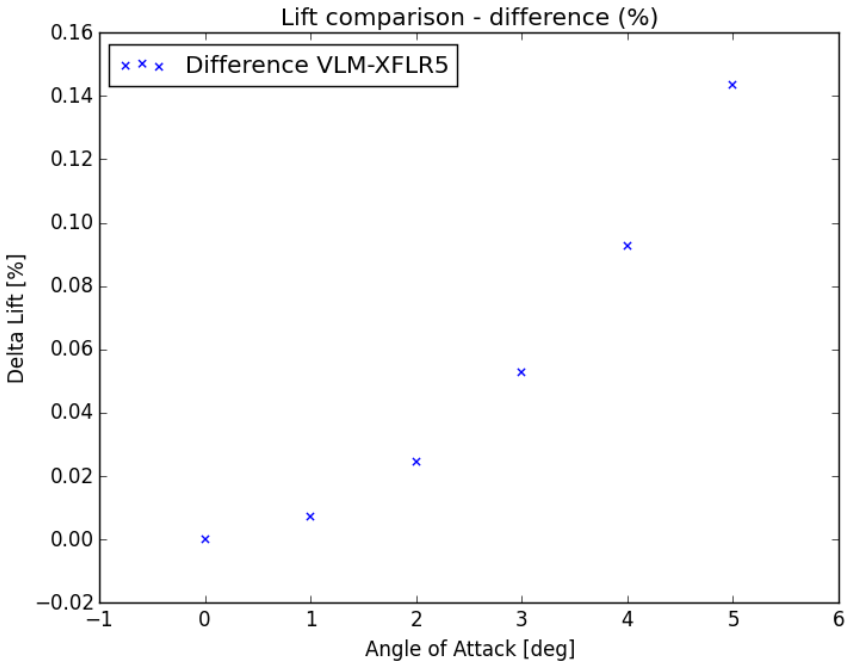

Figure 6.2: Lift difference percentage with XFLR5

6.3. Verification & Validation

VLM In order to verify that the vortex lattice method was working accordingly a comparison was made with a reference geometry in both the developed model and in XFLR5. Because XFLR5 is also a VLM code the differences should be small. The reference geometry consists of a flat wing with a wingspan of 8 m and a chord of 1 m. The wing consists of fifty spanwise elements and ten chordwise elements making for a total of 500 panels. For this model both lift and drag have been calculated over a range of six angles of attack and compared in order to verify the VLM code.

As can be seen in Figure 6.2 to Figure 6.3 the differences are very small. The maximum difference in lift is found at the highest angle of attack and was found to be 0.143%. In comparison to this however, the maximum difference in the drag calculation was found to be less than 1 thousandth of a percentage. From this it can safely be assumed that the VLM model is working correctly.

The mesh used for the aerodynamic model is shown in Figure 6.4. As mentioned in Section 6.2.4 the fuselage geometry is not included for the lift and drag calculations, but in the figure it is plotted for sake of completeness. For the verification process plots were also produced and the most interesting cases are presented. In Figure 6.5 the lift distribution is shown, this distribution is exactly as expected for this configuration. Figure 6.6 displays the change in lift during a rolling movement, this is one of the more complex cases due to the difference between left and right. But also for this case the results are exactly as expected. Finally, Figure 6.7 shows the change in lift due to an one degree increase of the sideslip angle. Here the results match expectations as well.

Stability derivatives The stability derivatives are calculated by changing the velocity vectors based on the condition the derivative is calculated for. This then gives a change in forces and moments that result in the determination of the stability derivatives. After passing the verification for flat plate the stability derivatives part of the code was tested on the full mesh. The results are shown in Table 6.1. For the stability derivatives a comparison is made with the stability derivatives of a Cessna 172 [62][65], which has comparable dimensions as the design, to see if the values are comparable. The fourth column of the table shows the verdict on the acceptability of the model value. The differences can to some extent be attributed to model limitations such as the missing fuselage.

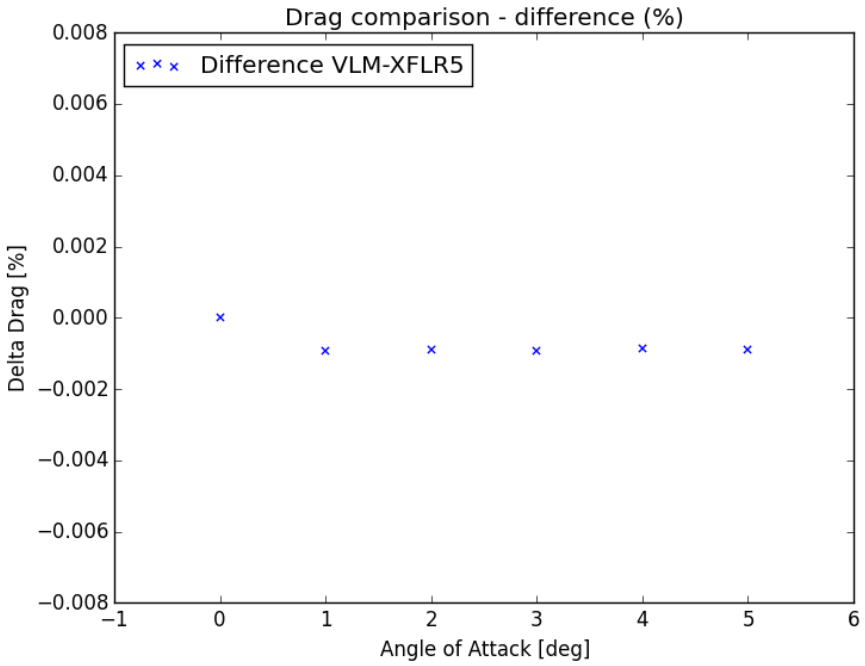

Figure 6.3: Drag difference percentage with XFLR5

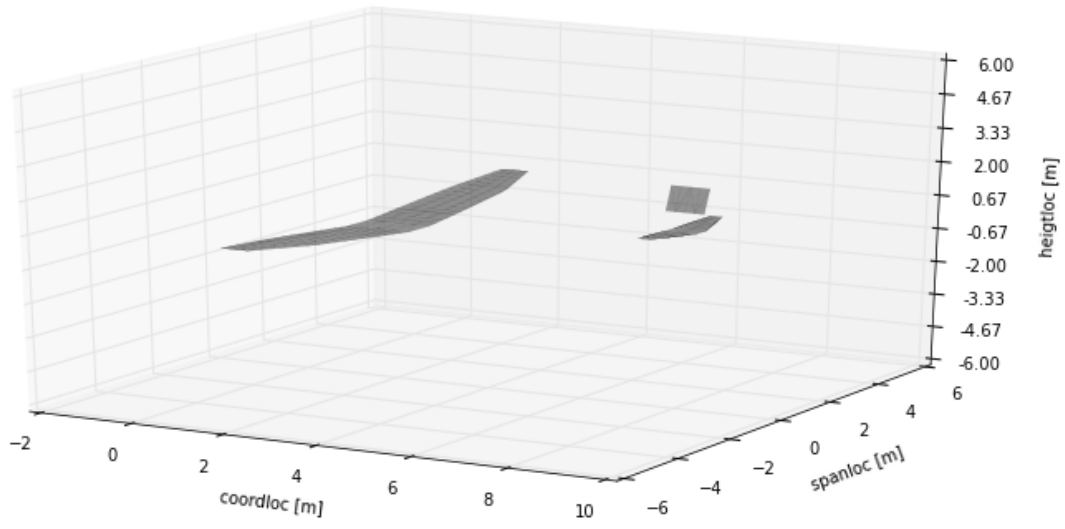

Figure 6.4: Mesh of the aircraft used for the aerodynamics model

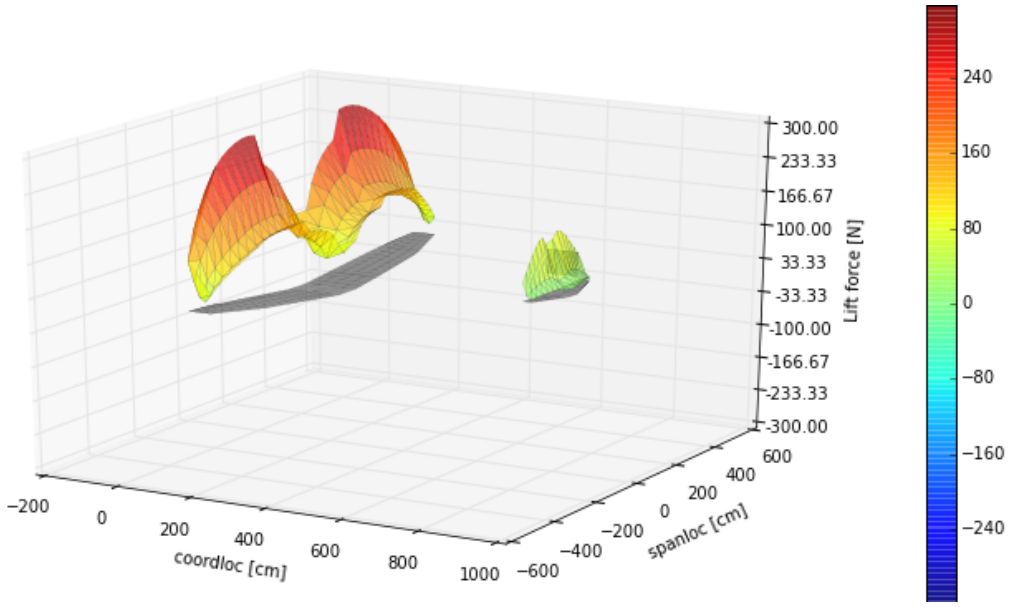

Figure 6.5: Lift distribution of the aircraft

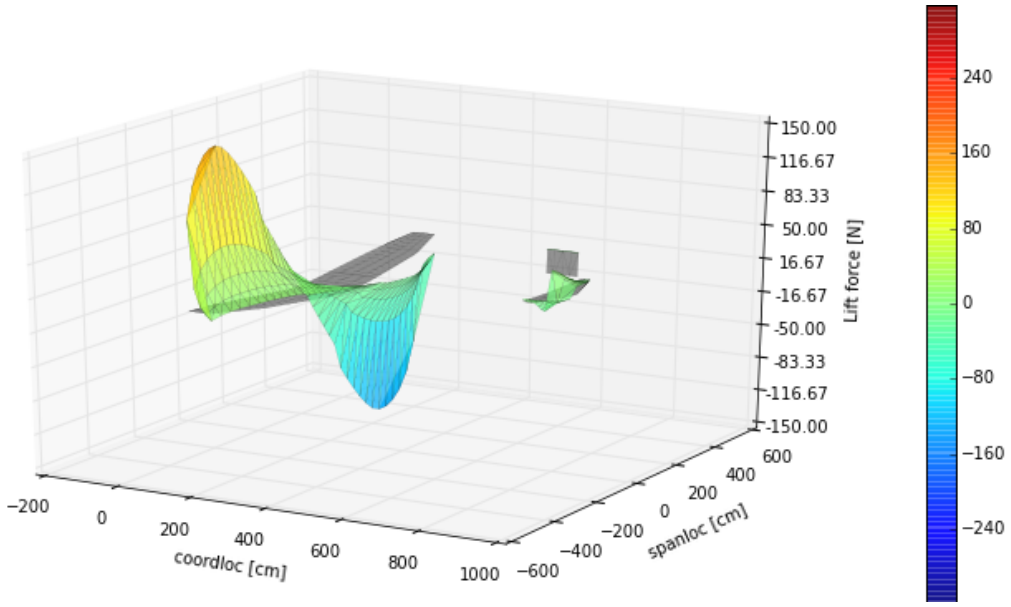

Figure 6.6: Change in lift distribution during a rolling manoeuvre

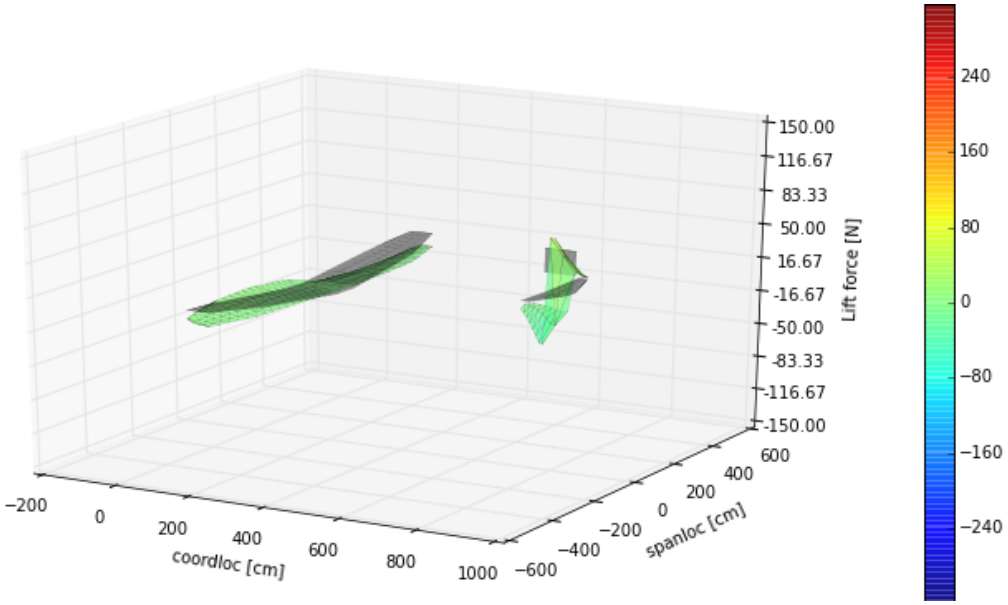

Figure 6.7: Change in lift distribution due to an one degree increase of the sideslip angle

Table 6.1: Results of verification of the aerodynamics model

Outcome	Value from model	Cessna 172	Verdict
C_{xu}	-0.03	-0.093	acceptable
C_{zu}	-0.77	-0.620	acceptable
C_{mu}	-0.002	0	acceptable
$C_{L\alpha}$	3.96	5.143	acceptable
$C_{D\alpha}$	0.23	0.13	acceptable
$C_{x\alpha}$	0.50	0.18	questionable
$C_{z\alpha}$	-3.94	-4.631	acceptable
$C_{m\alpha}$	-1.13	-0.89	acceptable
C_{zq}	-5.61	-1.95	**unacceptable**
C_{mq}	-6.79	-6.2	acceptable
$C_{z\dot{\alpha}}$	-1.07	-0.85	acceptable
$C_{m\dot{\alpha}}$	-3.21	-2.6	acceptable
C_{yb}	2.56	-0.31	**unacceptable**
C_{lb}	-0.48	-0.089	**unacceptable**
C_{nb}	1.52	0.065	**unacceptable**
C_{yp}	-0.03	-0.037	acceptable
C_{lp}	-0.54	-0.47	acceptable
C_{np}	-0.13	-0.03	questionable
C_{lr}	0.75	0.096	**unacceptable**
C_{nr}	-2.59	-0.099	**unacceptable**

Comparison of the values resulting from the model with those of the Cessna 172 resulted in multiple values that are deemed to differ too much. The model clearly included one or more errors that caused this discrepancy. Checking the code multiple times for the cause of the issue did not yield a solution within the available time. For this reason, the stability derivatives were instead calculated using XFLR5, for the rest of the values the VLM was used. This switch did not cause a lot of problems since the integration of all models, which was initially the reason not to use XFLR5 and develop the VLM method, had already been scrapped at an earlier stage as it would take too long. The stability derivatives given by XFLR5 were all comparable to similar aircraft and thus useable for other models.

6.3.1. Verification & Validation

Verification was done by doing unit test and checking for errors in the results from all units within the code. Afterwards the complete model is tested by inputting a flat plate to see if this simple case produces any weird outcomes. As a last verification test the model was run with the mesh as input and comparing the outcome to values of comparable aircraft, as well as data coming from XFLR5 for the same mesh. Validation of the aerodynamic model is not possible at this stage. To validate the model a windtunnel test will have to be executed and eventually a test flight with a concept aircraft should be performed by doing the same procedures as the model, just now in real-life to compare how the model performs. These tests will give the required data to validate the model completely.

6.4. Outcome

The model has several outcomes, most prominently the load distribution on the lifting surfaces. Other outcomes of the model are the stability derivatives, which are used in the stability model. Also various aerodynamic plots come from the model, which are helpful to visualise the general performance of the aircraft. The outcomes from the aerodynamic model are used by all three other models, being structures, stability & control and performance.

7

Structures

This chapter presents the structural model that was set up and used for the design of the aircraft. First the chapter will outline the assumptions that were made to be able to setup the model as well as the reason behind them and their possible consequences in Section 7.1. Secondly, the choice of material is explained in Section 7.2. Next, fundamental theory used and the model approach is presented in Section 7.3. The verification and validation process of the model is discussed and presented in Section 7.4. Finally, the outcome of the model is discussed shortly in Section 7.5.

7.1. Assumptions

All the assumptions, used for the structural model, are listed below.

AS-STRUC-01 *The aircraft is designed for the worst case scenario, with a composite safety margin of 2.0.* The aircraft may not ever be able to get in this situation and this will over design the aircraft and that is taken into account for further development. The primary reason for the high safety margin in comparison to metals (1.5) is the lower degree of knowledge about composite materials compared to metals, therefore a higher degree of over-designing is required with eye on safety [95]. Hence, instead of listed in the requirements maximum load of $+6g$, a worst-case load of $+12g$ is considered. the loads during minimum load of $-6g$ were also looked at early during the analysis, but they are not as severe as maximum loads. The worst-case loads on enpennage were determined by aerodynamical analysis.

AS-STRUC-02 *All structural elements are constructed using a sandwich composite material consisting of two laminate facesheets, a honeycomb core and adhesive layers between them*
This choice has been made because of the significant mass reduction when compared to aluminium. A more elaborate discussion on the material choice in presented in Section 7.2.

AS-STRUC-03 *The drag forces on the main wing, tail and fuselage are neglected*
From the aerodynamic analysis it is concluded that the drag force is negligible when compared to the lift loading on the wing and empennage from a structural perspective. Drag should be accounted for in further design where in-depth optimisation is performed.

AS-STRUC-04 *Shear centres of the wingbox and tailbox are located on the crossing of neutral axes of the respective cross-sections*
Computing the exact location of shear centre is a complex procedure and the result should be near the neutral axes crossing location due to the nearly symmetrical airfoils that are used. It was decided to make this assumption in order to save time to compute more important parameters.

AS-STRUC-05 *All stresses are carried by the facesheets of the sandwich composite*
The honeycomb core of the composite material does not carry any stresses. The core only distributes the stresses to the laminate facesheets.

AS-STRUC-06 *Total thickness of the composite material is uniform across each part of the structure, namely wing, fuselage and empennage*
This assumption contains two different considerations. First of all, it means that in the points of joining the honeycomb will not have a reduced thickness, which in fact needs to happen in order to connect parts. Secondly, it might not be optimal to keep the same thickness of the material across the part as the stresses vary throughout the structure. However, varying thickness would make modelling the design excessively difficult for this stage of the design process.

AS-STRUC-07 *Ribs are not accounted for in stress or Moment of Inertia (MOI) calculations*
The function of ribs is to prevent the wing or tail structure from buckling and to add extra stiffness. Their contribution to the stress distribution and MOI is small in comparison.

AS-STRUC-08 *The composite laminate is quasi-isotropic*
Any composite material used is assumed to have a $\pm 45°$, $0°$, $90°$ fibre alignment. This way the properties are almost constant in every direction, which simplifies the process at this design stage.

AS-STRUC-09 *For the MOI calculations the structure is assumed to be thin walled*
The wall thickness is significantly smaller than the overall dimensions of the wingbox which makes the thin walled assumption valid. Only Steiner terms from the parallel axis theorem are considered for thin walls.

AS-STRUC-10 *The fuselage structure is modelled using classical beam theory*
Therefore in the analysis the following factors are neglected: local load introductions, stress concentrations and warping. In the further development phases, it is advised to use a finite element model or other models which do not use this simplifying assumption.

AS-STRUC-11 *The bending relief is not considered in this phase of the design*
It initially posed a 'chicken and egg' problem - it was possible to calculate the lift needed for further calculations to end up with a mass which was calculated only at the end of these calculations, and it would then be possible to solve the problem of bending relief. The same goes for the fuel weight - only towards the end it became evident where the fuel would be placed, and only then it could be considered for bending relief.

7.2. Material selection

Two material categories are viable candidates for the airframe: metals and composites. In turn, composite materials can be divided into two categories: laminates and sandwiches. These three options and their properties are explained shortly.

- **Metals** have been used in aircraft construction for a long period of time, especially when compared to composites. For the large part of the aviation age metals were the default choice for aircraft design. As a result the properties of metals are known extensively, which allows for reduction in development risk and better optimisation. Metals are relatively cheap and easy to manufacture. The downside of metal usage for the airframe is a higher resultant mass of the structure, the risk of corrosion and increased risk of fatigue. Metal is the material of choice if cost is the driving factor.

- **Laminate composites** feature significantly reduced structural mass, increased corrosion resistance and nearly no risk of fatigue. This comes with multiple drawbacks. Composite materials are more expensive when compared to metal structures, in particular those composed of carbon

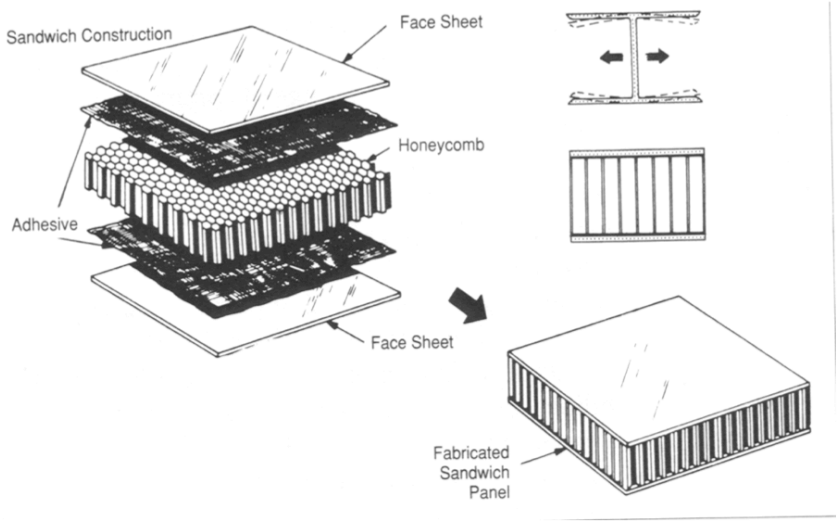

Figure 7.1: Basic sandwich composite with honeycomb [53]

fibres. Manufacturing and assembly of laminates is also more complex, including part replacement in the case of irreversible damage. When it comes to cracks or delamination, it is not always possible to detect the damage easily as it occurs inside the composite plate and therefore the damage is not directly visible. Therefore, more thorough maintenance procedures with non-destructive investigation methods are required to ensure safety. Composite structures also require a higher safety factor for this reason as mentioned by Ir. J Sinke at Delft University of Technology. Laminate composites are the preferred material if mass and performance criteria are more important than cost.

- **Sandwich composites** consist of a honeycomb structure, two laminar composite facesheets and an adhesive layer connecting these elements, as shown in Figure 7.1. Advantages of sandwich composite structures when compared to just laminate composite structures include a more simple overall structure, as the bending stiffness of the honeycomb increases buckling performance and thereby eliminates the need for stiffeners in the structure. This generally applies to GA aircraft. As the honeycomb core's mass is low, the overall structural mass is decreased when compared to pure laminates. With the stiffeners eliminated the total amount of connections between structural parts is reduced, but at the cost of increased complexity of remaining connections. To provide a reliable connection to other parts, the sandwich has to be made thin at the connection locations. From a manufacturing point of view, it is a complication that sandwich composite parts are very stiff and therefore the production has to be done very precise. A part of a slightly wrong size or curvature will not fit in the structure and remaking the entire part is required. Additional layers for the sandwich composite can be added to enhance properties such as water resistance, electrical insulation or impact resistance.

It was decided to use composite material over metals; mainly because of the reduced mass and the high corrosion resistance. The choice between the two types of composites was made in favour of the sandwich composite as it allows for structural simplicity because no stringers or stiffeners are required for sandwich components.
For the actual composite fibre, it is decided to use carbon fibre because of its vastly superior mechanical properties comparing to other fibres. The designed aircraft has to withstand loading cases of $-3/+6g$ ($-6/+12g$ including safety factor) and therefore carbon fibre is desirable to obtain a low structural mass. The only downside of using carbon is a relatively high price of it, but the weight reduction it provides benefits the overall design, especially considering that the aircraft is expected to be a state-of-art design. The primary function of the honeycomb core is transferring loads to the laminate composite facesheets. A major problem with using honeycomb structures in aircraft is the possible introduction of moisture in the honeycomb structure. This moisture can lead to degradation of the material if aluminium is used. Therefore the optimal choice for the honeycomb core is determined to be Kevlar® as it has

mechanical properties that are close to aluminium when used as honeycomb core material and it has a low mass, while having no moisture degradation.
Finally, the last basic layer, which is adhesive connecting the laminate and core, is taken to be epoxy film for this design stage, as it has good temperature tolerance (from $-55°C$ to $82°C$). A short overview of basic sandwich properties is given in Table 7.1.

Table 7.1: Basic sandwich components properties

Layer	Primary material	Density
Laminate [16]	Carbon fibre	1800 kg m^{-3}
Adhesive [70]	Epoxy	0.42 kg m^{-2}
Honeycomb core [82]	Kevlar®	96.1 kg m^{-3}

7.3. Theory and model approach

In this section the approach to creating the structural model is explained. The subsections each present and explain the applied equations. All the equations follow from the Aircraft Structures for Engineering Students book by T.G. Megson [71], unless stated otherwise.

7.3.1. Design load cases

The aircraft is designed for the worst case scenario it could find itself in, even if this is an unrealistic scenario. This results in a slightly over designed aircraft but this will also be accounted for in a later stage of the design as mentioned by Item **AS-STRUC-01**.
The bending relief is as well not considered in this phase of the design as it initially posed a 'chicken and egg' problem - it was possible to calculate the lift needed for further calculations to end up with a mass which was calculated only at the end of these calculations, and it would then be possible to solve the problem of bending relief. The same goes for the fuel weight - only towards the end it became evident where the fuel would be placed, and only then it could be considered for bending relief.
The worst case scenario for this aircraft is during a pull-up manoeuvre at the maximum speed which is the dive speed, $V_D = 1.55 \cdot V_{\text{cruise}}$ at 12g and at MTOW. The other worst case scenario considered is at the same speed but with a different load factor is -6g. Figure 7.2 shows the manoeuvre of the worst case scenario where $V = V_D$ and $N = 12 \cdot MTOW$.

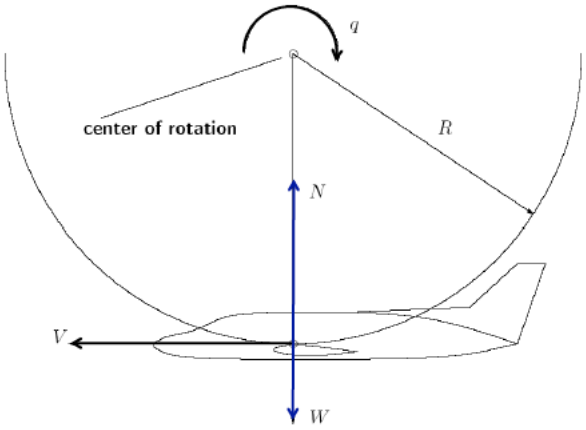

Figure 7.2: Pull-up manoeuvre [62]

7.3.2. Wing and tail

Second moment of inertia To begin with, some basic values need to be calculated that are used in further calculations. First of all the neutral axes of the cross section of the wingbox are calculated. Since the wing is tapered, the neutral axis changes with respect to the reference system for every

location along the span. The neutral axes locations x_{NA} and z_{NA} are calculated as in Equation (7.1) and Equation (7.2). Then the span of the wing was divided into sections and the calculation was repeated for every spanwise location. The approach is shown in Figure 7.3. In this figure it can be seen that the chord is split up into sections as well as the span of the wing. The horizontal and vertical lines should not be confused with stringers and ribs and neither should the shape of the picture.

$$x_{NA} = \frac{A_{\text{section}}\overline{x}}{A_{\text{total}}} \quad (7.1) \qquad z_{NA} = \frac{A_{\text{section}}\overline{z}}{A_{\text{total}}} \quad (7.2)$$

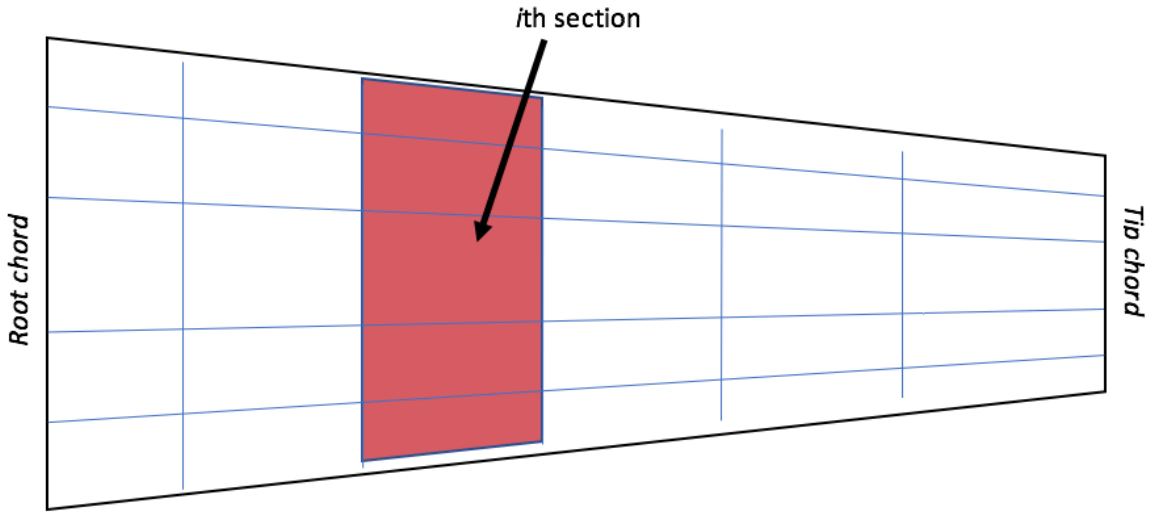

Figure 7.3: Sectioning approach for the wing and tail sections

For calculating bending stresses the MOI are required about the x and z axes, these are calculated using Equations (7.3) and (7.4). Since the airfoil is not fully symmetrical the product of inertia is also included, as calculated using Equation (7.5). Here too, the value changes for each spanwise section of the wing: it decreases towards the tip. As stated in assumption **AS-STRUC-09** the structure is assumed to be thin walled.

$$I_{xx} = \int_A \tilde{z}^2 dA \quad (7.3) \qquad I_{zz} = \int_A \tilde{x}^2 dA \quad (7.4) \qquad I_{xz} = \int_A \tilde{x}\,\tilde{z} dA \quad (7.5)$$

Bending Stress From the aerodynamics analysis, the distribution of loads was determined for each section of the wing and tail wingbox. This distribution is required in order to find the shear and bending stress at every point of the wing or tail wingbox for the spanwise positions. This is done according to Equation (7.6) where the lift of a section is calculated. Here c_i is the chord length at the respective spanwise location and dy is the width of such a section, which is constant. As mentioned Section 7.3.1, bending relief is not taken into account.

$$L_i = C_L \frac{1}{2} \rho V^2 c_i dy \quad (7.6)$$

The load acting at every section also contributes to the moment experienced at the root of the wingbox. In Equation (7.7) this moment is calculated. Here y_i is the distance from the root to the respective section. Only the moment about the x-axis is considered because the drag forces are negligible, as stated in assumption **AS-STRUC-03**.

$$M_{x_i} = L_i \cdot y_i \quad (7.7)$$

Summing up all lift and moment contributions gives the total lift and total moment at the root of the wing. Then starting from the total value and subtracting every section value from the total $(i-1)th$ value provides the shear and moment diagrams.
In order to determine the parameters such as the skin thickness, the bending stress must be calculated for the entire wingbox. Bending stress is one of the two stresses considered in the design of the aircraft at this stage. Thus far the moment has been calculated for the entire wing as well as the MOI's and the neutral lines. This allows for the bending stresses to be calculated for every section of the wing as well. As the drag force is neglected, as stated in assumption **AS-STRUC-03**, only a moment about the x-axis is applied. The general equation for bending stress with only M_x is Equation (7.8).

$$\sigma_y = \frac{M_x}{I_{xx}I_{zz} - Ixz^2}(I_{zz}\bar{z} - I_{xz}\bar{x}) \tag{7.8}$$

This allows the bending stress along the the wingbox contours to be investigated by checking for every z and x combination. This identifies the critical locations on the wingbox along the span of the wing, allowing the wingbox to be designed accordingly.

Shear Stress Alongside with bending stress, the wingbox and tailbox are subjected to shear stress. In the case of composite sandwich material, shear stress is transferred by the honeycomb core to the laminate sheets. In order to find the shear stress distribution, which relates to the shear flow according to Equation (7.9), the shear flow at every point of the wingbox and tailbox has to be determined. The general equation for the shear flow in a beam cross-section is given in Equation (7.10). In this form the equation is not usable for the model, therefore it has to be adapted for the wingbox and tailbox separately.

$$\tau = \frac{q}{t} \tag{7.9}$$

Using the aerodynamics model the force distribution over the wing and tail chord is determined. The resultant of that distribution does not necessarily pass through the shear centre of the wingbox or tailbox. Therefore the principle of superposition is applied, as illustrated in Figure 7.4. Here the total force S that is applied at a random point can be represented by a combination of the same force S applied at the shear centre and the torque T. The torque is defined as the product of force and horizontal distance between the shear centre and the point of action of the force.

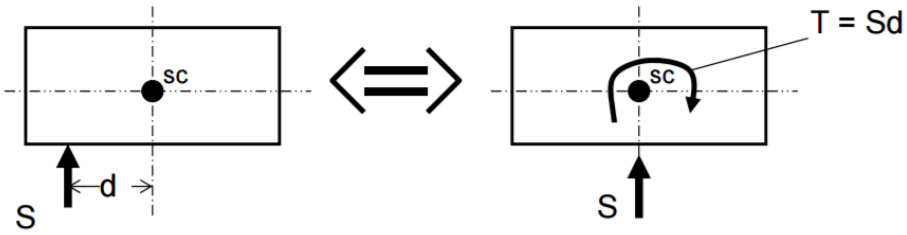

Figure 7.4: Illustration of superposition principle with respect to shear flow and shear centre [35]

Because of how the model is constructed it is possible to evaluate the shear flow point-by-point across the cross-section. The interpolation function allows for determining the change in length Δs between every point. Hence, the general equation in Equation (7.10) is simplified to Equation (7.11).

$$q = \left(\frac{S_x I_{xx} - S_z I_{xz}}{I_{xx}I_{zz} - I_{xz}^2}\right)\int_0^s txds - \left(\frac{S_z I_{zz} - S_x I_{xz}}{I_{xx}I_{zz} - I_{xz}^2}\right)\int_0^s tzds + q_t \tag{7.10}$$

$$q_i = q_{i-1} + \left(\frac{S_x I_{xx} - S_z I_{xz}}{I_{xx}I_{zz} - I_{xz}^2}\right)tx_i\Delta s_i - \left(\frac{S_z I_{zz} - S_x I_{xz}}{I_{xx}I_{zz} - I_{xz}^2}\right)tz_i\Delta s_i \tag{7.11}$$

The next step is to simplify Equation (7.11) further for the wingbox and tailbox specifically in order to reduce the required amount of computations. As stated in assumption **AS-STRUC-03**, the drag force, which in this case is represented by S_x, is assumed to be zero. This reduces the wingbox shear flow

equation to Equation (7.12). The same applies to the tailbox, but here the product of inertia I_{xz} is zero because a symmetrical airfoil is used. Therefore the tailbox shear flow equation is reduced to Equation (7.13).

$$q_{i_{wingbox}} = q_{i-1} + (\frac{S_z I_{xz}}{I_{xx} I_{zz} - I_{xz}^2}) tx_i \Delta s_i - (\frac{S_z I_{zz}}{I_{xx} I_{zz} - I_{xz}^2}) tz_i \Delta s_i \tag{7.12}$$

$$q_{i_{tailbox}} = q_{i-1} - \frac{S_y}{I_{xx}} ty_i \Delta s_i \tag{7.13}$$

The force distribution over the wing or tail chord generates a torque. This torque is added to the shear flow using the superposition principle as explained earlier using Figure 7.4. This is integrated through the means of setting an initial shear flow equal to the torque shear, as shown in Equation (7.14).

$$T = 2A_{encl} q_0 \tag{7.14}$$

7.3.3. Fuselage

The fuselage structure has the following main functions: to sustain the aerodynamic and pressurisation loads 3both under normal operating conditions and under emergency operations as well as to provide accommodation and protection to passengers and cargo. In addition to this, the fuselage structure must allow components such as the lifting surfaces and the engine to be mounted and it should offer adequate load paths to carry the resulting loads. During the design of the fuselage a compromise between structural efficiency, which includes withstanding operational loads and pressurisation while being light-weight, and aerodynamic performance has to be made.

Fuselage Shape Concepts Before determining the loads experienced by the structure and designing the structure to meet these loads, the cross-sectional shape of the fuselage and its lengthwise geometry must be established. The three fundamentals lengthwise shapes of a fuselage are, according to [55]:

- **Frustum-shaped** The empennage of this fuselage resembles a trapezoidal prism and in general has a tapered boxlike appearance. Examples of aircraft with this shape are the Cessna 172 and the Piper PA-28 Cherokee.
- **Pressure tube** This type of fuselage has a tubular main section and capped ends. It is commonly used in the industry in the design of large passenger aircraft.
- **Tadpole** The combination of the empennage and forward portion resembles the shape of a tadpole. It is the most encountered shape in sailplanes. Examples of aircraft with this shape are the Diamond DA-20 Katana and the Cirrus SR20.

Figure 7.5 provides a visual representation of the structural layout of the previously defined shapes. By evaluating the requirements, it becomes apparent that the second shape can be discarded for the design since the aircraft carries only four people. The pressure tube shape provides no structural or aerodynamic advantages in this case since it is better suited for transport aircraft. Finally, a trade-off can be performed between the remaining two shapes. Three criteria are assessed: aerodynamic efficiency, production cost and use of space. Each of the criteria is assigned the same weight and the score classes are as follows:

- Excellent (Green). The concept exceeds the requirements.
- Good (Blue). The concept meets the requirements.
- Correctable deficiencies (Yellow). The concept can meet the requirements.
- Unacceptable (Red). The concept cannot meet the requirements.

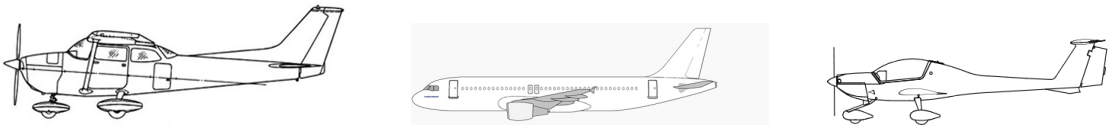

Figure 7.5: The fundamental shapes of a fuselage from left to right: frustum-shaped (Cessna 172), pressure tube (A320) and the tadpole (DA-20 Katana).[4, 7, 9]

Aerodynamic efficiency The tadpole design has proven to generate far less drag than the frustum shape, mainly due to the fact that its empennage shape results in a reduction of wetted area of 30-40% [40]. The main challenge encountered with such a design is the curvature of the geometry after the maximum height. Special attention must be paid to the transition as a too sharp transition can result in an increase in the overall drag of the fuselage.
Production cost This trade criteria is dependent on the choice of material. The frustum shape is inexpensive to produce out of folded sheet metal, while the tadpole design can be cheap to produce using composites [55]. Here assumption **AS-STRUC-09** is used, which states that the aircraft is made of composite.
Usage of space The frustum shape provides more space in the empennage to store equipment or cargo. However, the strict requirement on the maximum take-off weight does not allow for the passengers to bring cargo exceeding 25 kg. Therefore, additional space for cargo is not desired.

The trade-off summary can be found in Figure 7.6. The result of the trade-off is that the tadpole design is best suited for the design.

	Aerodynamic Efficiency	Production Cost	Usage of space
Frustum-Shaped	Nominal	More expensive than tadpole	Additional space in empennage to store cargo
Tadpole-Shaped	Less wetted area than frustum	Nominal	Less space than frustum

Figure 7.6: Trade-off of the fuselage shape

Now that the lengthwise structural layout of the design has been established, the cross-section of the fuselage must be selected. As stated in the requirements, the cruise altitude of the aircraft should be at least 18000 ft. Generally, people begin to suffer from oxygen deficiency from altitudes as low as 14000 ft. Therefore, for the comfort of the passengers, during the conceptual design stage, the design team opted for a pressurised cabin. This limits the cross-sectional shape of the fuselage to a circle as this is structurally the most efficient configuration for pressure loads.
A general shape of the fuselage has now been established and all that remains is defining its dimensions based on constraints imposed by the human body, the size of the equipment, the cargo and the structural components which are to be mounted on the fuselage. For the preliminary design process, there is not yet enough detail available to estimate the layout and dimensions of the fuselage with a high accuracy. Thus, it is more convenient to estimate the geometric properties of the aircraft with some generic shapes, such as a cylinder or a frustum [55]. For a reasonable accuracy, the fuselage is segmented into five of the above mentioned shapes, which are as follows:

- **Segment A** is the nose of the fuselage. It provides support for the engine, the main landing gear and the firewall. It is modelled as a cylinder, with the diameter D_A equal to the largest cross section dimension of the engine, plus some space for the landing gear. Its length L_A is defined by the length of the engine and firewall combined.
- **Segments B,C,D** are the cockpit, passenger cabin and cargo space. Their respective shapes are a frustum, a cylinder and another frustum. The diameter D_{B_2} is the maximum along the entire

fuselage length. The value was increased by 0.2 m from the one estimated during the conceptual design stage in order to allow for the wingbox to be mounted in this section as well as to fit the occupants comfortably. The length of each section was determined based on the estimations provided in General Aviation Aircraft Design [55].

- **Segment E** is the empennage segment, which is modelled as a frustum. Depending on the optimal size and position of the horizontal tail, the fuselage length L_f changes. The length L_E of this segment is set to vary depending on the length. The diameter D_{E_2} provides sufficient space to facilitate the tailbox.

Table 7.2 shows the dimensions of each segment, where D denotes a diameter and L denotes a length. The index 1 and 2 denote the beginning and end of a segment. The datum for the length of the fuselage is set at the nose.

Table 7.2: Fuselage Segments

A: Cylinder		**B: Frustum**		**C: Cylinder**		**D: Frustum**		**E: Frustum**	
D_A	0.8 m	D_{B_1}	0.8 m	D_C	1.4 m	D_{D_1}	1.4 m	D_{E_1}	0.8 m
L_A	1.35 m	D_{B_2}	1.4 m	L_C	0.9 m	D_{D_2}	0.8 m	D_{E_2}	0.2 m
		L_B	1.3 m			L_D	0.5 m	L_E	$L_f - L_A - L_B - L_C - L_D$

Stress calculations As mentioned in assumption **AS-STRUC-10**, the fuselage is modelled using classical beam theory and in the stress calculations local load introduction, stress concentrations and warping are neglected.
The coordinate reference frame selected for the assignment has its origin at the rear part of the fuselage (at the tail) in the geometrical centre of the circular cross section. The positive x-axis is pointing to the right wing parallel to the ground. The positive y-axis is perpendicular to the ground and the positive z-axis is pointing to the direction of the nose. The reference frame follows the one defined in the Aircraft Structures for Engineering Students book by T.G. Megson [71]. The correct signs of the internal force and moments in the structure are shown in Figure 7.7. The origin of the axis system is represented in Figure 7.8.

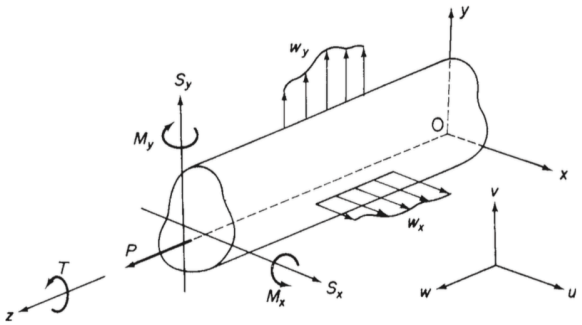

Figure 7.7: Reference frame and correct sign convention for the internal loads in the structure[71].

The fuselage is modelled as a static object, which means that all forces and moments are in equilibrium. The internal forces and moments in the fuselage generate normal and shear stresses as well as torque. The moments introduce normal stresses, while the shear and torque introduce shear stresses. In order to determine the stresses the structure was discretised at every centimetre along the z-axis. At these locations the moments M_x and M_y, the shear forces S_x and S_y and the torque T were calculated. This provides a satisfactory compromise between accuracy and computational cost. Since drag is neglected in calculations, as stated in assumption **AS-STRUC-03**, the normal stresses introduced by the normal forces are also neglected.
The next step is to split up the stress calculations into two parts normal and shear stresses. For each cross-section the minimum thickness required to sustain these stresses was calculated using the tensile

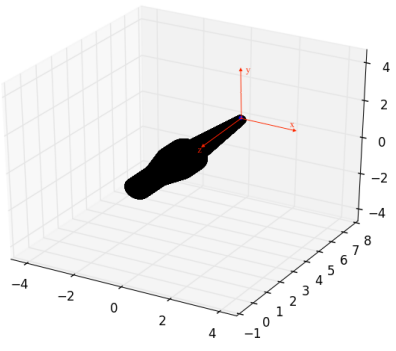

Figure 7.8: Reference frame

σ_t, compressive σ_c and shear τ_{max} stresses of the material. The following steps were taken for each cross-section element, where the *i* index denotes the i-th cross-section.

- *Calculate the moment of inertia of each cross-section* The general equation for a thin walled circular section is given by Equation (7.15). Assumption **AS-STRUC-09** is applied here. Given the circular shape, I_{xx} and I_{yy} are equal, while I_xy is zero.

$$I_{xx_i} = I_{yy_i} = \pi r_i^3 t \tag{7.15}$$

- *Cross-section is descritized into 360 points*, which are spaced evenly at one degree intervals. The numbering of the points begins at the positive x-axis and moves counterclockwise. The index j is used to denote the current point. Since the cross-section is in the xy-plane, the x and y coordinates of each point are determined using Equation (7.16).

$$x_j = r_i \cos(\theta_j) \qquad y_j = r_i \sin(\theta_j) \tag{7.16}$$

- *Calculate the minimum thickness to sustain the normal stresses in the cross-section*. Assuming failure will occur when the maximum or minimum applied stress equals the ultimate strength of the material, then the required thickness at each cross-section can be calculated using Equation (7.17), when the point on the cross-section is in tension and Equation (7.18) when the point is in compression. Finally, the largest thickness between the 360 points is set as the thickness of the cross-section. The thickness to the fuselage is set to the largest thickness among all the cross-sections.

$$t_j = \frac{M_{y_i} \cdot x_j + M_{x_i} \cdot y_j}{\pi r_i^3 \sigma_t} \tag{7.17}$$

$$t_j = -\frac{M_{y_i} \cdot x_j + M_{x_i} \cdot y_j}{\pi r_i^3 \sigma_c} \tag{7.18}$$

  In addition, the thickness required to sustain the normal stress due to pressurization must be added to this thickness. The pressure differential used for these calculation is $\Delta p = 63724.1$ Pa. It assumes a worst case scenario in which the aircraft is pressurized at sea level conditions. The thickness is calculated using Equation (7.19). The required thickness is reached at the location of the maximum radius.

$$t_h = \frac{\Delta p \cdot r_{max}}{\sigma_t} \tag{7.19}$$

- *Calculate the minimum thickness to sustain the shear stresses in the structure*. Since the cross-section of the fuselage is symmetric, the shear centre is located at the geometric centre. The

shear forces on the cross-section are moved to act through the shear centre and a torque T is introduced in the section. In order to determine the shear stresses on the closed section beam, the principle of superposition is applied. The shear flows produced by the shear load are added to the shear flows produced by the torque. First the shear flows due to the shear forces are calculated using Equation (7.20). An imaginary cut is made in the fuselage at the location of the positive x-axis. The shear flow is calculated between the 360 points. Solving the integral in Equation (7.20), the basic shear flows are determined using Equation (7.21).

$$q[j, j+1]_b = -(\frac{S_{x_i}}{I_{yy_i}}) \int_0^s txds - (\frac{S_{y_i}}{I_{xx_i}}) \int_0^s tyds \tag{7.20}$$

$$q[j, j+1]_b = -\frac{S_{x_i}}{\pi r_i^3} r_i^2 \sin(\theta_j) - \frac{S_{y_i}}{\pi r_i^3} r_i^2 (\cos(\theta_j) - 1) = -\frac{S_{x_i}}{\pi r_i} \sin(\theta_j) - \frac{S_{y_i}}{\pi r_i} (\cos(\theta_j) - 1) \tag{7.21}$$

Next, the shear flow in the cross-section due to the torque is determined using Equation (7.22).

$$q_{0_i} = \frac{T}{2A_{encl}} \tag{7.22}$$

The basic shear flows are then added to the shear flow due to the torque. From the total shear flow, q_t, the required minimum thickness in the cross-section to sustain the shear loads is determined, using the maximum shear strength of the material τ and Equation (7.23). The maximum thickness between all cross-sections is then compared to the current fuselage thickness. If it exceeded it the thickness was changed to the one determined for the shear stresses, otherwise it remained unchanged.

$$t_i = \frac{q_t}{\tau} \tag{7.23}$$

The model does not treat the concept of structural instability yet. This is mainly due to the choice of material, as composite buckling requires the development of a finite element model. This will be examined in the later stages of the deign.

7.4. Verification & Validation

As a self-created model, the structural part of the design has to be verified using analytical results and validated using real-life data.

For the verification part unit tests and system tests, standard verification methods, were applied to each part of the model. Structuring the model in the form of functions was of tremendous help for this purpose as the unit tests consisted of testing the individual functions. Smaller functions were combined as larger functions in order to perform complex calculations and output the final results of the simulation. These output values were verified as a part of the system test.

The main method of verification was making simplified calculations on paper and comparing the model results with these. Additional methods included varying the input for the functions in order to make sure results still made sense. This includes varying the force, dimensions and also discretisation grid to find out possible errors in formulae. For validation, the most reliable method would be testing individual structural components on withstanding the worst-case loading, for example bending the wingbox with the force of $+6g$ and recording the outcome. Considering the 2.0 composite safety factor, it is supposed to fail at $+12g$ to be deemed optimally designed. The structural components can also be tested for resisting crash loads (for the scenario of a bird strike) and buckling loads (by the means of applying shear the sandwich plate). Failing of the sandwich structure is not always visible, as it might happen inside the structure, so applying sonic or ultrasonic inspection methods is necessary during the validation.

7.5. Outcome

From applying the theory as presented above the most interesting outcome of the structural model is the mass of the aircraft structure. Apart from the mass, the dimensions of the structural parts of the aircraft are determined.

7.5.1. Main wing and empennage

The final outcome of the structural model for the main wing and empennage are the dimensions of the wing- and tailbox and the mass of the structure. However, to get to the final outcomes, first some other outcomes must be used. These outcomes are as follows:

- Shear and moment values at any point along the span, together with representing diagrams shear and moment diagrams.
- The neutral axes x_{NA} and z_{NA} at every position along the span of the wings.
- The moment of inertia I_{xx}, I_{zz} and I_{xz} moment of inertia at any point of the span.
- Bending stress distribution in the cross-section at any point of the span. Highest bending stress at a given point of the span. Highest bending stress plot along the span.
- Shear flow and stress distribution plot at any location along the span. Highest shear flow value at any location along the span.
- Wingbox and tailbox dimensions such as skin thickness, rib placement, spar placement, and wingbox volume.
- Total mass of the wing and empennage including the LE and TE structures, excluding control surface structures.

7.5.2. Fuselage

The outcome of the fuselage model is the smallest thickness necessary to withstand the applied loads. This thickness is then applied everywhere throughout the fuselage length. Finally, the mass of the fuselage is calculated.

8

Stability & Control

This chapter presents the stability & control model that was set up and used for the design of the aircraft. First the chapter will outline the assumptions that were made to be able to set the model as well as the reason behind them and their possible consequences in Section 8.1. Secondly, the fundamental theory used and the model approach is presented in Section 8.2. The verification and validation process of the model is discussed and presented in Section 8.3. Finally, the outcome of the model is discussed shortly in Section 8.4.

8.1. Assumptions

This section lists the assumptions that were made including an explanation of their possible impact on the results.

AS-STAB-01 *The stick-free neutral point is assumed to lie 5% MAC, ahead of the stick-fixed neutral point*
A conventional elevator tends to float trailing edge up with increasing angle of attack. Therefore the aircraft is less stable than if the elevator is fixed and the stick-free neutral point should be expected more forward than the stick-fixed one [55].

AS-STAB-02 *The mass per person is 86 kg. The cargo mass is 25 kg per person, which is stored in the cargo hold*
These are the guideline values for the average masses of the payload as prescribed by EASA [42].

AS-STAB-03 *A 2% MAC margin is applied to the most forward and most aft centre of gravity location.*
This is done to account for small variations in the loading of the aircraft.

AS-STAB-04 *The applied Stability Margin (S.M.) is 5% MAC*
This is the minimum required margin as stated in [85].

AS-STAB-05 *The effective tail and rudder area is reduced by 40% at an angles of attack range of 40-50 °*
Due to the placement of the horizontal tail the vertical tail and hence the rudder will partly be located in the downwash originating from the horizontal tail. As a result of this the rudder effectiveness will be decreased at these angles of attack [55].

AS-STAB-06 *The maximum control surface deflection during flight is 75% of the maximum deflection on the ground*
The aerodynamic loading will stretch cables and deteriorate the performance of the control system. As a result maximum control surface deflection will be limited during flight when compared to on-ground maximum deflection [55].

AS-STAB-07 *The elevator area is proportional to the elevator chord to horizontal tail chord ratio*
Since the elevator stretches along the entire horizontal tail plane and therefore takes

up a large part of the overall horizontal tail surface the surface area distribution could be described by the elevator chord to horizontal tail chord ratio.

AS-STAB-08 *When the vertical tail span equals the rudder span, the rudder area is assumed to be proportional to the rudder chord to vertical tail chord ratio*
For the same reason as mentioned in **AS-STAB-07** the rudder surface mainly relies on the rudder chord to vertical tail chord ratio. However, when the rudder span does not equals the vertical tail span and therefore not stretches along the entire vertical tail, this assumption should be revised by implementing **AS-STAB-08**

AS-STAB-09 *If the rudder span does does not coincide with the vertical tail span, the rudder area is assumed to be proportional to the rudder span to vertical tail span ratio*
This assumption implies that when the rudder span is greater or smaller than the vertical tail span, the rudder area should then be determined by multiplying the rudder area which stretches along the entire vertical with the rudder span to vertical span ratio.

8.2. Theory and model approach

This section provides the theory behind the models that determine the stability and control characteristics of the aircraft. The determination of these characteristics consist of the establishment of the the tail size, the possible centre of gravity locations, the control surfaces size and location, the longitudinal stability and at last the dynamic stability.

8.2.1. Horizontal tail size & wing placement

The horizontal tail is essential for longitudinal stability; therefore it has to be sized appropriately so it can fulfil its job in all scenarios. The surface size of the horizontal tail is dependent on the most forward and most aft centre of gravity location, therefore these locations were determined for different loading situations by setting up multiple loading diagrams. To minimise the horizontal tail drag it is desired to have a configuration of the wing and horizontal tail that minimises the horizontal tail size while still providing controllability and stability. Accordingly, the loading diagrams were generated for different locations of the wing. From these loading diagrams the optimum value of (S_h/S), that hence corresponds to a specific wing location, has been obtained from the stability and controllability curves in the scissor plot. The centre of gravity limits to ensure this controllability and stability were calculated using Equations (8.1) and (8.2) respectively.

$$\bar{x}_{cg} = \bar{x}_{ac} - \frac{C_{m_{ac}}}{C_{L_{A-h}}} + \frac{C_{L_h}}{C_{L_{A-h}}} \frac{S_h l_h}{S\bar{c}} \left(\frac{V_h}{V}\right)^2 \tag{8.1}$$

$$\bar{x}_{cg} = \bar{x}_{ac} - \frac{C_{L\alpha_h}}{C_{L\alpha_{A-h}}} \left(1 - \frac{d\epsilon}{d\alpha}\right) \frac{S_h l_h}{S\bar{c}} \left(\frac{V_h}{V}\right)^2 - S.M. \tag{8.2}$$

Hence, Equation (8.2) specifies the horizontal tail size that provides stability with the centre of gravity in most aft position. More specifically, the size of the horizontal tail is established such that the centre of gravity lies in front of the neutral point to maintain stability. The controllability line however, defines the most forward location of the centre of gravity at which the tail control for.

8.2.2. Control surfaces sizing

The sizing and placement of the control surfaces are directly influencing the controllability and manoeuvrability of the aircraft. Therefore, it is essential that the design of these surfaces is compatible with the mission requirements. The design approach that follows from these requirements is described for each control surface individually below:

Ailerons System requirement **REQ-SYS-03** states that the aircraft shall have a minimum roll rate of 180 degrees per second. From this requirement, the location and size of the two ailerons on the main wing can be determined. According to [55], the roll rate for a straight tapered wing can be obtained using Equation (8.3).

$$p = -\frac{48Sc_{l_{\delta_\alpha}}C_R V}{(c_{l_a} + c_{d_0})C_R b^3}\left[(b_2^2 - b_1^2) + \frac{4(\lambda - 1)}{3b}(b_2^3 - b_1^3)\right]\delta_{\alpha_{max}} \tag{8.3}$$

Assuming that the outer part of the aileron (b_2) is located at 95% of half the wing span, the aileron size can be determined by iterating upon the inner location (b_1) until the configuration meets the desired roll rate. Note that the $c_{l_{\delta_\alpha}}$, c_{d_0} values are obtained from [55] and that the c_{l_a} is defined by the DATCOM method [85].

Rudder The most critical flight condition for the sizing of the rudder, especially for an aerobatic aircraft, is the spin recovery condition since the rudder is the most significant element to stop the rotation. CS-23 states that a GA (aerobatic) aircraft must be able to recover from a one-turn spin, in not more than three seconds. From this yaw rate, the rudder can be sized by using equation Equation (8.4)[88] and iterating on the b_R/b_v ratio until the required restoring moment, initiated by maximum rudder deflection, is reached. Based on this ratio the rudder area can be determined according to **AS-STAB-08** and **AS-STAB-09**.

$$\delta_R = \frac{-\left(\frac{I_{xx}I_{zz} - I_{xz}^2}{I_{xx}}\right)_w \cdot \dot{N}_R}{\rho V_s^2 S b C_{L_{\alpha_v}} V_{VT} \tau \frac{b_R}{b_v}} \tag{8.4}$$

Note that the moment of inertia's that are used in this equation are in the aerodynamic reference frame at high angle of attack of 40 ° [88] and that $\dot{N}_R$ is the recovery roll rate stated by CS-23.

Elevator The design of the elevator strongly depends on its effectiveness. Based on the elevator chord to horizontal tail chord ratio (C_e/C_{ht}) the desired effectiveness (τ) of the elevator can be obtained using the statistic relation described in Equation (8.5) [55]. In addition to that, the (C_e/C_{ht}) ratio also describes the surface area of the elevator as mentioned in assumption **AS-STAB-07**. However, the most essential coefficient in determining whether the elevator is effective in longitudinal stability is the elevator efficiency $C_{m_{\delta_e}}$ presented in Equation (8.6).

$$\tau = -4.66\left(\frac{C_e}{C_{ht}}\right)^4 + 8.79\left(\frac{C_e}{C_{ht}}\right)^3 - 6.44\left(\frac{C_e}{C_{ht}}\right)^2 + 2.85\left(\frac{C_e}{C_{ht}}\right) + 0.0316 \tag{8.5}$$

$$C_{m_{\delta_e}} = \left(\frac{V_h}{V}\right)^2 \frac{S_h}{S}\left(\frac{X_{cg} - X_{AC_w}}{\bar{c}} + \frac{S_h l_h}{S\bar{c}}\right) C_{L_{\alpha_h}} \tau \tag{8.6}$$

Hence, dependent on the longitudinal stability characteristics of the aircraft, the elevator can be sized by changing the (C_e/C_{ht}) in such a way that the elevator can trim the aircraft at different airspeed while still being controllable. It is therefore desired to have elevator trim stability as described in Equation (8.7).

$$\frac{d\delta_e}{dV} = \frac{4W}{\rho V^3 S}\frac{1}{C_{m_{\delta_e}}}\frac{X_{cg} - X_{n_{fix}}}{\bar{c}} > 0 \tag{8.7}$$

It should be evident that this elevator trim stability is concerned with the condition that the is elevator in a fixed position. Due to encountered difficulty in relating the elevator geometry with the hinge moment coefficients it is assumed that the stick-free neutral point lies 5% MAC, ahead of the stick-fixed neutral point, as stated in assumption **AS-STAB-01**. Therefore the control system will be designed in such a way that the control forces are corresponding to this location by installing springs and mechanisms or a elevator control horn. As a result, the control forces should be within the limits described by CS-23.

8.2.3. Longitudinal stability

The longitudinal static stability is concerned with the aircraft's stability in the longitudinal plane under steady flight conditions. For the stability of a conventional aircraft it essential that the centre of gravity is located in front of this neutral point to maintain static stability. As already described in Section 8.2.1, the tail is sized such that this stability condition is met. However, for handling qualities it is still important to define the neutral point at which the elevator deflection is zero, or the stick fixed neutral point

(Equation (8.8)). The stick-free stability is assumed to follow from the stick-fixed neutral point according to assumption **AS-STAB-01**.

$$X_{n_{fix}} = \frac{C_{L\alpha_h}}{C_{L\alpha_{A-h}}}\left(1 - \frac{d\epsilon}{d\alpha}\right)\left(\frac{V_h}{V}\right)^2 \frac{S_h l_h}{\bar{c}} + X_{AC_w} \tag{8.8}$$

Aerobatic handling qualities The longitudinal static stability and manoeuvrability of the aircraft is significantly influenced by the moment arm between the centre of gravity and the neutral point. Reducing this moment by locating the centre of gravity closer in front of the neutral point, results in improved longitudinal control. Since the aircraft should be able to perform aerobatic manoeuvres, a specific payload configuration should be defined that decreases the arm distance between the cg and the neutral point which consequently increases the aircraft's handling qualities. However, placing the centre of gravity to close to the neutral point, makes the aircraft less stable. Therefore it of importance to strictly use the stability margin of 5% of the MAC as described in **AS-STAB-04**. Another point of interest for aerobatic aircraft is the elevator control characteristics during a pull up manoeuvres to determine the handling qualities at different loading conditions. This can be done by specifying the stick-fixed manoeuvre margin as presented in Equation (8.9) at different gravity location [51].

$$\frac{d\delta_e}{dn} = \frac{-1}{C_{m_{\delta_e}}} \frac{2W}{\rho V^2 S}\left(\frac{C_{m_q}}{2\mu} + \frac{X - X_{n_{fix}}}{\bar{c}}\right) \tag{8.9}$$

Where C_{m_q} follows from Equation (8.10) according to [62]

$$C_{m_q} = -1.1 C_{L_h} \frac{S_h l_h^2}{S\bar{c}^2} \tag{8.10}$$

Pitching moment versus angle of attack For longitudinal stability the partial derivative of pitching moment with respect to changes in a angle of attack should be negative to be able to restore from a disturbance in angle of attack. This stability criteria can be visualised by constructing a $C_m - \alpha$ curve using Equation (8.11) [62].

$$C_m = C_{m_0} + C_{L\alpha_{A-h}}(\alpha + \alpha_0)\left(\frac{X_{cg} - X_w}{\bar{c}}\right) - C_{L\alpha_h}(\alpha_0 + \alpha + i_h)\left(\frac{V_h}{V}\right)^2 \frac{S_h l_h}{S\bar{c}} \tag{8.11}$$

From this curve the required incidence angle of the horizontal tail plane can be determined such that the $C_{m_0} > 0$ condition is met. This condition is desired for take off rotation and trim capabilities at cruise with an angle of attack range of 2 to 8 °

8.2.4. Dynamic stability

The dynamic stability is concerned with both the longitudinal and lateral stability of the aircraft as a response to control surface input. For the longitudinal and lateral responses the equations motions are linearized for the symmetric and asymmetric motions respectively to create a state space model [62]. From the aerodynamics model, the stability derivative's that are required for the construction of this state space model are implemented to consequently obtain the stability characteristics by analysing plots and eigenvalues (shown in Equation (8.12)).

$$\lambda = \xi + j\eta \tag{8.12}$$

For the symmetric analysis a input on the elevator or a disturbance in angle of attack results into a short period and a phugoid motion. For the asymmetric motion. a aileron input or roll angle disturbance will result into a aperiodic roll while a rudder input or slide slip angle disturbance induces a dutch roll. Another aperiodic motion is the spiral motion which is initiated by an initial roll angle. To determine whether the aircraft is stable for these latter motions, the damping ratio (ζ), time to damp half the amplitude ($T_{\frac{1}{2}}$), neutral frequency (ω_n) and oscillation frequency (ω_0) can be deduced and analysed from the eigenvalues according to Equations (8.13) to (8.16) respectively.

$$T_{\frac{1}{2}} = -\frac{0.693}{\xi}\frac{\bar{c}}{V} \quad (8.13) \qquad \zeta = \frac{-\xi}{\sqrt{\xi^2+\eta^2}} \quad (8.14)$$

$$\omega_0 = \sqrt{\xi^2+\eta^2}\frac{V}{\bar{c}} \quad (8.15) \qquad \omega_n = \omega_0\sqrt{1-\zeta^2} \quad (8.16)$$

Note that these equations are relevant for the symmetric motions and that the $\bar{c}/V$ should be replaced by $\bar{b}/V$ to make them applicable for asymmetric motions. For dynamic stability purposes it is necessary that the real part (η) of the eigenvalue (Equation (8.12)) is negative to have a convergent response motion. This is relevant for the short period, phugoid and dutch roll motions since it is expected that for a conventional aircraft the dominant motion will be periodic. For the aperiodic roll however, the eigenvalue is expected to be real and negative. The damping of this motion is probably caused by the wing rotating about the longitudinal axis. A further discussion on the stability criteria with respect to the parameters described by the latter equation will be given in Section 8.2.4

8.3. Verification & Validation

This section describes the procedure that has been taken to verify the models and outlines the required validation process for future development. The elaboration on the verification and validation are subdivided between the first two subsections respectively.

8.3.1. Verification

In order to determine whether there are errors in the models, all models were verified by using the same input values and comparing the output values, which are obtained from a reliable source, with the outcome of the model. For the horizontal tail size and the wing placement, input and output values from the ADSEE course [100] where used as a reliable source to verify that the model did not contained any errors.

In case of the aileron and rudder sizing, the model described in the book [55] used examples to clarify the steps that were involved in constructing the model. By consistently following these steps with the input values as described in the book, the model has been tested, compared and hence verified. However, for the elevator sizing, no clear model was available for verification. Therefore the three models; elevator effectiveness model, elevator trim stability model and the stick-fixed manoeuvre model, were verified individually by using unit and system tests. To determine whether the results of these tests where within a reasonable range, the input parameters of the Cessna Citation 550 II where used to specify if they were acceptable. Since the longitudinal stability characteristics of the Cessna Citation where known from the 'Simulation, Verification and Validation' aerospace bachelor course, it was possible to verify these models.

Also for the verification of the dynamic stability analysis, the Cessna Citation was used as a reference aircraft. From the 'Simulation, Verification and Validation' Aerospace Bachelor course, the symmetric and asymmetric state space matrices can be used since they have been verified for this aircraft correctly [98]. However, although the model was correct, it turned out that the moment of inertia's and stability derivatives from the aerodynamic and structure department where not sufficient and forced the state space response model to go to infinity. Therefore it has been chosen to use the XFLR5 software instead, to determine the eigenvalues of the symmetric and asymmetric motions.

8.3.2. Validation

For the validation procedure, the results should be compared to test data. Since the stability and control is concerned with the behaviour of the entire aircraft, this test data could only be gathered by performing actual flight tests. However, it could be possible, to obtain the hinge moment coefficient by isolating the control system from the aircraft and determine the required springs and actuators to validate that the control forces are within the specified limits of CS23. The hinge moment coefficients, can consequently be obtained by setting up a experiment in a windtunnel.

8.4. Outcome

As described in the previous sections, the outcome of the stability and control model describes the weight distribution of the payload and its corresponding loading diagram. Note that this loading diagram is based upon centre of gravity location of OEW at which the horizontal tail size is minimised. This minimisation is visualised in the scissor plot where the most forward and most aft centre of gravity location as a function of the leading edge of the wing, is plotted along a second vertical axis. From this diagram the optimum (S_h/S) and its corresponding centre of gravity range can be obtained.

Based upon this diagram, the location of the stick fixed and stick free neutral point with respect to the centre of gravity range can be visualised. By plotting the stick fixed manoeuvre margin along this centre of gravity axis, the elevator deflection due to an increase in load factor could be visualised at different altitudes. This diagram can be used to optimise the payload configuration for aerobatic purposes. Besides, the required elevator deflection as a function of airspeed is presented for different centre of gravity locations. From this plot, the elevator trim stability and its effectiveness can be obtained. In addition to that, the effectiveness of the elevator is presented in a C_m/α curve for the most forward and most aft location of centre of gravity. Accordingly the size and position of the control surfaces are obtained

As described in Section 8.3, the XFLR5 model was eventually used for the determination of the dynamic stability characteristics. From this model the eigenvalues for the motions and consequently its corresponding parameters as described in Section 8.2.4 could be obtained.

9 Performance

This chapter presents the performance model that was set up and used for the design of the aircraft. First the chapter will outline the assumptions that were made to be able to set-up the model as well as the reason behind them and their possible consequences in Section 9.1. Secondly, the fundamental theory used and the model approach is presented in Section 9.2. The verification and validation process of the model is discussed and presented in Section 9.3. Finally, the outcome of the model is discussed shortly in Section 9.4.

9.1. Assumptions

The assumptions made for the performance model are listed below.

AS-PERF-01 *Take-off and landing are performed at sea level*
It is assumed that the take-off and landing distance would be determined at sea level with respect to fulfilling the take-off an landing distance requirements (**REQ-MIS-08** & **REQ-MIS-09**). The altitude naturally influences the atmospheric properties. At a higher altitude the lower air density limits the power that can be generated by the engine. Also, the take-off and landing speeds need to be higher in order to compensate for the lower air density to obtain the required lift. This results in a longer take-off distance as it takes longer to get to the required lift-off speed. It also results in a longer landing distance because the approach speed needs to be higher to obtain the necessary lift. Even though the requirements are only applicable to the take-off and landing distance at sea level, the distances are also calculated for these manoeuvres at different altitudes in case an airstrip in the mountains is used.

AS-PERF-02 *Take-off and landing are performed on a flat runway*
For simplification purposes it is assumed that take-off and landing will be performed on a flat runway. A runway with a slope causes the weight vector of the aircraft to not be orthogonal to the ground. As a result a component of the weight vector works perpendicular to the direction of the moving aircraft, either slowing it down or accelerating it depending on the slope angle. This either elongates or shortens the take-off or landing distance.

AS-PERF-03 *Take-off and landing distances are evaluated for dry asphalt or concrete surfaces*
The take-off and landing distances mission requirements (**REQ-MIS-08** & **REQ-MIS-09**) state that the aircraft should be able to take-off and land within a 500 m distance. It was established that compliance with these requirements is evaluated for dry asphalt or concrete surfaces. Mission requirement **REQ-MIS-06** states that the aircraft should be able to take-off and land on grass runways and therefore the landing and take-off distances are also determined for runways with different surface types. Since dry asphalt or concrete surface is the most optimal to land on a runway made out of a different material will cause an increase in the take-off and landing distances.

AS-PERF-04 *Climb rate is evaluated at sea level*
System requirement **REQ-SYS-04** states that the minimum climb rate shall be 15 m s^{-1}. This climb rate value was established to accommodate for aerobatic capabilities. Usually these aerobatic manoeuvres are performed at low altitudes where the public is able to see them well. Therefore the climb rate is evaluated at sea level. Since the power available becomes less with increasing altitude the maximum climb rate decreases as well with altitude. This means that at higher altitudes the climb rate will drop.

AS-PERF-05 *Climb rate is evaluated at an aerobatic payload mass of 172 kg*
System requirement **REQ-SYS-04** states the minimum climb rate should be at least 15 m s^{-1}. However, this requirement was established to accommodate aerobatic flying. Therefore climb rate is evaluated using an aerobatic payload mass rather than the full design payload. It is established that when the aircraft is going to be used for aerobatics only two people and no luggage will be taken on as payload. This means that the aerobatic payload mass is 172 kg instead of the design payload mass of 444 kg. As a consequence the total mass during aerobatic manoeuvres is lower than the MTOW, which results in a higher climb rate.

AS-PERF-06 *Service ceiling equals 25000 ft*
The service ceiling of the aircraft is assumed to be 25000 ft. This altitude follows from two considerations. The first consideration was the fact that the Reduced Vertical Separation Minimum (RSVM) changes from 2000 ft to 1000 ft between FL290 (29000 ft) and FL410 (41000 ft) [89]. In order to be allowed to fly in this airspace the aircraft should include specifically certified altimeters and autopilot systems. Since mission requirement **REQ-MIS-13** states that the required cruise altitude should be at least 18000 ft, far below 29000 ft, it is deemed unnecessary to accommodate and certify the aircraft to fly above 29000 ft. When uncertified for this altitude, the aircraft is only allowed to go up to 28000 ft. The second consideration is that flying above 25000 ft with a pressurised cabin puts additional constraints and requirements on the cabin and pressurisation system and it has to be specifically certified to fly above this altitude as is outlined in CS-23 [61]. Since the extra 3000 ft do not give a significant performance increase at such a high altitude, it was deemed to be unnecessary to certify the aircraft to fly above this altitude.

AS-PERF-07 *Fuel fractions for flight phases other than the cruise and loiter phases are taken from literature*
When compared to the cruise and loiter phases, these flight phases (start, taxi, take-off, climb, descent & landing) are relatively short. They also largely depend on the flying style and the actual flight path; hence, an elaborate analysis would not give an accurate representation of reality. Therefore the fuel fractions were assumed to be constant and are taken from literature for comparable aircraft [100].

AS-PERF-08 *Approach angle (θ_{app}) is 3°*
The approach angle, which is used for calculating the approach distance while landing, is assumed to be 3°. This value was taken because both the T-Visual Approach Slope Indicator System (T-VASIS) and the Precision Approach Path Indicator (PAPI), two systems that are used to assist the pilot during the approach, use three degrees as the standard slope[68]. The three degree slope follows from IFR flight path criteria, and the approach indicator systems are set accordingly[59]. Since the systems are adapted to this angle, it is ideal if the aircraft is sized for this angle so the pilot can easily coordinate the landing manoeuvre.

AS-PERF-09 *Loiter phase duration is 45 minutes*
The loiter is a required part of the IFR fuel load [42, CS 23.25].

AS-PERF-10 *The Ivchenko Motor Sich AI-450C turboprop engine is used*
The engine was chosen based on its decent fuel consumption and power. The fuel consumption is similar the the Garrett TPE331, but this engine is newer. It has a single stage compressor and turbine combined with a single stage free power turbine. [20]

9.2. Theory and model approach

The performance model was divided into the propulsion system and the flight phases, which were analysed separately. The first will analyse the propeller in combination with the selected engine, mainly to calculate the power available, and the latter will analyse the performance of the aircraft using this available power. The theory used to write the model functions is stated below.

9.2.1. Propulsion System

The propulsion system was analysed by means of blade element theory (BET) and Rankine-Froude momentum theory. All theories and formulas are taken from [55, 87]. The BET and momentum theory is used to calculate the thrust and power needed to turn the propeller. This results in a propeller efficiency (η_p) which can be used in the models of the different flight phases.

Model The blade element theory relies on sectioning a blade and calculating the aerodynamic characteristics of each section separately. Each section or element has a certain airfoil with the associated aerodynamic properties. These properties are calculated using an airfoil analysis program like XFoil. The lift and drag coefficients are used to calculate elemental lift and drag forces as shown in Equations (9.1) and (9.2).

$$dL = c_l \frac{1}{2} \rho V^2 c \, dr \qquad (9.1) \qquad dD = c_d \frac{1}{2} \rho V^2 c \, dr \qquad (9.2)$$

These forces have to be transformed to thrust and torque vectors. First the forces are converted to a tangential force dK and a normal force dT with respect to the propeller disk. This is shown in Figure 9.1. With torque equalling force times distance the differential torque dQ can be calculated easily. From Figure 9.1 one gets Equations (9.3) to (9.5) to calculate dT, dK and dQ:

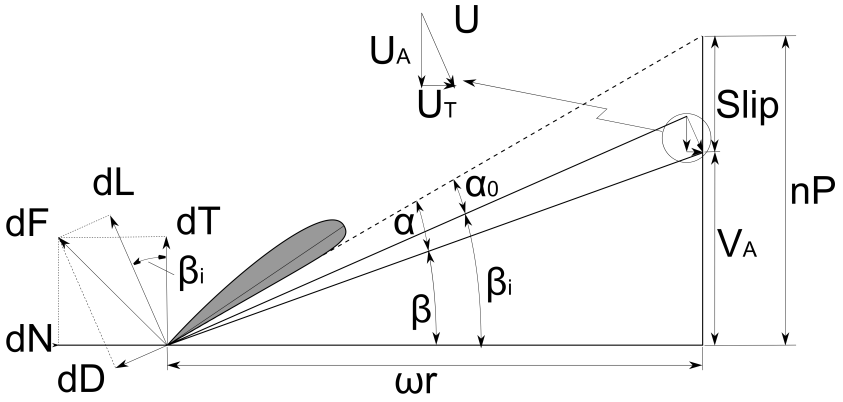

Figure 9.1: A blade element with angles [28]

$$dT = dL \cos\phi - dD \sin\phi \quad (9.3) \qquad dK = dL \sin\phi + dD \cos\phi \quad (9.4)$$

$$dQ = r \, dK \qquad (9.5)$$

Integration yields Equations (9.6) and (9.7), here N_b is the number of propeller blades and H is the hub radius.

$$T = N_b \int_H^R dT \qquad (9.6) \qquad Q = N_b \int_H^R dQ = N_b \int_H^R r \, dK \qquad (9.7)$$

The power needed to turn the propeller is given by the rotational equivalent of $P = FV$, as shown in Equation (9.8).

$$P = Q \, \omega \qquad (9.8)$$

Induced angle of attack 'Pure' BET does not account for the induced velocity seen in Figure 9.1. Rankine-Froude momentum theory does, so this was incorporated in the model. Skipping the derivation and using the Newton–Raphson method, one ends up at the recursive scheme as shown in Equation (9.9) [101].

$$w_n = w_{n-1} - \frac{f(w_{n-1})}{f'(w_{n-1})} \tag{9.9}$$

Here f and f' are defined in Equations (9.10) and (9.11)

$$f(w) = \frac{8\pi r}{N_b c} w - \frac{V_E}{(V_0 + w)}[C_l(\omega r) - C_d(w + V_0)] \tag{9.10}$$

$$f'(w) = \frac{8\pi r}{N_b c} - C_l(\omega r)\left(\frac{1}{V_E} - \frac{V_E}{(V_0 + w)^2}\right) + C_d \frac{(w + V_0)}{V_E} \tag{9.11}$$

This scheme is executed until the difference between w_n and w_{n+1} is smaller than a set value, which in this case is set to 0.001. Then the induced angle of attack α_i is defined as in Equation (9.12). This induced angle of attack is used to calculate the total angle of attack as shown in Equation (9.13).

$$\tan(\alpha_i) = \frac{w}{V_E} \Leftrightarrow \alpha_i = \arctan\left(\frac{w}{V_E}\right) \tag{9.12}$$

$$\alpha = \beta - \phi - \alpha_i \tag{9.13}$$

The full derivation can be found in [55, Chapter 14]

Correction factors The blade element theory does not account for hub and tip losses, nor does the XFoil analysis account for Mach effects and wave drag.
In reality, the lift coefficient at the end of a lifting surface goes to zero. The BET ignores this and as such the resulting thrust is more than in reality, thereby rendering the analysis invalid. Ludwig Prandtl realised this and developed hub and tip correction factors that are easily incorporated in the model. The tip correction parameter is defined in Equation (9.14) and the hub correction parameter is presented in Equation (9.15).

$$P_{tip} = \frac{N_b}{2} \frac{R - r}{r \sin\phi} \tag{9.14}$$

$$P_{hub} = \frac{N_b}{2} \frac{r - R_{hub}}{r \sin\phi} \tag{9.15}$$

The resulting parameters are then inserted in Equations (9.16) and (9.17) to obtain the tip and hub correction factors.

$$F_{tip} = \frac{2}{\pi} \arccos\left(e^{-P_{tip}}\right) \tag{9.16}$$

$$F_{hub} = \frac{2}{\pi} \arccos\left(e^{-P_{hub}}\right) \tag{9.17}$$

The total correction factor F_p is obtained by multiplying the two correction factors. This factor can be included in Equations (9.6) and (9.7) to arrive at the final equations for thrust and torque, Equations (9.18) and (9.19).

$$T = N_b \int_H^R F_p \, dT \tag{9.18}$$

$$Q = N_b \int_H^R dQ = N_b \int_H^R r F_p \, dK \tag{9.19}$$

This leaves the Mach effects and wave drag to be accounted for. For the first the lift coefficient is corrected using the Prandt-Glauert correction, as shown in Equation (9.20). Here C_{L_0} is the lift coefficient at low Mach numbers and M the Mach number itself. Drag is more difficult to account for as aerodynamic drag is composed of many different drag sources. The different effects of the Mach number on the different drag components produce a fairly constant drag up until the critical mach number number M_{cr}. Wave drag occurs from the moment the local velocity somewhere on the airfoil exceeds $M = 1$. The wave drag component C_{D_w} is added to the base C_d if the Mach number exceeds the drag divergence number. C_{D_w} is defined as in Equation (9.21).

$$C_L = \frac{C_{L_0}}{\sqrt{1-M^2}} \tag{9.20}$$

$$C_{D_w} = 20(M - M_{cr})^4 \tag{9.21}$$

The main outputs of this model are the propeller efficiency η_p, power required to turn the propeller P_{p_r} and the thrust T.

9.2.2. Flight phases

This section presents the performance model. It is divided into the flight phases, take-off, climb, cruise, descent and landing. Each of these phases has been separately modelled. The theory used to set-up these models and the results that flow from these models are explained for each phase and presented below.

Take-off The take-off performance part is mainly concerned with determining the required take-off distance. This is of special importance because mission requirement **REQ-MIS-08** states that the take-off distance should not exceed 500 m. In order to get a clearly defined result for the take-off distance a number of assumptions were made. These assumptions were listed in Section 9.1.
The total take-off distance is made up out of different phases with their respective distance. Namely the ground roll distance (S_G), rotation distance (S_{ROT}), transition distance (S_{TR}) and climb distance (S_C). Together they add up to the total take-off distance as shown in Equation (9.22).

$$S_{TO} = S_G + S_{ROT} + S_{TR} + S_C \tag{9.22}$$

To determine the ground roll distance the following method was used. The equation of motion for the ground roll part, as seen in Equation (9.23), describes the acceleration as a function of the forces working on the aircraft during take-off. Here μ_g is the ground friction coefficient. The value of this parameter depends on the surface type and the weather condition, the take-off distance is evaluated for various surface types and presented in Section 13.3.3.

$$\frac{dV}{dt} = \frac{g}{W}[T - D - \mu_g(W - L)] \tag{9.23}$$

Using a numerical integration method with a small time step (<1 s), the acceleration, speed, thrust, lift and drag could be determined at every step and added up. Using Python this could be very accurately modelled. The model then checks the time at which the accumulated speed equals the lift-off speed (V_{LOF}) which is defined by Equation (9.24) in which V_{S1} is the stall speed in take-off configuration [55]. When this condition is satisfied the model determines the ground run distance based on the accumulated time, acceleration and speed data determined at every step.

$$V_{LOF} = 1.1 \cdot V_{S1} \tag{9.24}$$

The rotation distance (S_{ROT}) was found to be approximately equal to the value of V_{LOF} since the rotation time for small aircraft is approximately 1 s [55], see Equation (9.25).

$$S_{ROT} = |V_{LOF}| \tag{9.25}$$

The transition distance starts when lift-off occurs and finishes when the climb angle is achieved that should be maintained at least until obstacle height. This distance was calculated using Equation (9.26).

$$S_{TR} \approx 0.2156 \cdot V_{S1} \cdot \left(\frac{T}{W} - \frac{1}{L/D}\right) \tag{9.26}$$

After the transition phase the aircraft is at a certain height $h_{transition}$. The regulations for take-off performance specified in CS-23 determined that the take-off distance is measured until an altitude of 50 ft above the take-off surface is reached [42]. This height is referred to as the obstacle height (h_{obst}). In case the transition height is less than 50 ft above the take-off surface, an extra climb phase and its distance must be added to the total take-off distance. Using the climb angle that is calculated using Equation (9.27) this distance could be calculated using Equation (9.28).

$$\theta_{climb} = \arcsin\left(\frac{T}{W} - \frac{1}{L/D}\right) \quad (9.27) \qquad S_C = \frac{h_{obst} - h_{transition}}{\tan(\theta_{climb})} \quad (9.28)$$

Climb The main importance of the climb performance model is to estimate the climb rate to fulfil system requirement **REQ-SYS-04** that states that the minimum rate of climb (RoC) that the aircraft can achieve should be 15 m s^{-1}. As was already discussed in assumption **AS-PERF-04** the climb rate requirement is assessed at sea level.

Using a simplified drag model, the airspeed for best RoC (V_Y) could be determined using Equation (9.29) [55]. This equation determines the speed at which the excess power is maximum and thus the largest RoC is achievable. The parameter k is determined using Equation (9.30).

$$V_Y = \sqrt{\frac{2}{\rho}\left(\frac{W}{S}\right)\sqrt{\frac{k}{3 \cdot C_{D_{min}}}}} \quad (9.29) \qquad k = \frac{1}{\pi A e} \quad (9.30)$$

Using the resulting airspeed the maximum achievable RoC can be determined with Equation (9.31) [55].

$$RoC_{max} = 60\left(\frac{\eta_p P}{W} - V_Y\left(\frac{1.1547}{(L/D)_{max}}\right)\right) \quad (9.31)$$

As can be observed, both the values for Equation (9.29) and Equation (9.31) will change with altitude due to changing density and changing power. The model that was set up in Python uses the standard atmosphere to model how the speed and RoC change with increasing altitude. Using this it can established at what point the RoC becomes zero and thus at what altitude the absolute ceiling is. It is however not of interest to determine the ceiling above an altitude of 25000 ft as was already established in assumption **AS-PERF-06**. A plot that shows the maximum rate of climb as a function of altitude will be presented in Chapter 13.

Furthermore, the model calculates the time it takes to reach cruise altitude while using the maximum RoC throughout the climb phase. This was done by fitting the curve for RoC versus altitude with a cubic polynomial of the form presented in Equation (9.32) and using the coefficients from this polynomial as an input for Equation (9.33) to determine a representative RoC_a for the entire climb phase [55].

$$Ax^3 + Bx^2 + Cx + D \quad (9.32)$$

$$RoC_a = \frac{A(h_1 - h_0)^3 + B(h_1 - h_0)^2 + C(h_1 - h_0)}{\ln(Ah_1^3 + Bh_1^2 + Ch_1 + D) - \ln(Ah_0^3 + Bh_0^2 + Ch_0 + D)} \quad (9.33)$$

Using this representative RoC the time it takes to achieve to get to cruise altitude can be approximated using Equation (9.34).

$$t_{cruise} = \frac{h_1 - h_0}{RoC_a} \quad (9.34)$$

Even though the climb rate requirement will be evaluated for an aerobatic mass, the climb phase will naturally also be performed with MTOW. In Chapter 13, the climb characteristics for both an aerobatic mass and MTOW will be presented. Furthermore, CS23 states a minimum requirement on the climb gradient when flying with MTOW[42], which was calculated using Equation (9.35)[55], and can be found in Chapter 13 as well.

$$\text{Climb gradient} = \frac{\text{Vertical distance}/\Delta t}{\text{Horizontal distance}/\Delta t} \quad (9.35)$$

Cruise & Range The design range of the aircraft is set at 1400 km, as stated in mission requirement **REQ-MIS-05**. The range is analysed using the Breguet range and endurance equations (9.36 and 9.37 [100]). As stated in assumption **AS-PERF-09** the plane should be able to loiter for 45 minutes after the cruise phase. The fuel fractions for the phases before cruise and after loiter are taken from reference aircraft, as stated in assumption **AS-PERF-07**.

$$R = \left(\frac{\eta_p}{g \cdot c_p}\right)_{\text{cruise}} \left(\frac{L}{D}\right)_{\text{cruise}} \ln\left(\frac{W_4}{W_5}\right) \quad (9.36) \qquad E = \left(\frac{\eta_p}{V \cdot g \cdot c_p}\right)_{\text{loiter}} \left(\frac{L}{D}\right)_{\text{loiter}} \ln\left(\frac{W_8}{W_9}\right) \quad (9.37)$$

To minimise the amount of fuel required for the mission range, the optimal cruise altitude has to be determined. Therefore, the required power to fly at the most efficient airspeed is calculated for different altitudes. Together with the available power and the engine efficiency at those altitudes, the most efficient cruise altitude could be determined. 'Most efficient' is defined as the flying condition with the highest distance covered over fuel burned ratio.

The most efficient cruise speed is found by optimising $\frac{1}{c_p}\frac{L}{D}$. Computing the lift over drag ratio for different air speeds is straightforward. Finding the accompanied specific fuel consumption proved to be more difficult, since the manufacturer of the selected Ivchenko Motor Sich AI-450S turboprop engine, see assumption **AS-PERF-10**, only provides one specific fuel consumption c_p-value for one particular power setting. To get around this, data from the Pratt & Whitney PW127 [14] regarding c_p was interpolated and scaled to fit the Ivchenko. It was found the efficiency of turboprop engines drops significantly when being run at a power setting lower than 50 %. For this reason flying at the highest lift over drag ratio is not always the most efficient. In such cases the speed should be increased until the optimal balance between aerodynamic and propulsive efficiency is found.

Using the lift-drag polar obtained from the aerodynamics model, the power requirements for the most efficient and the specified cruise speed are calculated. Additionally, the maximum speed is determined at the maximum power setting. The range is then analysed for those different air speeds as a function of payload.

Descent The main purpose of the descent performance model is to determine the glide distance in case of engine failure. Since the aircraft is a single engine aircraft this is of particular interest for safety reasons. Section 23.71 of CS-23 states that it is required to determine the maximum horizontal distance travelled in still air and the speed necessary to achieve this with the engine inoperative and the aircraft in the most favourable configuration for gliding [42]. The best gliding speed (V_{BG}) with engine inoperative and the gliding distance are determined with Equation (9.38) and Equation (9.39), respectively. Here k is determined using Equation (9.30). The equations were obtained from "General Aviation Aircraft design" [55].

$$V_{BG} = \sqrt{\frac{2}{\rho}\sqrt{\frac{k}{C_{D_{min}}}}\frac{W}{S}} \quad (9.38) \qquad R_{glide} = h \cdot \left(\frac{L}{D}\right)_{max} \quad (9.39)$$

Since the best gliding speed V_{BG} changes with altitude it will not be presented in the results. However, it will be part of the POH (Pilot Operating Handbook). The mass used for determining the descent performance is the MTOW minus the masses calculated by the fuel fractions up until the cruise phase. The model determines the glide distance from cruise altitude using the standard atmosphere model for the density and using the aerodynamic properties from the aerodynamic model.

Landing Similar to the take-off performance model, the landing performance model is mainly concerned with determining the landing distance in order to fulfil the maximum landing distance of 500 m as specified in mission requirement **REQ-MIS-09**. A number of assumptions were made in order to make a clear assessment of the landing distance. These assumptions and their consequences are

outlined in Section 9.1.

The total landing distance ($S_{landing}$) can be divided into four parts, namely the the approach distance (S_A), flare distance (S_F), free-roll distance (S_{FR}) and braking distance (S_{BR}) as is shown in Equation (9.40). The approach distance is measured from the moment the aircraft goes past the obstacle height (h_{obst}), which is specified in CS-23 as 50 ft above the landing surface [42].

$$S_{landing} = S_A + S_F + S_{FR} + S_{BR} \tag{9.40}$$

To determine the approach distance Equation (9.42) was used, using the approach angle as specified in assumption **AS-PERF-08** [55]. The flare height is calculated by Equation (9.41) in which V_{SO} is the stall speed in landing configuration. During the flare manoeuvre the nose of the aircraft is raised.

$$h_f = 0.1512 \cdot V_{SO}^2 \cdot (1 - \cos(\theta_{app})) \tag{9.41}$$

$$S_A = \frac{h_{obst} - h_f}{\tan(\theta_{app})} \tag{9.42}$$

When flare height is reached the flare manoeuvre is initiated. The distance covered during the flare manoeuvre is calculated using Equation (9.43) [55].

$$S_F = 0.1512 \cdot V_{SO}^2 \cdot \sin(\theta_{app}) \tag{9.43}$$

For the free roll distance it is estimated that small aircraft have approximately one second of free roll until the braking is initiated. This distance is thus calculated by Equation (9.45) [55]. Here V_{TD} is calculated using Equation (9.44), as is specified in CFR 23.73 [60].

$$V_{TD} = 1.1 \cdot V_{SO} \tag{9.44}$$

$$S_{FR} = |V_{TD}| \tag{9.45}$$

After one second of free rolling, the braking phase is initiated. The brake distance is calculated using Equation (9.49) in which the drag is calculated using a drag coefficient as specified by Equation (9.46) and μ_g depicts the ground friction coefficient that depends on the landing surface [55]. The $\Delta C_{D_{flaps}}$ for different flap types is elaborated upon in Section 9.2.3. Similarly to the take-off distance, the landing distance was calculated for several different surface types, all these distances are presented in Section 13.3.3. Furthermore, the landing distance is also calculated using reverse thrust. This distance is not the landing distance that can be used for certification [42] but it is of interest for the pilot since it can significantly reduce the necessary landing distance. The idle and reverse thrust are estimated using Equation (9.47) and Equation (9.48) [55].

$$C_{D_{ldg}} = C_{D_0} + C_{D_{induced}}(@C_{L_{ldg}}) + \Delta C_{D_{flaps}} \tag{9.46}$$

$$T_{idle} = 0.07 \cdot T_{static} \tag{9.47}$$

$$T_{reverse} = -0.6 \cdot T_{static} \tag{9.48}$$

$$S_{BR} = \frac{V_{BR}^2 W}{2g\left[\sqrt{2} \cdot \eta_p \cdot 550 \cdot \frac{P}{V_{BR}} - D_{ldg} - \mu_g(W - L)\right]} \tag{9.49}$$

9.2.3. High-lift device sizing

In order to achieve the minimum take-off and landing distances a sufficiently high wing lift coefficient is required. The wing lift coefficient at clean configuration is not enough to accommodate for this and therefore high-lift devices need to be sized. For high-lift devices plain, split and slotted flaps are considered. The estimated achievable $\Delta C_{l_{max}}$ for these flap types is shown in Table 9.1.

Table 9.1: Estimated achievable $\Delta C_{l_{max}}$ for three types of high lift devices [100]

High lift device	$\Delta C_{l_{max}}$ when fully deployed
Plain and split	0.9
Slotted	1.3

To calculate the increase in wing lift coefficient as a result from using one of these flap systems Equation (9.50) is used [29]. Here S_{wf} is the reference wing flapped surface and $\Lambda_{hingeline}$ is the sweep angle of the hinge line for the flap system. It should be noted that this is the increase in lift coefficient when the flaps are fully deployed, as they will be during landing. For take-off, 80 % of this value is used to limit drag [29].

$$\Delta C_{L_{max}} = 0.9 \cdot \left(\frac{S_{wf}}{S}\right) \cdot \Delta C_{l_{max}} \cdot \cos(\Lambda_{hingeline}) \tag{9.50}$$

The increase in drag due to the flaps is taken from a table provided in "General Aviation Aircraft design", reproduced here in Table 9.2 for clarity [55]. Note that this table was established with the assumption of the flaps covering 60% of the wingspan and 25% of the chord. The resulting drag values are used to determine the total drag coefficient in landing configuration.

Table 9.2: Flap induced drag coefficients for different flap types and deflections [55]

Flap type	**Reference deflection, δ_f**	$\Delta C_{D_{flaps}}$
Split or plain flap	30°	0.05
	50°	0.10
Slotted flap	30°	0.02
	50°	0.05

9.3. Verification & Validation

This section gives an overview of the verification procedures that were taken to verify the models and presents the outline for the validation methods that are to be performed in the future.

Verification For verification unit tests and system tests were applied to each element of the model. Since the model is structured in the form of functions this could be done very efficiently. The unit tests consisted of testing the individual functions. Smaller functions were combined in larger functions in order to perform more complex calculations that required several inputs. These output values were verified as a part of the system test. The main method of verification was making simplified calculations on paper and comparing the model results with these. Additional methods included varying the input for the functions in order to make sure results still made sense.

For the model setup of the climb, descent, landing and take-off performance, methods from the book "General Aviation Aircraft design" were used [55]. This book provides extensive methods as well as worked-out examples, mostly performed based on data from the Cirrus SR-22. To verify the four model elements the example data was used and it was found that all models produced the same results as shown in the book.

Validation To validate the models, the results should be compared to test data. For the performance models this is only possible by flight test. This is because the performance model relies on a vast amount of aircraft parameters that work together to provide the performance output. It is therefore impossible to isolate a certain part of the performance and validate it, as every single aircraft part has a contribution to overall lift and drag during the flight, so isolated testing results would be meaningless. One part that could be considered separate, the propulsion system, did not produce any credible results. The obtained efficiency values were way too high (92% - 95%, where the maximum lies around 90%) and the calculated power required to rotate the prop was higher at 50 m s^{-1} than at 100 m s^{-1}. Therefore it was decided not to include it in the performance model. There could be different reasons for that; one possibility is that the compressibility effects aren't calculated properly for the airfoil sections. XFoil cannot do it due to the method it uses and the corrections applied are not the most accurate so the drag estimation might be lower than in real life. This might explain the higher efficiency and the higher power at 50 m s^{-1}. Another possibility could be that the induced angle of attack calculations were off.

9.4. Outcome

An overview of the output parameters resulting from the performance model is shown in Table 9.3. For the prop efficiency an assumption was made based on literature on reference aircraft [55].

Table 9.3: Outputs that follow from the performance model

Output	Unit	Output from	Output	Unit	Output from
S_{TO}	m	Take-off performance	V_{cruise}	m/s	Cruise & Range
$V_{stall_{@TO}}$	m/s	Take-off performance	$V_{efficient}$	m/s	Cruise & Range
$RoC_{sealevel}$	m/s	Climb performance	V_{max}	m/s	Cruise & Range
R_{glide}	km	Descent performance	R_{ferry}	km	Cruise & Range
$S_{landing}$	m	Landing performance	R_{MTOW}	km	Cruise & Range
$V_{stall_{@landing}}$	m/s	Landing performance	h_{cruise}	ft	Cruise & Range
$CL_{max_{TO}}$	-	High lift device sizing	SFC	kg/hp/hr	Propulsion
$CL_{max_{landing}}$	-	High lift device sizing	P	SHP	Propulsion

10

Aerodynamic characteristics

Previous chapters have outlined methodology behind the models, used to analyse and improve the system performance of the aircraft. The following chapters, starting with this one, are going to introduce the outcomes of iteration between those models.
This chapter shows the aerodynamic characteristics of the design. First the airfoil used for the lifting surfaces is shown in Section 10.1, subsequently the aerodynamic polars are presented in Section 10.2 and finally in Section 10.3 the lift and drag distribution during cruise conditions are given.

10.1. Airfoil

The airfoil is a custom airfoil created in the 2D inverse design environment of XFLR5 for a design lift coefficient of 0.5. It has a focus on laminar airflow over a large portion of the surface. The expected Reynolds number during cruise allows for the large section of the flow over the airfoil to remain laminar by using a favourable pressure gradient. In addition, care has been taken to ensure that the airfoil is not only optimised for this particular point. Both off-design drag and maximum lift have been taken into consideration during this process. The shape of the airfoil is presented in Figure 10.1 and the 2-dimensional drag polar for the airfoil is presented in Figure 10.2 for a Reynolds number of 5 000 000. This Reynolds number is representative for the wing during cruise. The drag bucket around a C_L of 0.5 is clearly visible.

10.2. Aerodynamic polars

This section shows various aerodynamic polars: Figures 10.3 and 10.4 show the C_L-α polar and C_D-α polar, respectively. Figure 10.5 shows the C_L-C_D polar and Figure 10.6 shows the C_m-α polar. Since the VLM uses flat panels there is an angle of attack for which the camberline is perpendicular to the incoming flow, resulting in zero lift, and drag. From the lift and drag polars it can be seen that this angle equals -2 degrees. In the real world zero drag is of course impossible, so both Figure 10.4, and Figure 10.5 will shift in a real application of this mesh. The lift polar shows no value for CL_{max}, this is due to the fact that the VLM method does not account for flow separation and thus will never peak out.

10.3. Lift and drag distribution

This section shows the lift and drag distributions during cruise conditions. The lift distribution is shown in Figure 10.7 and the drag distribution is shown in Figure 10.8. Please note that due to the way Python plots these graphs, the drag distribution is filled up in the middle to make it a smooth surface; looking past this however shows the actual drag distribution. Both the lift and drag distribution show expected results with high lift and thus drag over the wing and low amounts over the gap of the fuselage and the tailplane.

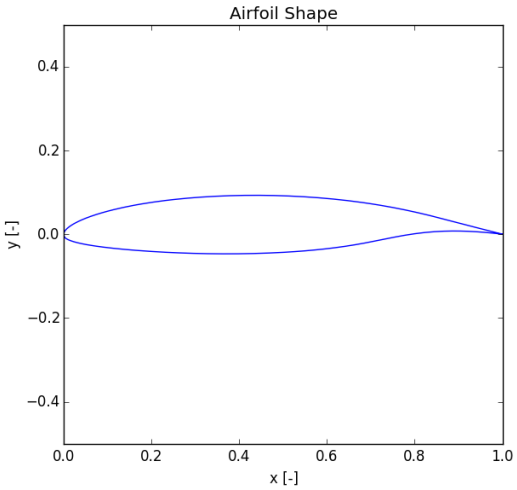

Figure 10.1: Airfoil Shape

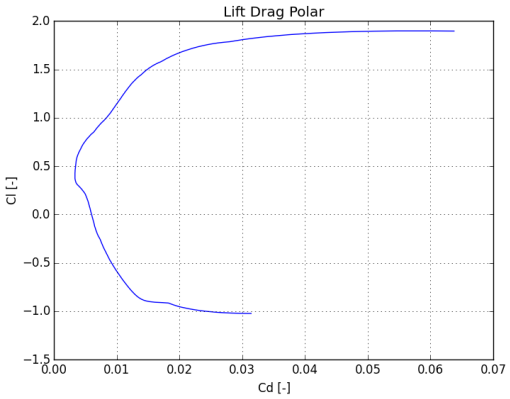

Figure 10.2: Drag polar for 2D foil at Reynolds number 5,000,000

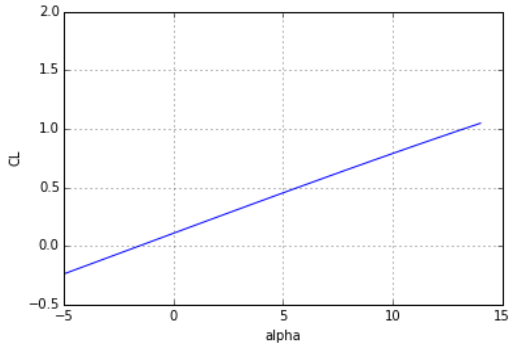

Figure 10.3: C_L-α graph

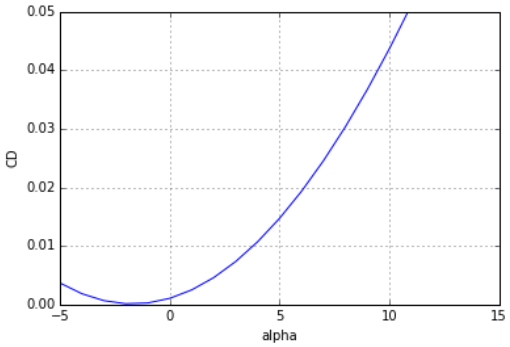

Figure 10.4: C_D-α graph

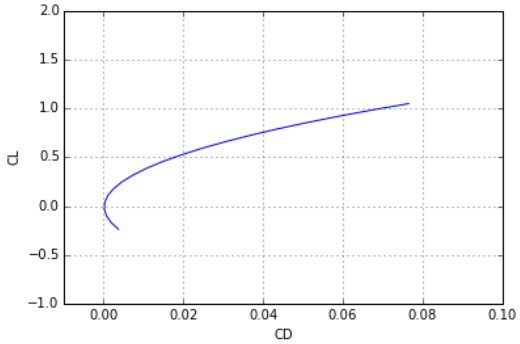

Figure 10.5: C_L-C_D graph

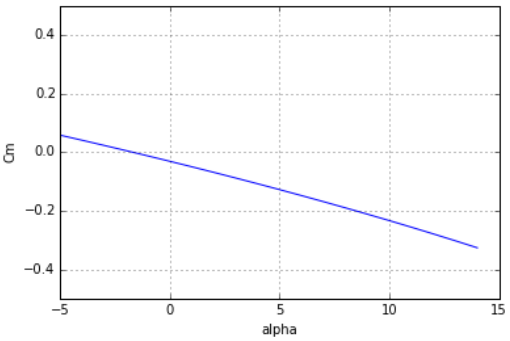

Figure 10.6: C_m-α graph

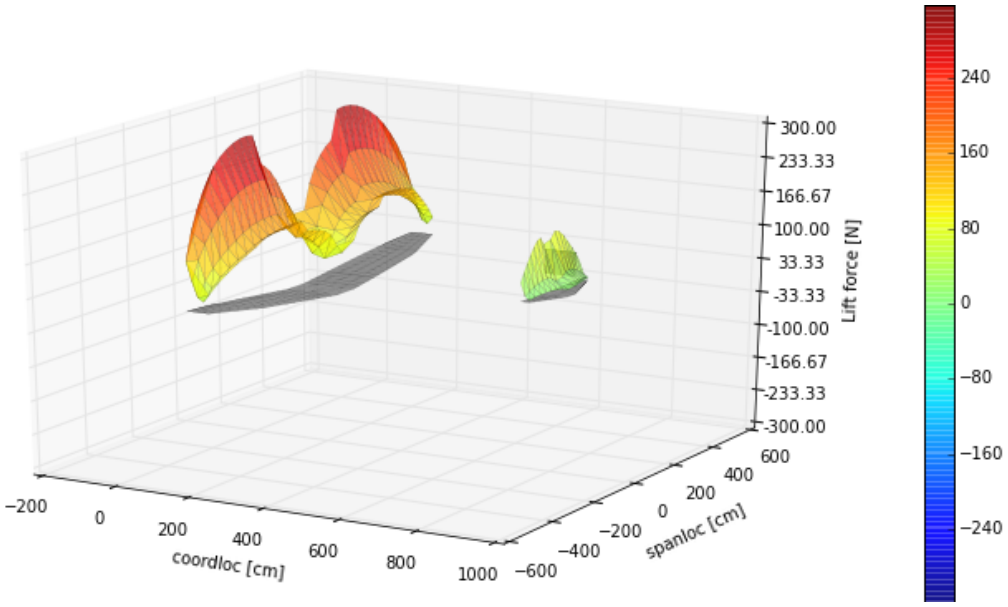

Figure 10.7: Lift distribution during cruise

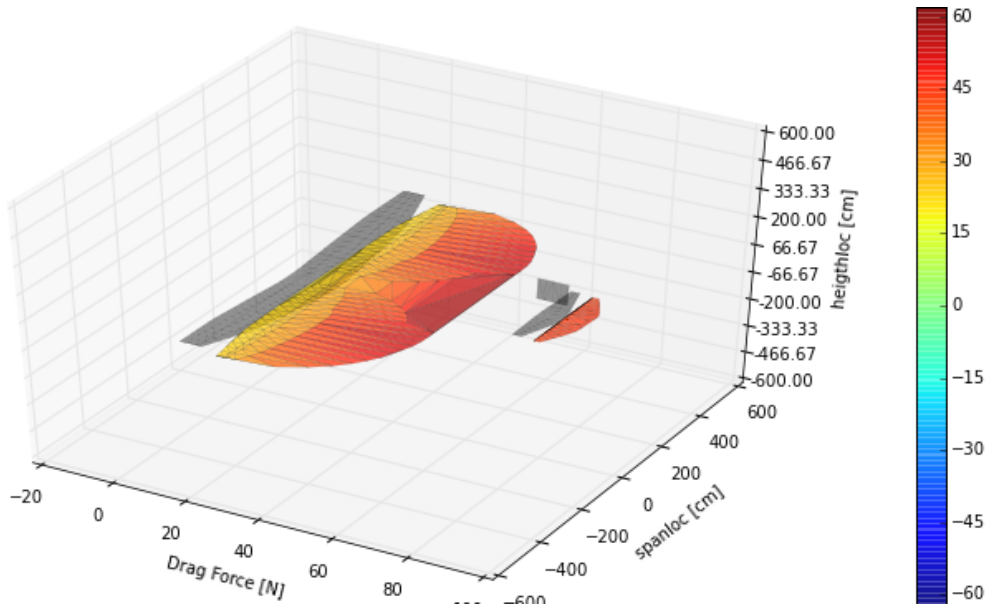

Figure 10.8: Drag distribution during cruise

11

Structural characteristics

This chapter outlines the main structural characteristics of the design. The properties of the wing are presented in Section 11.1, while the empennage is described in Section 11.2. Finally, The properties of the fuselage are outlined in Section 11.3.

11.1. Main wing

For the main wing it was decided early in the process to use a wingbox that covers the entire span of the wing with the fuselage mounted on top of it. This was a starting point from which to create the loading diagrams. The aircraft is designed for the 'worst case scenarios' as explained in Section 7.3.1. To start with, as mentioned in Chapter 7, the wing was sectioned into pieces. For each section, the lift was determined to finally create a shear loading diagram as seen on the left hand side of Figure 11.1 and Figure 11.2. In these figures, the shear loading for +12g and -6g can be seen, this includes the safety factor of 2 for composites as discussed in Section 7.3.1. At the left hand side of the diagrams the total lift is shown, which is 100 kN for 12g and -50 kN for -6g. Moving towards the right of the diagram, the shear forces decrease and eventually reach 0 N at the tip of the wing. The diagrams are plotted for just half the wing.

Moving on, the moment diagrams must be created to calculate the bending stresses in the wingbox along the entire wing. The moment diagrams can be seen on the right hand side of Figure 11.1 and Figure 11.2. The perhaps, unexpected shape of the moment diagrams can be explained by the irregular shape of the wing as presented in Chapter 10, because the wing is sectioned in 3 with 1 different taper ratio per section, this creates a sudden jump in moment of inertia. The maximum values for the bending moment for +12g and -6g are 237 kNm and -118kNm, respectively.

Now with the bending moments calculated for each section of the wing, the bending stresses for the wingbox can be calculated. Using Equation (7.8), the following two bending stress graphs are created.

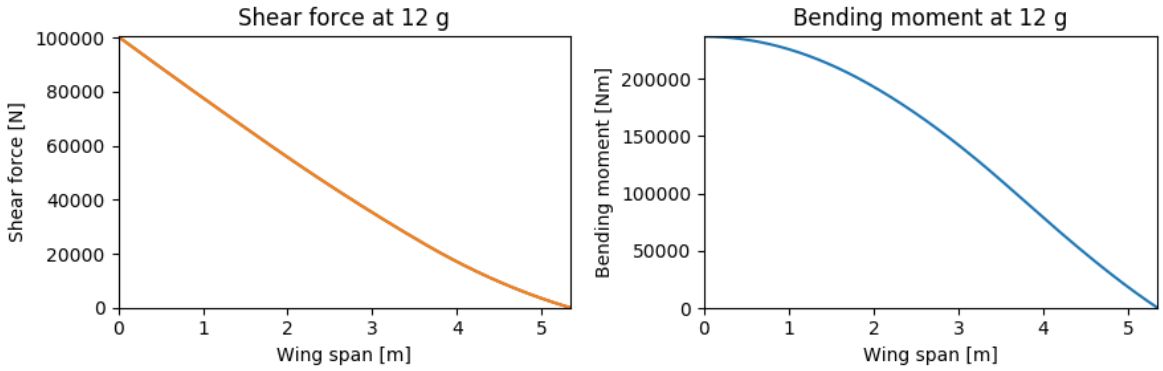

Figure 11.1: Shear and moment diagram for +12g

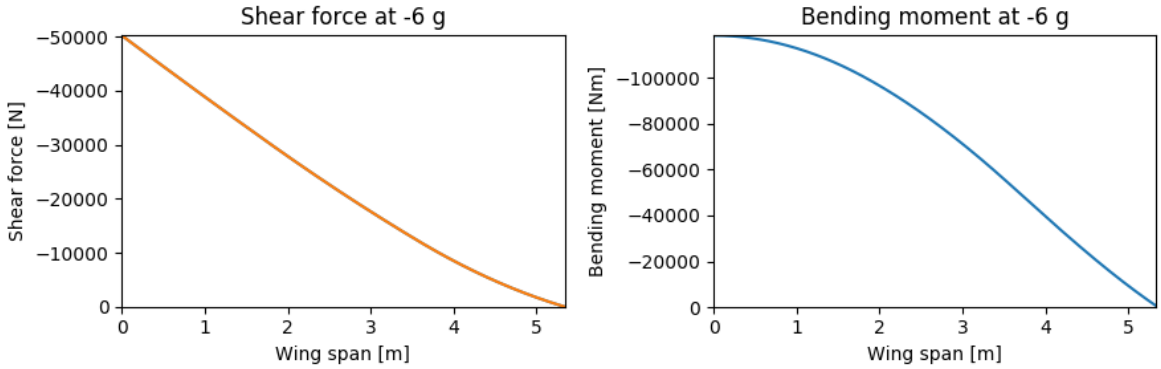

Figure 11.2: Shear and moment diagram for -6g

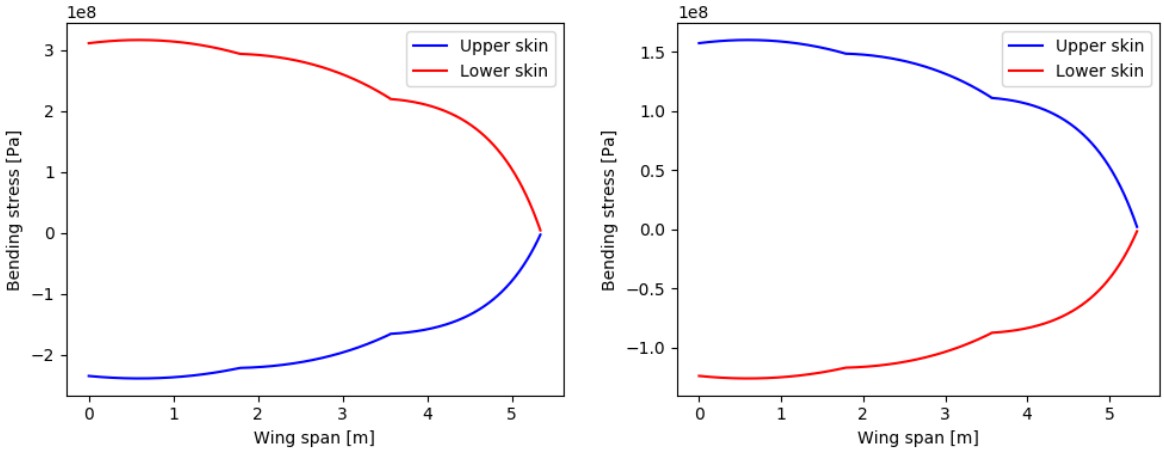

(a) Maximum bending stresses in upper and lower skin for +12g

(b) Maximum bending stresses in upper and lower skin for -6g

Figure 11.3: Maximum bending stressed along the top and bottom skin of the wingbox for +12g and -6g

The graphs show the maximum bending stress along the top and bottom skins for each section of the wing, starting from the root and ending at the tip. Here again, because of the three wing sections, there are kinks in the graph.

To determine buckling loads of a composite sandwich structure proved to be beyond the scope of this phase of the design as it requires very complicated calculations. After some research it was found that the average ultimate tensile stress of carbon fibres is 4500 MPa which was taken as an initial value to work with [8]. Making a quasi isotropic plate would require some additional calculations however. To find the ultimate tensile stress of a quasi isotropic plate (including the resin) [0°, 90°, ±45°] the ultimate stress must be multiplied by 0.2 as suggested by Ir. J. Sinke who is involved in research on composites. The multiplication with 0.2 results in an ultimate tensile stress of 900 MPa. Since buckling was beyond the scope of this design phase, the assumption needed to be made that the ultimate compressive stress is equal to the ultimate tensile stress and it will be shown later that this poses no big issue for this phase of the design.

From Figure 11.3 it can be seen that the maximum experienced bending stress is in the lower skin at 12g and is equal to 317 MPa, which is well below the ultimate tensile stress. A thickness of only 0.71 mm would be required to carry the bending stresses, however with this thickness the plate would most almost certainly buckle. On top of buckling, manufacturing of such a thin plate can prove to be a challenge. To account for all the contingencies, a final plate thickness of 2 mm was decided upon for the entire wingbox; which means each plate of the honeycomb structure is 2 mm so essentially 4 mm in total. Another assumption which was needed to be made at this stage because of incapability

of calculating for buckling was the placement of the ribs. A total of 5 ribs have been installed on the wingbox, each at the transition from one section to another (where the taper changes, where the kinks happen in the graphs in Figure 11.3).

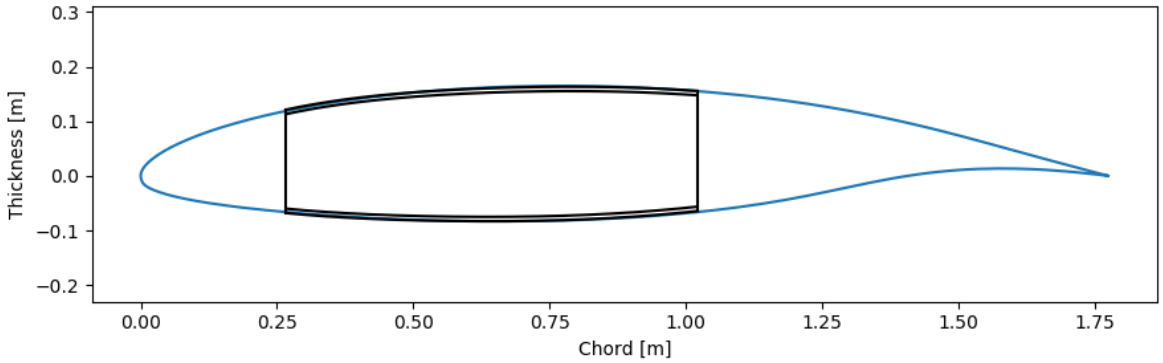

Figure 11.4: Outline of the wingbox including sandwich structured skins

To clearly present the results for the main wing Table 11.1 is presented below. The abbreviations US and LS have been used for upper skin and lower skin, respectively. Also CF has been used for carbon fibre. From the results it can be seen that that the maximum tensile stress is 317 MPa which is only 35% of the ultimate tensile strength. That shows that the wingbox can sustain 2.85 the amount of tensile load that it is designed for, showing that a 2 mm skin thickness covers all contingencies.

Table 11.1: Main wing results

Parameter	Value	Unit
V_{max}	100	kN
M_{max}	237	kNm
$\sigma_{ult,CF}$	900	MPa
$\sigma_{max,US}$	-239	MPa
$\sigma_{max,LS}$	317	MPa
τ_{max}	72.9	MPa
t_{skin}	2	mm

The final layout of the wingbox can be seen in the drawing in Figure 11.4 by the black lines. The drawing shown includes the dimensions of the wing at the root.

11.2. Empennage

The critical loads for the empennage were taken from the aerodynamics analysis. The critical load on each horizontal tail half is 21.3 kN (42.7 kN in total), which occurs during the dive. The highest considered load for the vertical tail is 38.4 kN, which occurs during the tightest slipping turn. The outcome summary of structural tail model is presented in Table 11.2 for horizontal tail, and Table 11.3 for vertical tail. For the exact bending and shear stress distributions in horizontal tail, refer to Figure 11.5 to Figure 11.8. The distribution in vertical tail follows identical pattern, but with higher bending stress, shear flow and stress values. Finally, the root cross-section of the horizontal tail can be seen on Figure 11.9. Vertical tail has the same cross-section, but of different cord at root (1.159 m).
In order to sustain the loads, the sandwich composite should have carbon laminate with a thickness of at least 1 mm and honeycomb with a thickness of 1.5 cm. The value of 1 mm for carbon fibre laminate is very high, however it is because the laminate is fully quasi-isotropic, which in reality might not be needed. In fact, quasi-isotropic laminate has only 20% of the strength of the pure fibre, while fully anisotropic laminate has 50%. Therefore, looking into isotropic requirements might significantly reduce the required material thickness. The thickness of the honeycomb is also high, however it can be reduced by in-depth sandwich composite analysis, the outcome of which would be the required

Table 11.2: Loads and stresses on horizontal tail

Load type	Highest absolute value	Location
V_{max}	38400 N	Tailbox root
M_{max}	8736.7 N m	Tailbox root
σ_{max}	95.03 MPa	Tailbox root, points of maximum airfoil thickness
q_{max}	121.2 kN m^{-1}	Tailbox root, middle of the spar
τ_{max}	60.6 MPa	Tailbox root, middle of the spar

Table 11.3: Loads and stresses on vertical tail

Load type	Highest absolute value	Location
V_{max}	38400 N	Tailbox root
M_{max}	15740.1 N m	Tailbox root
σ_{max}	92.54 MPa	Tailbox root, points of maximum airfoil thickness
q_{max}	160.4 kN m^{-1}	Tailbox root, middle of the spar
τ_{max}	80.2 MPa	Tailbox root, middle of the spar

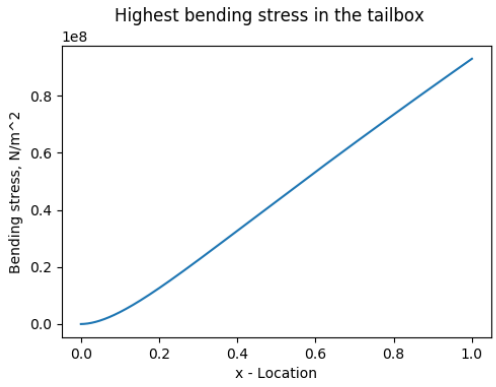

Figure 11.5: Highest bending stress along the horizontal tail span (tip to root)

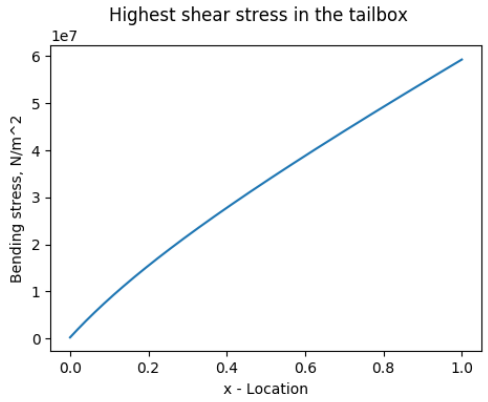

Figure 11.6: Highest shear stress along the horizontal tail span (tip to root)

honeycomb thickness so it can withstand vacuuming manufacturing loads and stress redistribution loads. The resultant total mass of horizontal tail is 10 kg, and of vertical tail is 7 kg.

11.3. Fuselage

Loading The fuselage has been designed with the worst case scenario, a twelve times larger inertial loading, in a pull-up manoeuvre. This includes an safety load factor of two, which was determined to be more appropriate for composites[95]. As previously mention in Section 7.3.3, the fuselage was modelled as a beam, which means that it is a static object and equilibrium exists between all forces and moments in the structure.

The main loads acting on the fuselage in the symmetric manoeuvre are the self-weight and the aerodynamic loads on the main wing and horizontal tail. The self-weight was determined based on the conceptual design weight estimation. The fuselage was determined to weight 20% of the OEW. This was designed as constant distributed load over the entire length of the fuselage. The lift on each section of the main wing was calculated as explained in Section 7.3.2. For the design of the fuselage, the lift forces on all sections were summed up, resulting in the lift being treated as a point load at the aerodynamic centre of the wing. The remaining forces and moments acting on the fuselage are the lift generated by the horizontal tail and the moment about the aerodynamic centre of the wing. Table 11.4 shows the external forces acting on the fuselage. As mentioned in Section 7.3.3, the z-axis begins at

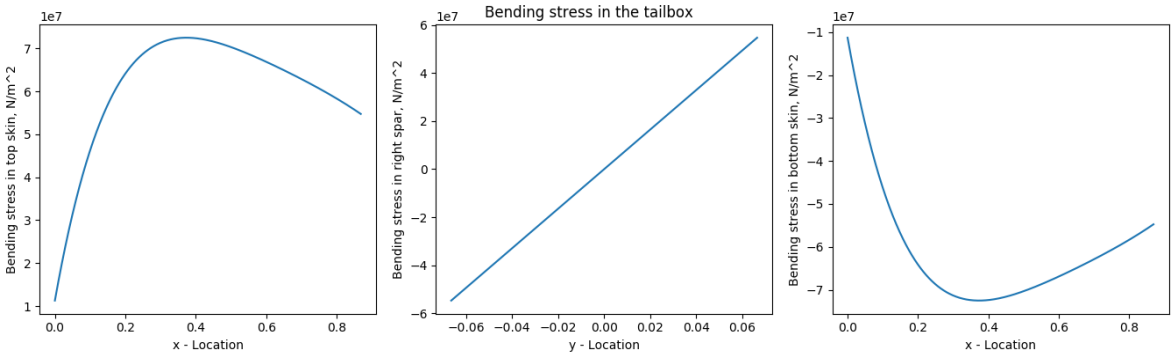

Figure 11.7: Bending stress distribution in the horizontal tailbox at the root

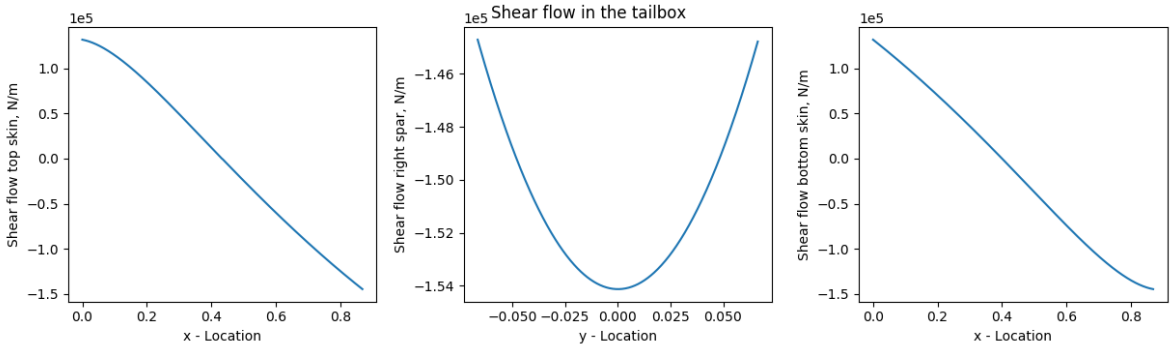

Figure 11.8: Shear stress distribution in the horizontal tailbox at the root

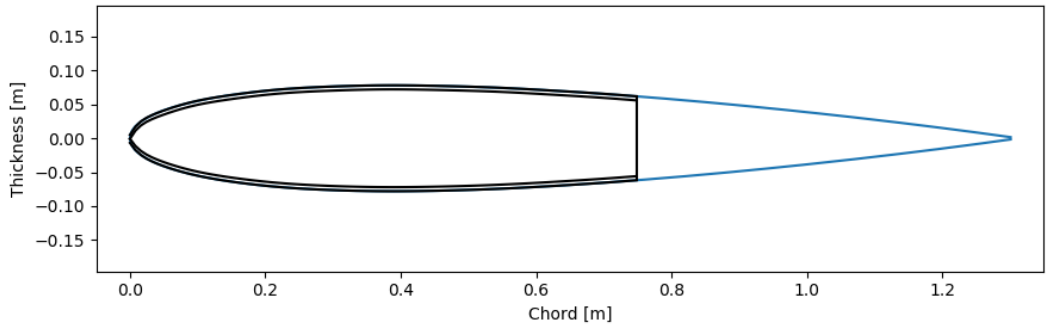

Figure 11.9: Position of the horizontal tailbox in tail structure

the aft of the fuselage, at the tail, and points towards the nose of the fuselage. Since the manoeuvre is symmetric and the drag is neglected, there are no forces acting along the x-axis or the z-axis, and the only moments present are those about the x-axis. The internal reaction forces and moments along the length of the fuselage are shown in Figure 11.10.

Table 11.4: The external loads on the aircraft.

Force	**Value**	**Location**
L_w	200825 N	0.57 m
L_h	-160816 N	5.1 m
w_{fus}	-5335 N m^{-1}	-
Moment	**Value**	**Location**
C_m	867416 N m	5.1 m

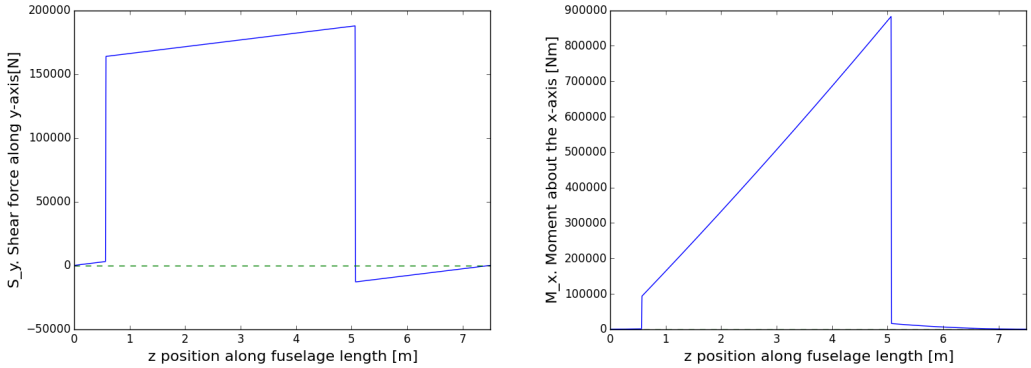

(a) Internal reaction shear force along fuselage length.

(b) Internal reaction moment along the fuselage length

Figure 11.10: Internal loads along the fuselage length

Results With the forces and moments in the structure determined, the model established in Section 7.3.3 is used to obtain the required thickness. Figure 11.11 shows the thickness required to sustain the normal stresses and the shear stresses respectively, along the fuselage length. The analysis showed that the thickness needed is 4.5 mm, when using only a quasi-isotropic carbon fibre laminate, with the mechanical properties displayed in Table 11.5 and the density outlined in Table 7.1. The determination of the tensile strength has been previously discussed in Section 11.1. The remaining two values have been obtained from literature.

Table 11.5: Composite Material Properties

Mechanical Property	**Value**
Tensile Strength	900 MPa
Compressive Strength	657 MPa [25]
Shear Strength	107.9 MPa [25]

As a sandwich structure proved to be better suited for the design at hand, due to the feasibility of developing the fuselage without the need of frames [99], the single skin panel determined previously, with a t_{eq} = 4.5 mm must be translated into a sandwich panel. For this stage of the design the equivalent weight method is considered [63]. The elastic and shear moduli of the equivalent single skin panel are assumed to equal those of facesheet materials. The core thickness was set to that of the minimum

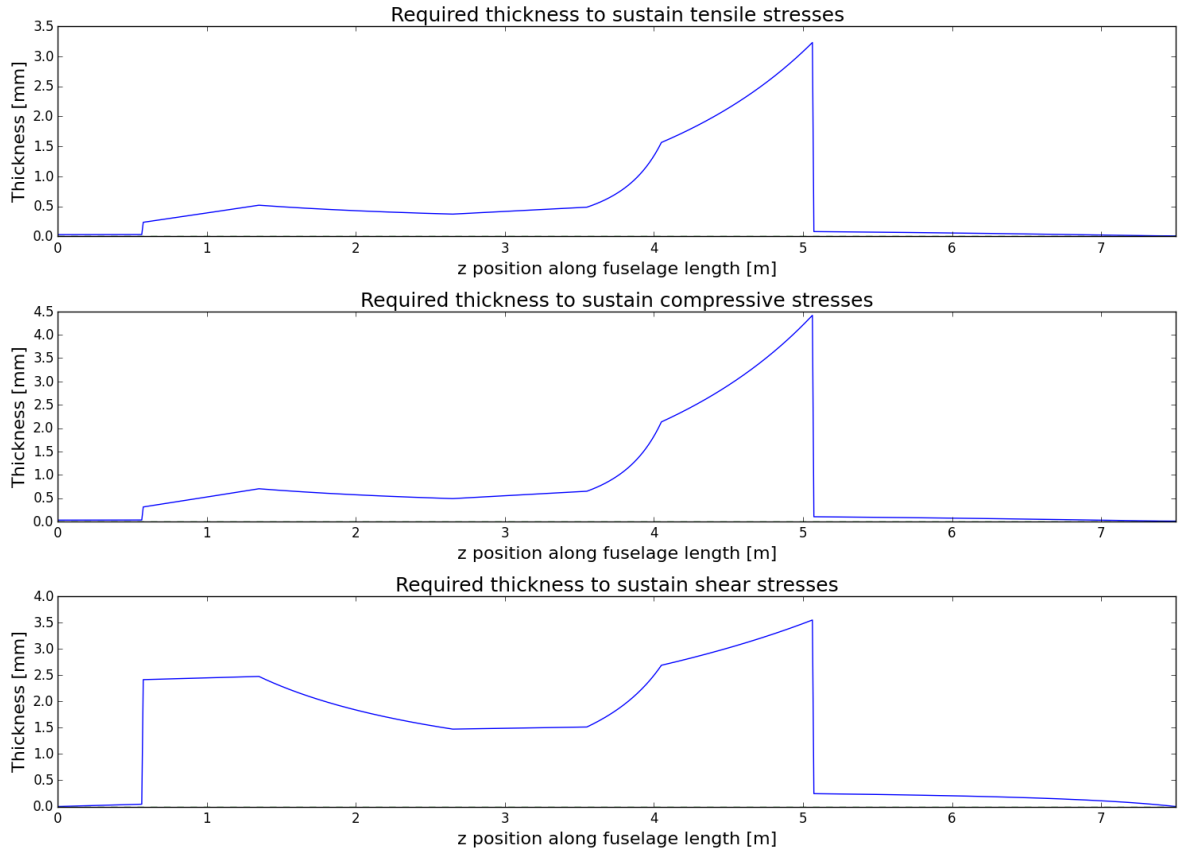

Figure 11.11: Required thickness to sustain the internal loads stresses along the fuselage length. The reference frame used is presented in Section 7.3.3.

allowable h_c= 5 mm [99]. The facesheet thickness was then calculated using Equation (11.1).

$$t_f = \frac{t_{eq}\rho_f - h_c\rho_c}{2\rho_f} \tag{11.1}$$

Thus, the resultant sandwich panel has a facesheet thickness of t_f=2.1 mm, a core thickness of t_c= 5 mm and an overall thickness of t_{total}= 9.2 mm. This reduced the total required thickness of the laminate by 0.3 mm, which reduces the mass of the structure. The mass of the fuselage is 137.5 kg and was obtained by summing up the mass of each segment along the fuselage length. The mass of a segment was calculated using Equation (11.2), where the dl= 1 cm.

$$dm_i = (2t_f\rho_f + h_c\rho_c) \cdot 2\pi r_i \cdot dl \tag{11.2}$$

To account for the effects of the engine mount and cut-outs in the fuselage, such as doors and windows, which typically require local reinforcement and thus generate an increase in mass, the mass of the fuselage structure is multiplied by a factor of 1.33 [41]. This puts the final mass of the fuselage structure at 182.9 kg.

12

Stability & control characteristics

This chapter presents the stability and control characteristics of the aircraft that follow from the models and methods described in Chapter 8. The results that are obtained are presented and discussed in four sections. Section 12.1 elaborates on how the position of the wing and the horizontal tail size is determined while Section 12.2 discusses the longitudinal static stability and manoeuvrability. Section 12.3 defines the dimensions and location of the control surfaces and Section 12.4 elaborates on the dynamic stability characteristics.

12.1. Horizontal tail

The horizontal tail was sized to provide controllability and stability in all scenarios. A plot was created to visualise the result, see Figure 12.1, the most forward and most aft centre of gravity locations were determined for different x_{LEMAC} locations to find the optimal combination.. The optimal horizontal tail over main wing area ratio was found to be 0.11, resulting in an area of 1.68 m^2. The location of the leading edge of the mean aerodynamic chord, x_{LEMAC}, associated with this ratio is 2.22 m from the tip. A loading diagram illustrating how the most forward and most aft loading situations are achieved can be consulted in Figure 12.2. The cargo was loaded first, then the people and lastly the fuel. For the aft loading case, one of the pilots was loaded before the two passengers since it is impossible to fly without a pilot..

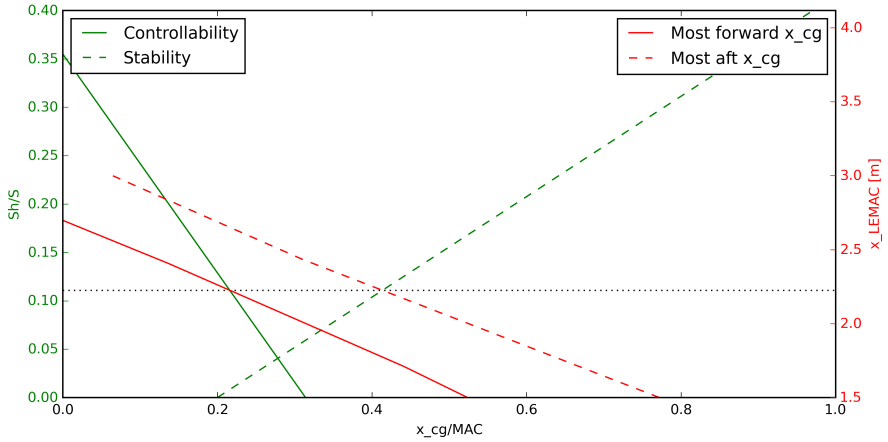

Figure 12.1: Stability and controllability centre of gravity limitations for different S_h/S ratios.

The payload distribution used to construct the loading diagram is presented in Table 12.1. Note that the full loading condition as described in Figure 12.2 refers to the maximum loading condition as presented in the table. The light loading condition however, only includes two pilots in the front.

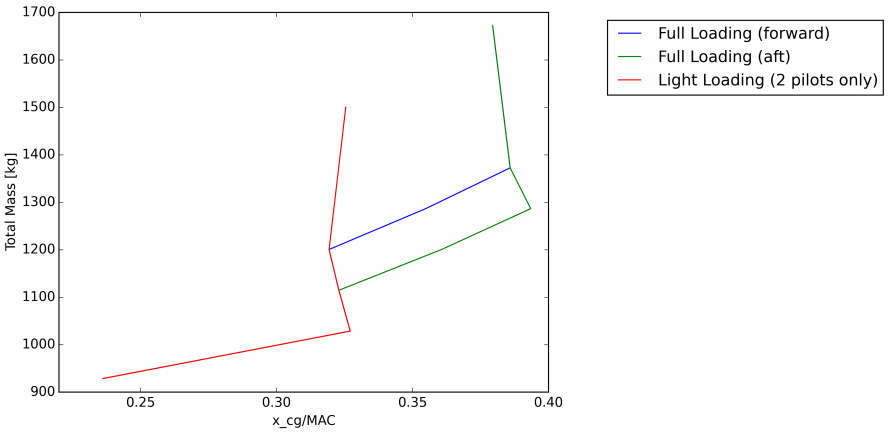

Figure 12.2: Loading diagram of the aircraft for the optimal x_{LEMAC}.

Table 12.1: Load distribution

Item	Mass	c.g. location w.r.t the nose
Operational empty mass	1043 kg	2.48 m
Pilot left seat	86 kg	2.65 m
Pilot right seat	86 kg	2.65 m
Passenger left seat	86 kg	3.55 m
Passenger right seat	86 kg	3.55 m
Cargo	100 kg	4.05 m
Max. mission fuel	300 kg	2.61 m

12.2. Longitudinal stability

As already mentioned in Section 8.2.3, it is essential for stability that the centre of gravity lies in front of the neutral point. The left plot in Figure 12.3 visualises the centre of gravity locations with respect to the stick-fixed and stick-free neutral point. Note that the different centre of gravity ranges are corresponding to different loading conditions. For these loading conditions the range of centre of gravity is defined by the centre of gravity location before flight and the centre of gravity after flight, when all the fuel is burned up. From this plot it becomes evident that the required elevator deflection decreases when the centre of gravity moves through the neutral point.
Since the maximum elevator deflection is 25°, the aircraft with the light loading condition can perform a pull up manoeuvre at 10000 ft with a maximum load factor of approximately 4. When the aircraft is fully loaded, it can in theory perform a pull up manoeuvre with a smaller turn radius and thus higher load factor at the same airspeed and altitude. However, the difference in weight between the two loading conditions will have disadvantages performance-wise. For example, the climb performance will deteriorate and more lift and thus velocity is required to perform the manoeuvre when the aircraft is fully loaded.

Therefore it has been chosen that the centre of gravity range for the aerobatic configuration should lie somewhere halfway between the light and full loading condition. This corresponds to a configuration with the two pilots up front and a load of 100 kg in the baggage compartment of the aircraft. The manoeuvre-margins corresponding to the loading conditions can be seen in the left plot of Figure 12.3

It should be mentioned that the manoeuvres-margin curves in the left plot of Figure 12.3 rely on the fact that the C_e/C_{ht} is set to 0.4. This value is based on statistics as stated by [55]. Accordingly, the right plot in Figure 12.3 could be generated which visualises the corresponding trim stability of the aircraft. As can be seen in this plot, the stability condition $d\delta/dV > 0$ is satisfied for all loading conditions. To visualise static longitudinal stability with the effectiveness of the elevator under the different loading conditions a C_m/α curve is generated and presented in Figure 12.4. Note that the enclosed area indicates the

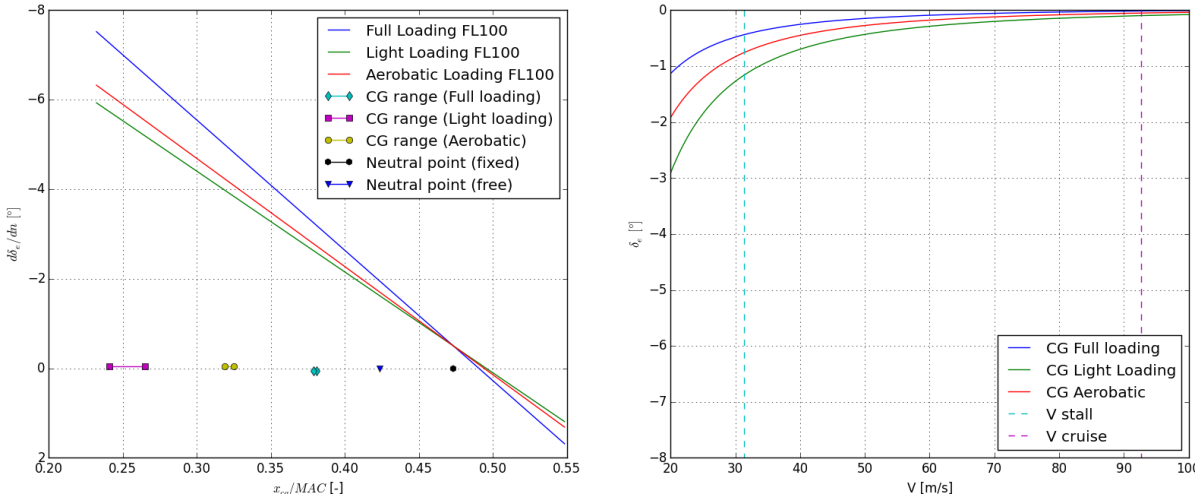

Figure 12.3: The left plot visualises the effect of the elevator during a pull up manoeuvre as a function of c.g. location while the right plot presents the trim stability as a function of airspeed

effectiveness of the elevator deflection.

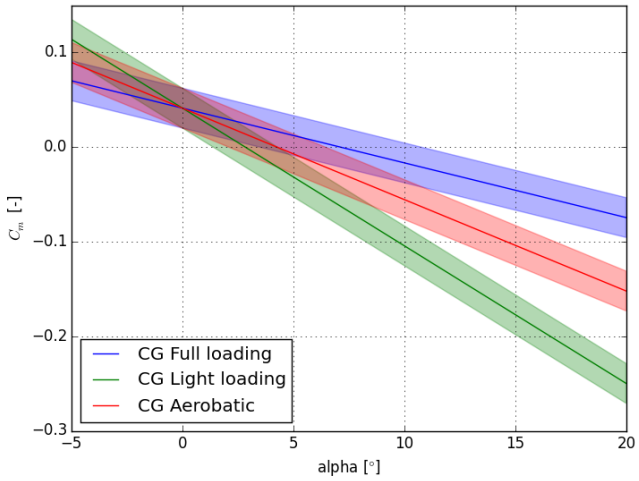

Figure 12.4: $C_m - \alpha$ curve for different loading conditions with trim capabilities at different alphas.

From this plot is should also be evident that the moment coefficient at zero angle of attack is positive due to the fixed angle of incidence of the horizontal tail plane at -6°. Without this angle of incidence, the C_{m_0} would be negative which is not preferable during take-off or landing due to the limited trim capabilities of the elevator. Note that this incidence angle is set such that the aircraft can also be trimmed at cruise with positive angle of attack for different loading conditions.

12.3. Control Surfaces

As mentioned in the previous section (Section 12.2) the elevator is sized based on statistics and reference aircraft. The aileron and rudder instead, are sized using the model as described in section Section 8.2.2. However, according to this model the required span of the rudder was greater than the span of the vertical tail span. Since the rudder area is proportional to the rudder span to vertical tail span ratio according to **AS-STAB-08** and **AS-STAB-09**, some modifications on the rudder dimensions are made to increase the rudder area:

- To reduce the wake on the vertical tail plane during a spin at high angles of attack, the horizontal

tail plane is moved forward with respect to the leading edge of the vertical tail. As a result the rudder becomes more effective and less rudder area is required.

- The rudder extends further down and aft at the lower side of the vertical tail to improve its effectiveness at high angle of attack.

Note that these modifications are essentially increasing the effective vertical tail span and area to 1.8 and 1.8 respectively. By taking into account these modifications, a new (b_R/b_v) ratio of 0.96 could be obtained. Accordingly the rudder area could be determined using Equation (12.1) and is presented Table 12.2.

$$_R/C_{vt} \cdot S_{vt} \cdot b_R/b_v \tag{12.1}$$

Table 12.2: Control surface dimensions and locations

Control surface	Chord ratio	Surace area	location
Elevator	0.4	0.64 m^2	evenly distributed along the span
Aileron	0.3	0.91 m^2	from 55% to 95% of half the wing span
Rudder	0.5	0.86 m^2	increasing chord from top to bottom

12.4. Dynamic stability

The results that were obtained from the dynamic stability XFLR5 model are presented in Table 12.3. As can be seen in third column of this table the damping coefficients for each motion is smaller than one. Next to that, the real part of the eigenvalue of the aperiodic roll is negative. This implies that the aircraft is dynamically stable for longitudinal and lateral motions. However, determining in which terms the aircraft is dynamically stable turned out to be a difficult task since there are no stability criteria available for the specific missions that the aircraft should perform. Therefore it has been chosen to focus only on determination of whether the aircraft is stable or not. Further investigation and development should reveal these criteria by performing tests and design modifications which are described in Section 27.2

Table 12.3: Dynamic stability results

Motion	Eigenvalue	Damping (ζ)	Neutral frequency (ω_n)	Period (P)	($T_{\frac{1}{2}}$)
Short period	$-0.7983 \pm 2.703j$	0.283	2.818 sec^{-1}	2.33 sec	-
Phugoid	$-0.004649 \pm 0.1593j$	0.029	0.16 sec^{-1}	39.29 sec	-
Dutch roll	$-0.2984 \pm 2.156j$	0.137	2.178 sec^{-1}	2.912 sec	-
Aperiodic roll	-9.622	-	-	-	0.072 sec
Aperiodic spiral	0.01874	-	-	-	3.699 sec

Its obvious that the difference in neutral frequency and damping ratio between the short period and pugiod motion are corresponding to its characteristics. The short period motion is a rapid pitching of the aircraft about the centre of gravity and has therefore usually a higher damping ratio than the longer period motion or phugoid. It could be stated that the aircraft is pretty lateral stable since the time to damp to half the amplitude of the aperiodic roll is short and the neutral frequency of the dutch roll is quite high. However, during the further development process the latter stability characteristics should be reconsidered to improve the aerobatic capabilities.

13

Performance characteristics

This chapter contains all the results that followed from the performance models that were outlined in Chapter 9. Together they resemble the performance characteristics of the final design.

13.1. Propulsion model results

As stated in Chapter 9, the results of the propulsion model were not credible and therefore not included in the performance model. A few assumptions had to be made to include the propulsion effects in the model:

- The propeller efficiency at flight speeds was assumed to be 0.82, a value that is reasonable for the varying flight conditions [52], the landing propeller efficiency was set to be 0.45 to simulate the effect of low speed on propeller efficiency.
- The static thrust was calculated from the static thrust for the Cirrus SR22 given in [55]. This thrust was divided by the power of the Cirrus' engine and then multiplied by the power of the designed aircraft's engine. The difference between blade number is negligible, this is caused by the adjusted blade geometry of the four-blade propeller, as propellers are designed for a certain power or thrust [36, 58].
- The power available is constant with flight speed and scales over altitude with $(\frac{\rho}{\rho_0})^{0.7}$ This is a generally accepted simplification for turboprop engines at medium speeds [64].

13.2. High lift device sizing

During the performance analysis it was found that the landing phase was the most critical when it comes to the required lift coefficient that is needed to reach the desirable landing distance. The high lift device sizing has thus been done parallel to the landing performance calculations and adapted accordingly. Using the method as presented in Section 9.2.3, the high lift devices were sized and an overview of the resulting system can be found in Table 13.1.

Table 13.1: High lift devices design.

Type	$\frac{S_{wf}}{S}$	$\frac{c_f}{c}$	$C_{L_{max@TO}}$	$C_{L_{max@landing}}$	$\Delta C_{D_{flaps}}$
Slotted flaps	0.6	0.25	1.81	1.95	0.05

13.3. Climb, descent & field performance

This section presents a clear overview of the results from the climb, descent and field performance models, which include landing and take-off performance.

13.3.1. Climb performance

The climb rate was established at sea level while using an aerobatic weight, as was discussed in Chapter 9. This results in the final values as shown in Table 13.2, with t_{cruise} being the time it takes to reach the cruise altitude of 25000 ft with maximum rate of climb during the entire climb phase.

Table 13.2: Climb performance results for Aerobatic mass

Aerobatic mass [kg]	RoC$_{sealevel}$ [m/s]	t_{cruise} [s]
1397	17.3	669

Furthermore, the maximum rate of climb, time to cruise altitude and absolute ceiling were determined for the aircraft climbing with MTOW. These values were established by modelling the maximum rate of climb as a function of altitude, as can be seen in Figure 13.1. Also, in order to comply with CS23, the climb gradient should be above 4% at take-off. These are the requirements applicable to a high speed (V_{MO} > 250 KCAS) level 2 airplane (2 to 6 passengers)[42]. The values found can be seen in Table 13.3. It should be noted that even though the absolute ceiling is at 38930 ft, the aircraft will only be certified and fly up to an altitude of 25000 ft as was specified in Chapter 9.

Table 13.3: Climb performance results for MTOW

MTOW [kg]	RoC$_{sealevel}$ [m/s]	t_{cruise} [s]	$h_{absolute}$ [ft]	Climb gradient [%]
1658	13.6	917	38930	26.7

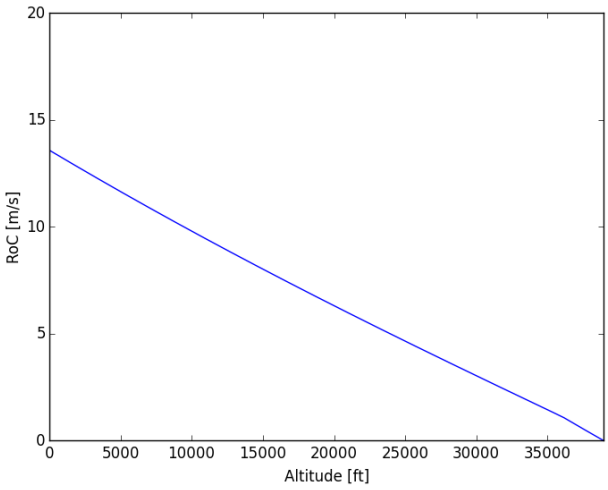

Figure 13.1: Maximum rate of climb at every altitude up to the absolute ceiling

13.3.2. Descent performance

The descent performance model determined the maximum obtainable glide distance and best gliding speed at every altitude. However, since this speed changes with altitude it will not be presented. It is however available and could be presented in the POH. The results presented in Table 13.4 are relevant parameters that are used or follow from the descent performance model, the altitude from which the glide distance was calculated is the cruise height.

Table 13.4: Descent performance results

Descent mass [kg]	R_{glide} [km]
1600	133.7

13.3.3. Field performance

The field performance includes both the take-off and landing performance. As was already stated in Section 9.2.2 and Section 9.2.2, the take-off and landing distances were initially determined for a runway made out of dry asphalt or concrete. To model this, a ground friction coefficient of 0.05 was taken for a situation when no brakes are applied and a coefficient of 0.5 when brakes are applied [55]. Besides this the landing and take-off distances were determined for several different surface types, under which grass runways to fulfil requirement **REQ-MIS-06**. To make an estimation of these distances, rules of thumb provided by the UK Civil Aviation Authority were applied to the results [96]. Furthermore, the landing distance was also calculated in case reverse thrust would be used. These landing distances cannot be used for certification nor can they be included in the Aircraft Flight Manual (AFM). However, it is of practical use for the pilot to know these distances. For both landing situations, idle and reverse thrust, a prop efficiency of 0.45 was used as already specified in Section 13.1. The resulting distances as well as the rules of thumb used are shown in Tables 13.6 and 13.7. Furthermore, the stall speeds during take-off and landing are presented in Table 13.5.

Table 13.5: Stall speeds in take-off and landing configuration

Configuration	Stall speed [m/s]	Stall speed [kn]
Take-off	31.1	60.5
Landing	30	58.3

Table 13.6: Take-off performance results

Surface	Take-off distance [m]	Obtained by
Dry asphalt/concrete	373.4	Take-off performance model
Grass runway dry (5 cm)	394.8	Increasing ground roll by 10%
Grass runway wet (5 cm)	473.7	Increasing dry grass runway by 20%
Soft ground	480.3	Increasing ground roll by 50%
Uphill slope (3%)	496.6	Increasing ground roll by 15% for every 1% slope

Table 13.7: Landing performance results

Surface	Landing distance [m]		Obtained by
	Idle	*Reverse Thrust*	
Dry asphalt/concrete	496.8	409.6	Landing performance model
Grass runway dry (5 cm)	555.1	441.7	Increasing ground roll by 30%
Grass runway wet (5cm)	525.9	425.7	Increasing ground roll by 15%
Soft ground	525.9	425.7	Increasing ground roll by 15%
Downhill slope (3%)	555.1	441.7	Increasing ground roll by 10% for every 1% slope

In case a take-off or landing manoeuvre would be attempted on an airstrip located in the mountains, it is of interest to know how the take-off and landing distances will increase with altitude. For this reason, the take-off and landing distances were plotted versus the altitude. The altitude influences the density, and therefore the power, lift and drag during these operations, as was already outlined in Chapter 9. The resulting plots can be seen in Figure 13.2 and Figure 13.3.

Take-off and landing with crosswinds

The requirements state that the aircraft should be able to perform take-off and landing with 25 kn crosswinds (**REQ-MIS-10** & **REQ-MIS-11**). Whether the aircraft is able to manage this amount of crosswind is mainly determined by the rudder authority. Crosswind performance is hard to measure and real limits

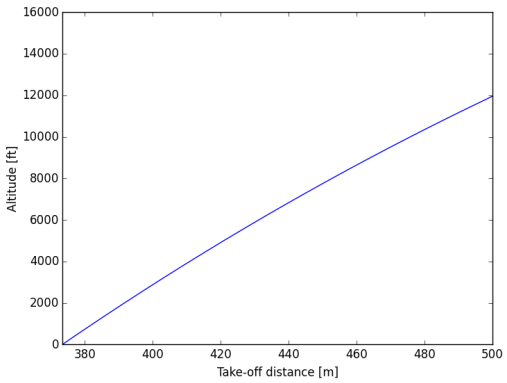

Figure 13.2: Take-off distance at different altitudes

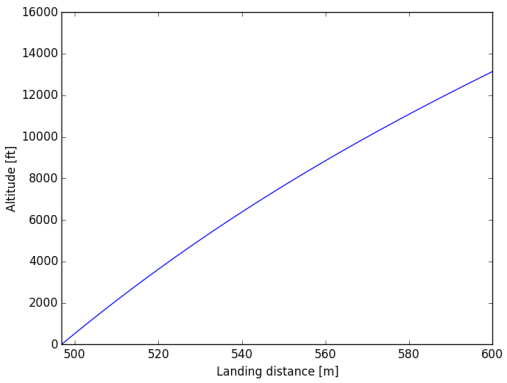

Figure 13.3: Landing distances at different altitudes

can usually not be found, therefore aircraft companies provide a ”maximum demonstrated crosswind” as a useful boundary. Both the Diamond DA40 and the Cirrus SR22 have a maximum demonstrated crosswind performance of 20 kn [21][33]. Since the rudder authority of this aircraft will be sized for spin recovery during aerobatics, in contrast to the Cirrus SR22 or Diamond DA40, it is believed that the rudder authority will be higher and result in a better crosswind performance. However, the actual crosswind performance cannot yet be analysed or demonstrated in this stage of the design and should be investigated further.

13.4. Cruise & Range

To begin with, the optimal cruising altitude was determined. Figure 13.4 shows the most efficient cruise speed at different altitudes. For relatively low altitudes, the aerodynamic efficiency is dominant. Around 26000 ft the engine efficiency takes over, resulting in the first sudden rise in the speed curve. As the associated speed of the highest aerodynamic efficiency keeps increasing with altitude; at some point the required power approaches the maximum. Since the engine is most efficient at this setting, this results in the best overall efficiency. This happens at about 39000 ft, where the speed curve follows a second steep rise. Above this point the aircraft is nearing its service ceiling and hence the velocity drops as a result of insufficient available power.

The above mentioned cruise efficiency can be expressed by a distance covered per fuel amount burned ratio. A plot of this ratio versus altitude can be seen in Figure 13.5. The altitude where the highest efficiency can be achieved is 42000 ft. However, this is higher than assumption **AS-PERF-06** dictates. Furthermore, flying at this altitude requires maximum power output. This means there is no margin to compensate when conditions are less favourable than assumed. Therefore the cruise altitude is set to the maximum allowable altitude of 25000 ft. At this altitude the aircraft can achieve a fuel efficiency of 5.7 km/L.

The required power was calculated for different speeds. A plot of this analysis at cruise altitude can be seen in Figure 13.6. The most efficient cruise speed was found to be 207 kn. Hence the cruise speed mission requirement, **REQ-MIS-12**, is met. This also means that specifying the plane for cruise at 180 kn does not make sense, since that is slower than the most efficient speed. Therefore the specified cruise speed was set to 250 kn. This is substantially faster than the most efficient speed, but it does not affect the range as much as the maximum cruise speed; as will be discussed in the next paragraph. At maximum power setting the plane is able to reach 299 kn.

A payload-range diagram for different speeds at cruise altitude was constructed, as can be seen in Figure 13.7. For the specified cruise speed, the range with maximum payload is 1422 km, which is only 18 km less than the range at the most efficient speed. Since the range is more than 1400 km, mission requirement **REQ-MIS-05** is met. With only one pilot and his luggage (111 kg payload), the range at 250 kn is 4020 km.

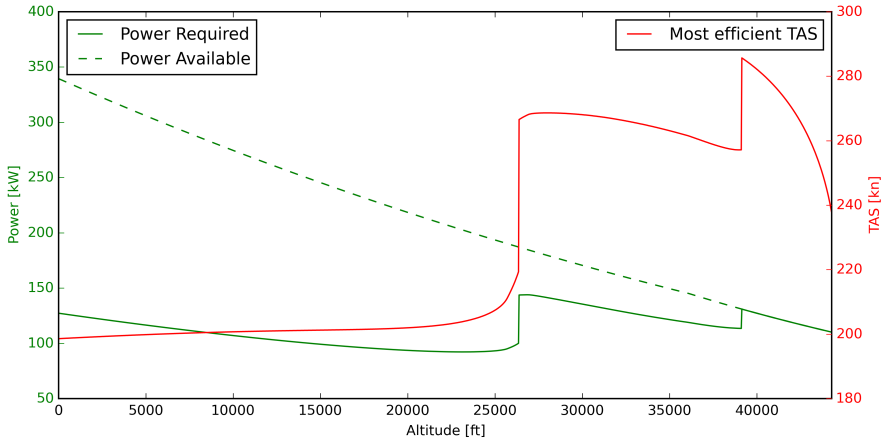

Figure 13.4: Most efficient true air speed at different altitudes in ISA conditions.

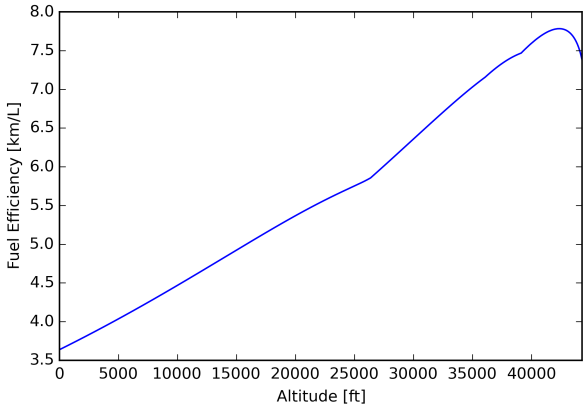

Figure 13.5: Fuel efficiency at different altitudes. Expressed as distance covered over fuel burned.

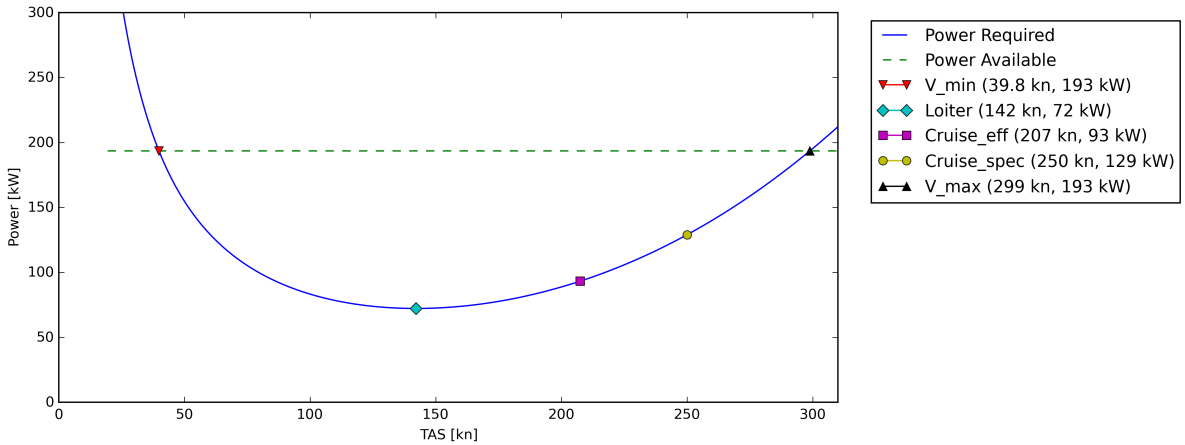

Figure 13.6: Required and available power at cruise altitude.

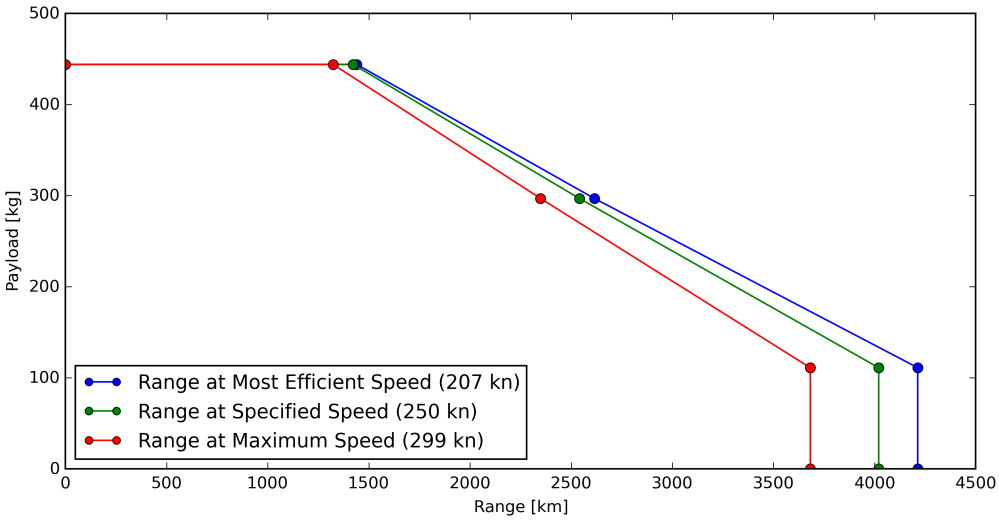

Figure 13.7: Payload-range diagram at cruise altitude.

14

Aircraft system characteristics

Several subsystems do not need a separate chapter. They are therefore described below. First the environmental control system, then the ice protection system, electrical system, control system, fuel system, landing gear, avionics and finally the ballistic recovery system.

14.1. Environmental control system

The aircraft will fly at altitudes up to 25000 ft. The temperature at that altitude is -40 °C at ISA conditions and the pressure is about a third of the sea-level pressure. These are theoretical values calculated with the 1976 International Standard Atmosphere model [17]. The human body is used to an oxygen pressure of 0.2 bar which is the sea-level partial pressure[1]. The partial pressure drops as the ambient air pressure drops, which leads to a lack of oxygen.
To counter the low temperatures, one can install an air conditioning unit. The lack of oxygen can be countered by either providing supplemental oxygen or pressurising the cabin. Providing oxygen can be done in two ways: via a mask or a nasal cannula. These methods do not contribute to the 'ultimate' feel of the aircraft so another method; pressurisation. This method just compresses the air and creates a suitable oxygen pressure; no masks or cannulae required.
Bleed air from the turbine's compressor stage is routed through the AC unit to provide a suitable atmosphere. This air is hot and under high pressure. Pressure relief valves are installed to protect the fuselage from ex- or imploding if the pressure differentials are too big. A regulator is installed to control the pressure differential. The pressure inside can be expressed as an altitude, the pressure altitude. CS-23 states that the maximum pressure altitude in the cabin should not exceed 15000 ft in an event of failure [42, CS 23.841]. Above 8000 ft the partial pressure has dropped to around 0.16 bar. This is the limit altitude where people still function without ill effects like loss of concentration [66]. Therefore it was decided to make this the maximum pressure altitude during normal flight.

14.2. Ice Protection system

One of the original requirements, **REQ-MIS-14**, stated that the aircraft should be all-weather capable. Hence there is a possibility that ice will form on the aircraft. This will deteriorate the flight characteristics, thus this should be prevented.
Two different techniques can be implemented; prevention of ice forming called anti-ice and removal of ice which is called de-ice. There are a few systems that can be applied to aircraft:

- **Pneumatic boots**
  Boots are inflatable pieces of rubber that cause the ice to break apart when suddenly inflated. This is has to be done periodically to keep the wing free from ice. The boots are not aerodynamically perfect.

- **Electro-thermal**
  Electro-thermal systems use a heated element that can operate in both de-ice mode and anti-ice

[1] Partial pressure is the fractional amount of a gas mixture component times the total pressure of the gas mixture $p_x = \frac{n_x}{n_{tot}} p_{tot}$

mode. It is just a matter if it is switched on and off periodically or not. This method can be applied to a whole range of aircraft and does not interrupt the laminar flow.

- **Fluid based (TKS)**
  A glycol-based anti-freeze can be pumped through a perforated leading edge, through perforations at the bottom of the windshield or on the propeller blades. This requires little power but is limited by the amount of fluid carried and the amount of ice that has accumulated.
- **Bleed air**
  Turbine engines have a bleed air system and some of this hot air can be routed through small channels and heat the leading edge this way. This is only done on aircraft with enough bleed air to spare.
- **Electro-mechanical**
  This system uses electronic actuators to send shockwaves through the wing's leading edge to knock ice off. This system can be combined with an electro-thermal system to have an anti-ice mode as well. The main benefit is the low power consumption.

As the aircraft relies on a laminar airflow over the wing a boot is not applicable because it disrupts the airflow and creates a turbulent boundary layer. The AI-450S will most likely not be able to supply enough bleed air to provide enough heating for both main wing and empennage while maintaining a pressure altitude of 8000 ft so bleed air heating is also ruled out. Because the turboprop engine has power to spare during cruise, an electro-thermal system was chosen. This will protect both the main wing and the tail. The propeller will also have such a system. A system for kit aircraft - dubbed the Therm-X - relies on a 75 V / 100 A generator to produce 7500 W of heating energy [37]. It combines both de-ice and anti ice methods. A part of the element is heated continuously while another is operated in a 60 second de-ice mode. This 7500 W is 2.5% of the maximum cruise power of 283.37 kW. Maximum T/O power (continuous) is 339.39 kW. This system will not cause the plane to fall out of the sky.

14.3. Electrical system

Several subsystems like avionics, environmental control, ice protection, etc. all need power to operate. This power is provided by the engine which drives a generator. During start up, power will be provided by a battery. In case of an engine failure this battery also serves as a backup power supply.
Cable bundles throughout the aircraft will provide power to the lights, avionics, TCAS, etc. These need to be sized according to the electrical current they have to transmit.
The total current and voltage of every system will have to be analysed in detail so a detailed power budget can be set up; but this is beyond the scope of this report.

14.4. Control system

The first option to consider is whether to put a fly-by-wire or mechanical control system in the aircraft. Control loads are low enough to be handled by a mechanical system, so a fly-by-wire system would add unnecessary complexity to the system. Cost was another criteria to evaluate because a fly by wire system is costly when compared to a mechanical system. Based primarily on these trade off criteria, a mechanical system was chosen as the control system mechanism.
Furthermore, the cockpit controls must be considered. While designing the cockpit there were three apparent options to evaluate:

- **The control yoke** This is basically a wheel which is held in front of the pilot. The yoke gives the pilot a better feeling and feedback for his movements, however for rapid movements the yoke is not very suitable. Important to consider is also movements at maximum g-loads pulled. It will be close to impossible for the pilot to hold up his arms in front of him at 6g and makes the yoke completely unsuitable for this purpose of the aircraft.
- **Centre stick** The centre stick looks literally like a control stick which is positioned in the pilot's chair between his/her legs. The centre stick could be used for the purpose of this aircraft as it is operable in rapid and high g environments. However, the aircraft also must fly long distances and the centre stick is considered to be uncomfortable to have between the legs for long hours and also this option was disregarded for that purpose.

- **Side stick** The side stick is similar to a centre stick, but the stick (or joystick) is positioned on the pilot's left or right hand side, depending on where he/she is sitting. The advantage of this side is that it can offer the pilot a comfortable arm rest, and it is not positioned in a particularly bothering place for the pilot. The side stick is considered to be the best overall option for the purpose of this aircraft and is therefore also chosen as the winner between these three options.

As explained in their description the yoke and centre stick are disregarded as options, so the side stick is thus chosen as the best option for the overall purpose of this aircraft. In Figure 14.1, all three considered options are shown to make clear what they look like.

(a) Control yoke (or control wheel) of a C-208 [13]

(b) Centre stick (or centre joystick) of a Diamond aircraft [6]

(c) Side stick (or joystick) of an A320 [11]

Figure 14.1: Three different cockpit control options

14.5. Fuel system

There are many choices for fuel tanks ranging from rigid, metal fuel tanks which are commonly used on older aircraft to ultra-lightweight tanks like used in Challenger ultralight aircraft. However a very common fuel tank used and selected for this aircraft is the bladder fuel tank. The advantages of this tank are its low weight, easy instalment and easy maintenance. Also, since the aircraft will fly aerobatics as well, fuel flow and sloshing of fuel is much better manageable as the bladder expands and contracts, thereby maintaining a pressure on the fuel [10]. A picture of a bladder tank can be seen in Figure 14.2.

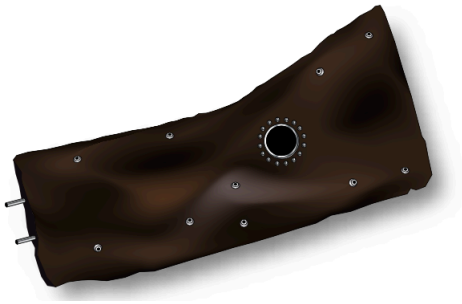

Figure 14.2: A drawing of the bladder tank [10]

In Figure 14.3 the placement of the fuel tanks for one wing can be seen by the green colour, the dashed lines indicate the ribs and the green lines indicate the wingbox structure with the top of the drawing being the LE. The placement is kept the same for the other half wing. It can be seen that the fuel tanks range from the second section of the wing until a small part of the third section of the wing and are all placed inside of the hollow wingbox structure. The total volume of the fuel tank for both wings in total is 0.56 m^3 with this arrangement. This placement of the fuel tanks needed to be taken to avoid interference with the landing gear in the first section and to provide as much bending relief as possible for the wing structure. The tanks are difficult to extend further to the wing tip as the structure gets more narrow and other subsystems such as ailerons must be fitted as well.

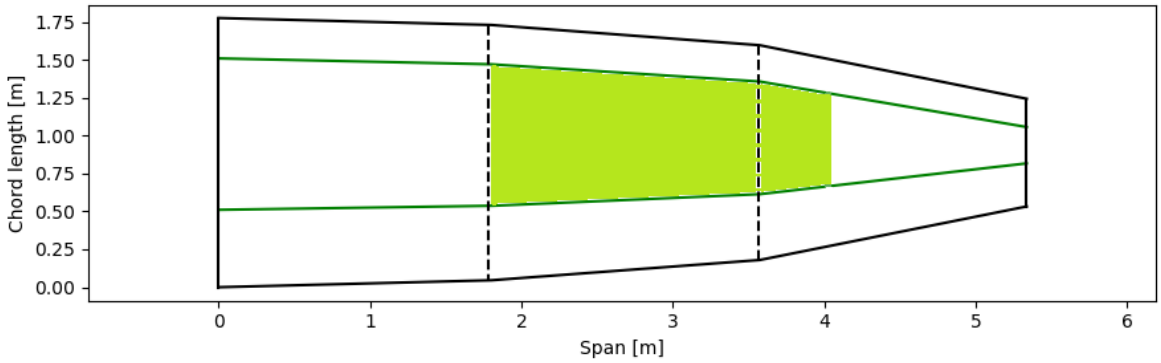

Figure 14.3: The placement of the fuel tanks in the wing

Since this is also an aerobatic aircraft with a low wing configuration, gravity will not feed fuel to the engine so an extra system is installed to feed fuel [10]. The aircraft therefore has two pumps installed: an electrical and mechanical pump (engine-driven). The electrical pump is used to start up the engine while the mechanical pump takes over once the engine is started. The fuel tanks will also be equipped with a system that can draw fuel from either tank so that the pilot can trim the aircraft laterally if necessary, this is also implemented for safety reasons. Additionally a separate small fuel tank is installed that will provide fuel during inverted flight, this fuel tank will be small and thus the time of inverted flight will be limited accordingly.

14.6. Landing gear system

The landing gear provides ground support to the aircraft, allowing it to taxi, take-off and land without causing damage to the structure. The undercarriage arrangement has been established during the conceptual design stage of the project, in which the most suitable configuration resulted to be a retractable tricycle landing gear. The main advantages of this type of landing gear are: good ground control in crosswinds, dynamic stability on the ground which makes it easier to manoeuvre and the fact that the shorter wheelbase permits a tight turning radius. The retractable features allows the aircraft to fly at a higher cruise speed due to the drag reduction. Since the landing gear is one of the most important mechanisms in the aircraft system, several of its key design features are addressed below.

14.6.1. Positioning

The landing gear must be positioned correctly with respect to the centre of gravity of the aircraft to allow for ease of rotation during take-off and to facilitate steering on the ground. The main landing gear position is determined by the need to achieve the former of the two, in addition to the most aft centre of gravity position and the propeller strike limit. On the other hand, the nose landing gear is positioned as to facilitate the latter, by ensuring that the nose is not overloaded for the entire range of centre of gravity locations. Using a geometrical layout approach [55] with the centre of gravity range determined in Section 12.1, the undercarriage position was determined and can be seen in Table 14.1. The datum is set at the nose of the aircraft. The wheel track was established such that the aircraft can have a turning radius of 60 m, which allows it to be easily steered on narrow runways and allows it to be comfortably stored between the fuselage and the first rib.

Table 14.1: Landing gear position and dimensions

Nose [x_N]	0.7 m	Wheelbase	2.32 m
Main [x_M]	3.02 m	Wheel track	4.64 m

14.6.2. Tyres and Wheels

The tyres of the landing gear are selected based on the static loads caused by the aft-most centre of gravity position in normal operations. An inertial load factor of 2 is considered to comply with the Certification Authorities [42]. Based on the resultant reaction loads the tyres were selected from a manufacturer, in this case Dunlop Aircraft Tyres. Additionally, based on the selected tyres the required internal pressure on the loaded tyres was determined using Equation (14.1) [55], where F is the load, and πab is the tyre footprint. Additionally, from the manufacturer the wheel size was obtained. The tyre and wheel specifications are presented in Table 14.2.

$$P = \frac{4F}{\pi ab} \tag{14.1}$$

Table 14.2: tyre and wheel specifications [94]

Main Landing Gear		**Nose Landing Gear**	
Tyre Type	III	Tyre Type	III
Ply Rating	10	Ply Rating	4
Reaction Load	709 lbs	Reaction Load	6576 lbs
Tyre Rated Load	800 lbs	Tyre Rated Load 6650 lbs	
Rated Inflation	126 psi	Rated Inflation	31 psi
Size	5.00-5 in	Size	7.00-8 in
Maximum Inflated Outside Diameter	21.36 in	Maximum Inflated Outside Diameter	14.2 in
Wheel Specified Rim Diameter	8 in	Wheel Specified Rim Diameter	5 in

14.6.3. Brakes

The two most common forms of breaks used in the aerospace industry are: drum brakes and disc brakes. Due to the fact that there is sufficient space in the wing to store the main gear, and in the nose to store the nose gear, the aircraft will be equipped with disc brakes as they have good heat dissipation, are lighter than drum brakes and are easier to maintain. Besides, drum brakes are outdated comparing to other brake methods. A component will be selected from a manufacturer, based on the kinetic energy of the aircraft that the brakes need to absorb. This is calculated using a conservative approach [55], from which the kinetic energy was found to be KE = 727 kJ. This was calculated using the stall speed during landing and the maximum landing weight.

14.6.4. Kinematics of the Landing Gear

An oleo-pneumatic shock absorber will be designed for both the nose and the main landing gear in the future stages of the design. In addition, due to difficulty of estimating the retraction and deployment loads during approach and transit with high accuracy [55], the landing gear actuation mechanism is also left for future design stages. In order to avoid the need for the pilot to opt for a belly landing in case the normal actuation system fails, an emergency actuation system which will allow the pilot to manually deploy the landing gear will be installed.

14.7. Avionics

To contribute to the 'ultimate' feel of the aircraft a glass cockpit was chosen as our main avionics system. The specific system is the Garmin G1000 with GFC 700 autopilot. These consist of two 10.4 in displays. Commonly one is configured as primary flight display (PFD) while the other is a multi-function display (MFD). This flight system is complemented by an array of switches and levers which actuate the lights, fuel system, landing gear, throttle etc. The panel itself will be simple to design and produce [49]. As an option the Garmin G3000 could be installed, but since the G3000 costs 3-4 times as much as the G1000 ($210000-$250000 depending on exact specification), this will be an optional upgrade whereas the standard version would have the G1000 installed.

14.8. Ballistic recovery system

The BRS (ballistic recovery system) is a system that releases a parachute in case something happens to the aircraft and there is a loss of control, to safely bring the pilot and his passengers back down to the ground. This will be an option provided to the customers and will not be provided as standard equipment because a BRS can weigh up to 100 kg and the aircraft was not initially designed to incorporate this.
There are many situations where a BRS could be used, to mention a few: loss of control of the aircraft such as a spin. If impossible to get out of the spin, the BRS can be activated and the aircraft will be safely brought back to the ground. Another dangerous situation could be a loss of consciousness of the pilot, a structural failure or an unlikely mid-air collision. According to Cirrus, up to 85 lives have been saved by it up to date and 120 could have been saved with the BRS if they would have activated it [32].
The parachute is stored in the back of the fuselage with two cables attached to the front of the fuselage and one cable attached to the aft part of the fuselage. The cables are embedded in the fuselage by fragile material so that it can come lose easily and the aerodynamic shape of the fuselage is maintained. When the BRS is activated a solid rocket will launch the parachute out of its container and the chute will decelerate the aircraft and bring it to the ground. A schematic representation of the BRS is shown in Figure 14.4.

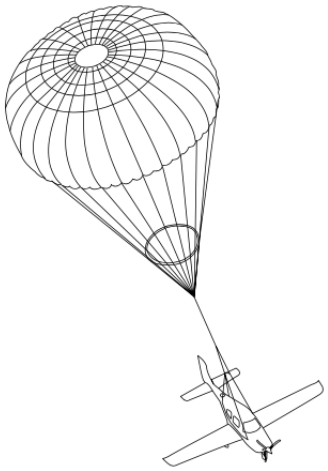

Figure 14.4: Schematic representation of a BRS [32]

15

Configuration

This chapter shows the basic specifications and geometry of the aircraft. The most important specs of the aircraft are found in Table 15.1.

Table 15.1: Aircraft Specification Sheet

Parameter	Value	**Parameter**	Value
Airfoil	Custom	Material type	Sandwich
S	15.12 m^2	Laminate material	Carbon
S_h	1.68 m^2	Honeycomb material	Kevlar
S_{elev}	0.64 m^2	Skin thickness wing	2 mm
S_{ailer}	0.91 m^2	Honeycomb thickness wing	1.5 cm
S_{rud}	0.86 m^2	Skin thickness tail	1 mm
Wing span	10.54 m	Honeycomb thickness tail	1.5 cm
Aspect ratio	7.35	Skin thickness fuselage	2.1 mm
Oswald factor	0.58	Honeycomb thickness fuselage	0.5 cm
L/D_{max}	17.55	Maximum Take-Off Weight	1657.57 kg
Flap type	Slotted	Operating Empty Weight	907.01 kg
$CL_{max,TO}$	1.8	Max Payload Weight	444 kg
$CL_{max,Land}$	1.952	Mission Fuel weight	300 kg
V_{cruise}	250 kn	Max Fuel Weight	450 kg
V_{eff}	207 kn	Aerobatic Weight	1397 kg
V_{max}	299 kn	Number of seats	4
Mission range	1422 km	Engine	Ivchenko AI-450C
Ferry range	4213 km	Avionics	Garmin G1000
Rate of Climb	17.3 $m\,s^{-1}$	Climate control	Air-conditioning
Roll rate	180 $°s^{-1}$	Ice protection	Electro-thermal
Gliding range	133.7 km	Fuel tanks	Bladder,1 per wing
Take-off distance	373.4 m	Tires	Dunlop type III
Landing distance	496.8 m	Brakes	Disc
Service Ceiling	25000 ft	Ballistic Recovery System	Optional Parachute
Fuel consumption	5.7 $km\,l^{-1}$	Listing Price	920,000 $
Power	450 hp	Operating cost	229 $/hr

A Catia model of the aircraft was constructed for visual purposes. Renders of the model from different angles can be seen below.

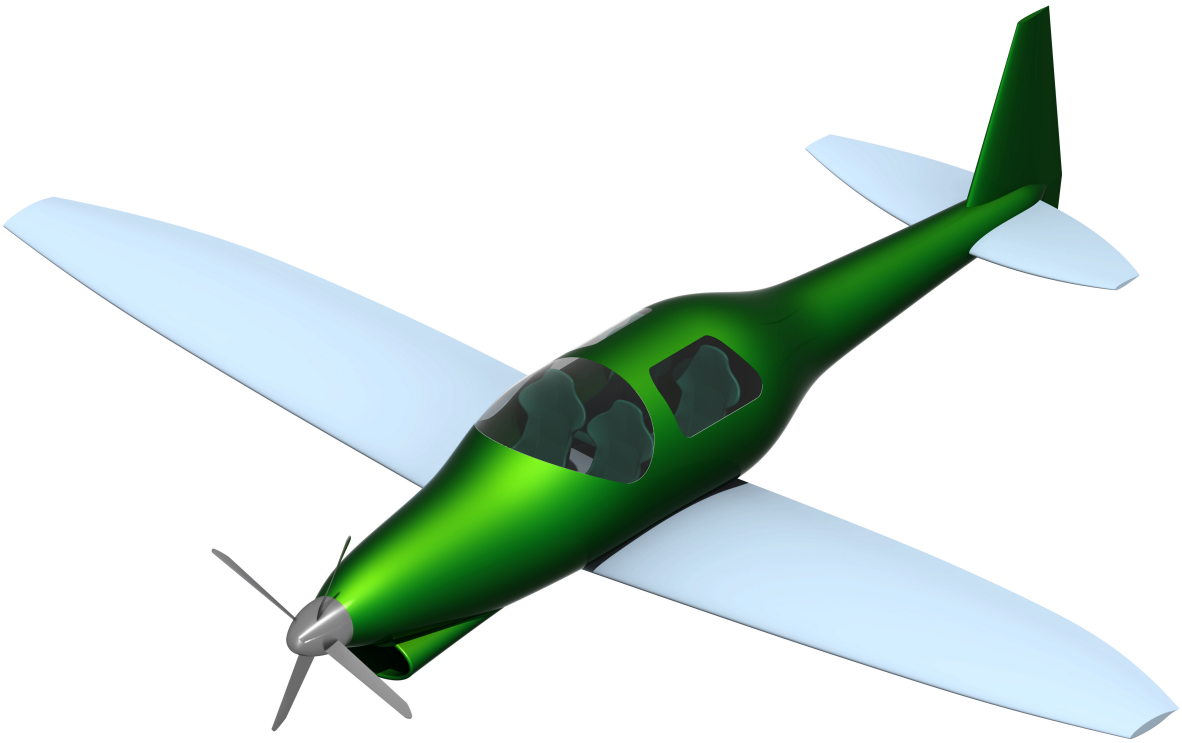

Figure 15.1: CATIA render of the aircraft. Isometric view.

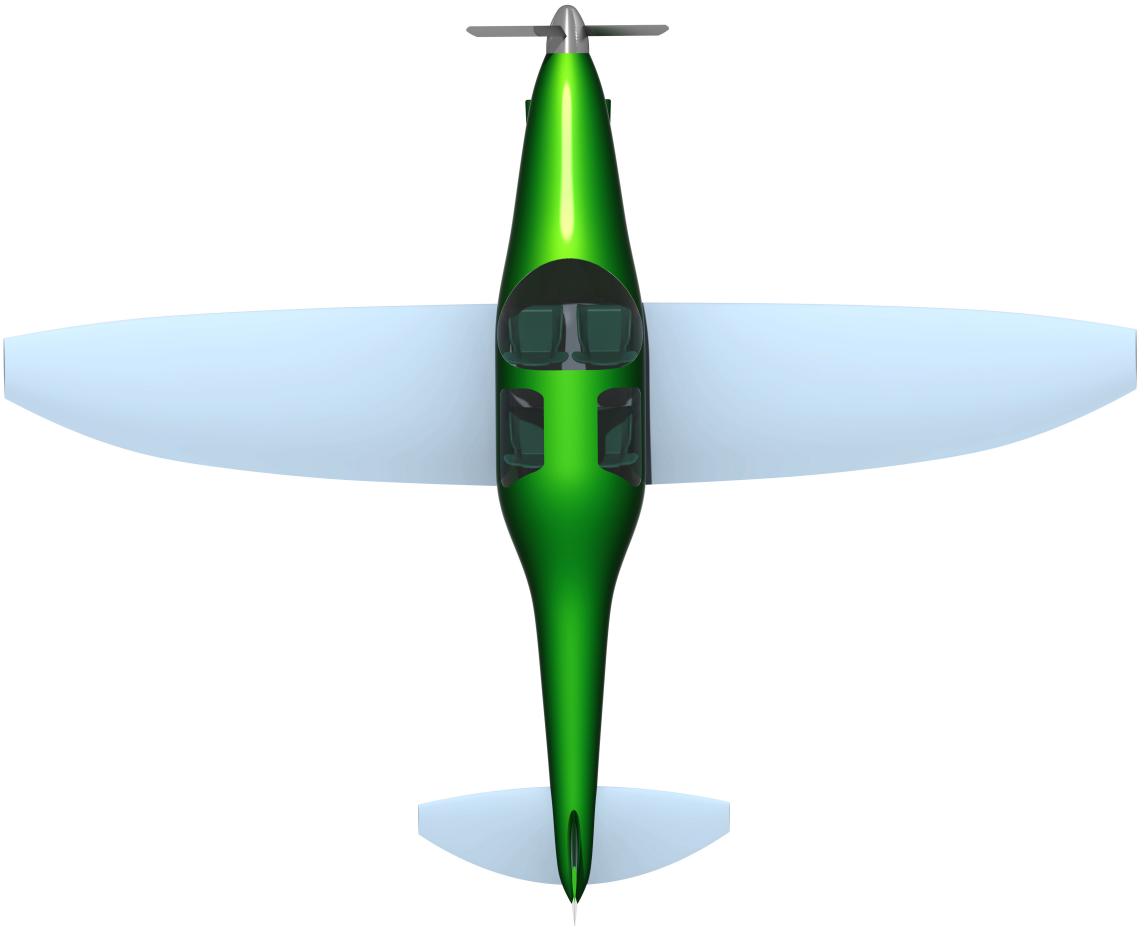

Figure 15.2: CATIA render of the aircraft. Top view.

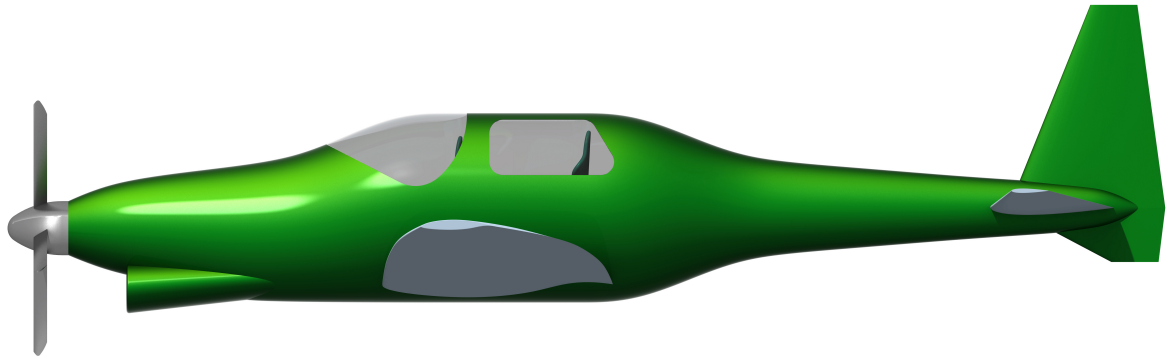

Figure 15.3: CATIA render of the aircraft. Side view.

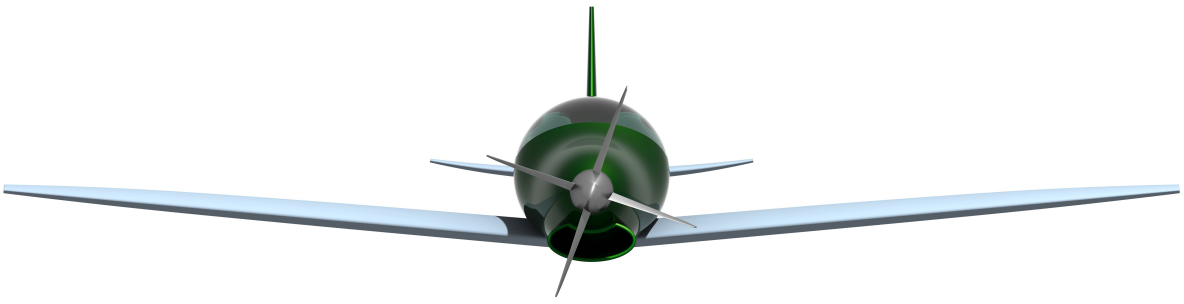

Figure 15.4: CATIA render of the aircraft. Front view.

16

Resource budget

In the baseline report a first resource budget plan was presented, this chapter covers an updated version as well as an evaluation of the resource budget plan.

16.1. Mass Budget

During the design process of an aircraft parameters change all the time and one of the most important ones for an aircraft is the mass. The mass has an impact on and is impacted by practically all design parameters. Therefore it is a major indicator for the design. Keeping the mass of the aircraft as low as possible is of great importance. A limit of 2000 kg MTOW is set by mission requirement **REQ-MIS-01**. Experience from other aircraft design processes indicates that over the course of the process the mass is almost certainly bound to increase. To make sure that the requirement is met by the final design a contingency plan has been devised in the earlier baseline report. The contingency plan states that during the baseline phase of the design a 20% contingency factor was to be used, meaning that during that phase of the design the aircraft was being designed for a MTOW of 1600 kg instead of the limit of 2000 kg. This ensured that during the design the mass was allowed to increase within the stated limits. For later stages lower contingencies were used as the design will be more detailed and less parts of the design are bound to change. For the final report a contingency factor of 10% was selected, which means that at the end of this stage the MTOW should not exceed 1800 kg. If it does exceed this value, some potentially major changes are to be made to the design to ensure it will comply with the requirements at later stages.

One of the most important parameters of the aircraft is the operating empty mass. This mass consists of all the structural weight and equipment fitted to the aircraft. For the structural mass of the aircraft a detailed estimation has been made by the structural model as presented in Chapter 7. However, with the exception of the avionics and the engine, no detailed mass estimation has been made for the other equipment on board. Instead, a mass estimation has been made on the basis of the class II estimation from Roskam [86]. An overview of all masses is given in Table 16.1

16.2. Evaluation

Figure 16.1 presents the evolution of the MTOW during the different stages of this project. Also, it shows the contingency at that stage and the final requirement of 2000 kg.

At this stage of the design the MTOW is 1658 kg, which is well under the limit of 1800 kg it should achieve to comply with the contingency factor of 10%. This means no radical changes need to be made to the design to reduce its mass at this point. However, it should be noted that some systems still use estimations made at an earlier stage. For example for the furnishing weight the class II estimations are still used. These subsystems that do not have an updated mass assigned might thus still increase the MTOW by more than would otherwise be expected at this stage. This mass increase is expected to stay within the proposed contingency value for the current stage and eventually also within the ultimate value of 2000 kg at the end of the design process.

Table 16.1: Aircraft component mass

Component	Weight [kg]
Installed Power plant	215
Avionics	20.0
Fuel system	39.7
Landing Gear	47.6
Flight Controls	84.1
Electrical System	68.7
Anti Icing + Pressurisation	39.1
Oxygen system	4.7
Furnishing	50.7
Wing structural mass	139
Empennage structural mass	17.0
Fuselage structural mass	182
Total operating empty mass	907

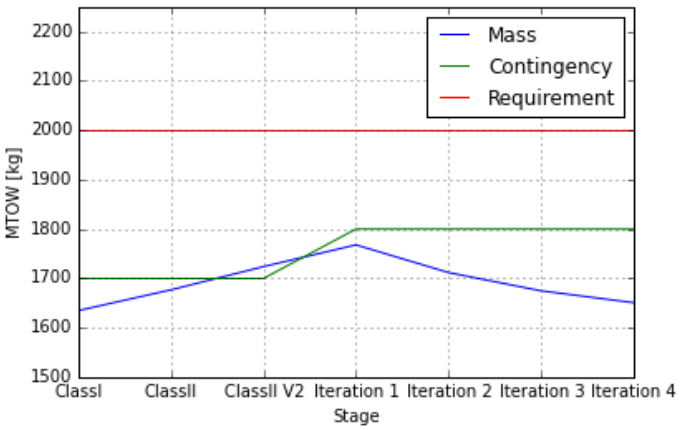

Figure 16.1: MTOW during different stages of the project

17

System interactions

This chapter shows the communication within the aircraft system, which is necessary for successful mission completion. Section 17.1 represents the relationships between the aircraft during operation and the surroundings, like other aircraft and ground segment, while Section 17.2 covers electrical communication within the aircraft. A short introduction on the Garmin G1000 system is given in Section 17.3.

17.1. Communication Flow

During the actual flight, the aircraft is not going to fly being isolated from the world. It is going to have a communication system, which is going to ensure efficient and safe flight not only for the aircraft itself, but for other air traffic as well.

The general communication flow diagram is presented in figure Figure 17.1. Rectangular blocks contain items aboard the aircraft, rhombic blocks represent the human segment, and elliptical blocks contain items not included within the aircraft.

In the aircraft communication system, there are 2 segments represented by humans: the pilot, who makes decisions regarding the aircraft operations and aircraft traffic control, which monitors the air traffic to ensure safe flights for everyone. Between themselves they communicate during ground flight phases (namely take-off and landing) to ensure smooth take-off and landing runway operation, and during the flight when it is necessary. Also, the pilot receives the cruise data (such as airspeed, altitude, angle of attack, surrounding air traffic, weather) that the avionics screen displays during the flight. In case of collision risks, which can be observed on the traffic map, traffic control can communicate directly to the pilots and prevent the collision through slight changes to flight paths.

The aircraft avionics is the primary data collector and storage unit in the aircraft. It receives the information from the aircraft ambient sensors which, in processed form, is displayed on the screen, sent to the company operations and control centre (collected data can be used to improve the aircraft model, especially in early days of the company). Communications to the company data control centre is entirely optional, as some customers might prefer to operate the flight privately, however this data might greatly benefit reliability and maintainability by identifying the least reliable aircraft subsystems.

Although ambient sensors of the aircraft can sense approaching weather, it is too short-term to be useful. For this reason, automated weather observing system (AWOS) collects as accurate as possible weather changes, transmits the resultant weather map to the aircraft avionics. Pilot can analyse the approaching weather and possibly change the course in case undesirable weather is inbound.

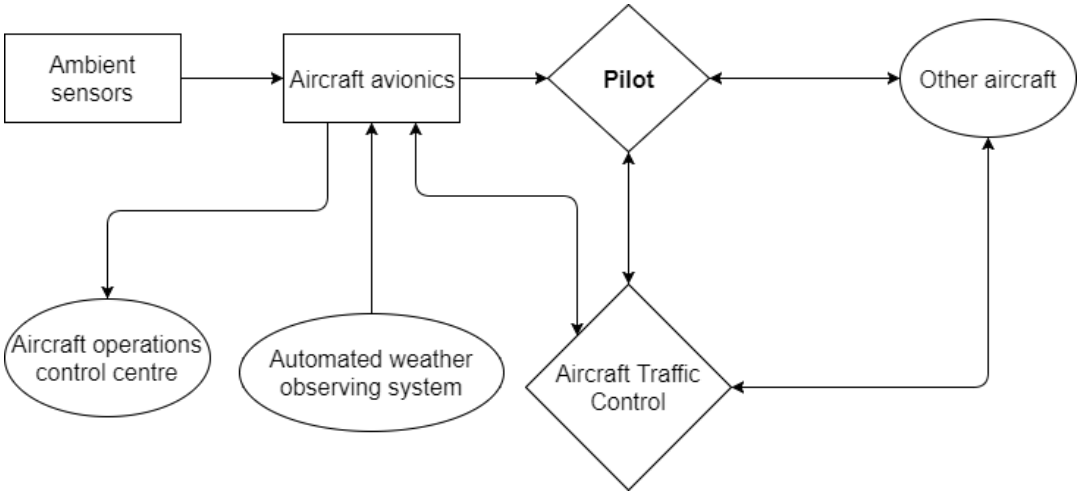

Figure 17.1: Communication diagram during aircraft operation

Like all other aircraft, VHF (very high frequency) bands are going to be used for the communications, namely frequencies between 108 and 137 MHz. For this purpose, several antennae (both transmitters and receivers) have to be placed on the aircraft structure. Antennae are going to be placed on the top and bottom of the fuselage, the exact amount and locations are going to be determined in later stages of the design.

17.2. Electrical Diagram

The electrical is presented in the Figure 17.2. During start-up, when the engine is not providing electrical power to generator yet, the battery is used to operate the required items: avionics, communication, lights (if necessary), de-ice system (if necessary), engine and environmental control (if necessary). The battery charges during the flight using the power from the generator. In case of generator failure, the battery can be used as a back-up source of electricity. In this emergency case, the performance of the electricity consuming systems can be adjusted so the battery charge is sufficient to operate the aircraft until an emergency landing can be made.

An additional item listed on the diagram is the outlets. These outlets can be used as a source of electricity for the passengers in case if they need it for tasks like charging the mobile phone or laptop. This is a useful feature for example for customers who use aircraft primarily for cruise, and want to use and charge their electronics during the flight. There is no need for these outlets to operate from the battery, as they are purely for passenger comfort and entertainment.

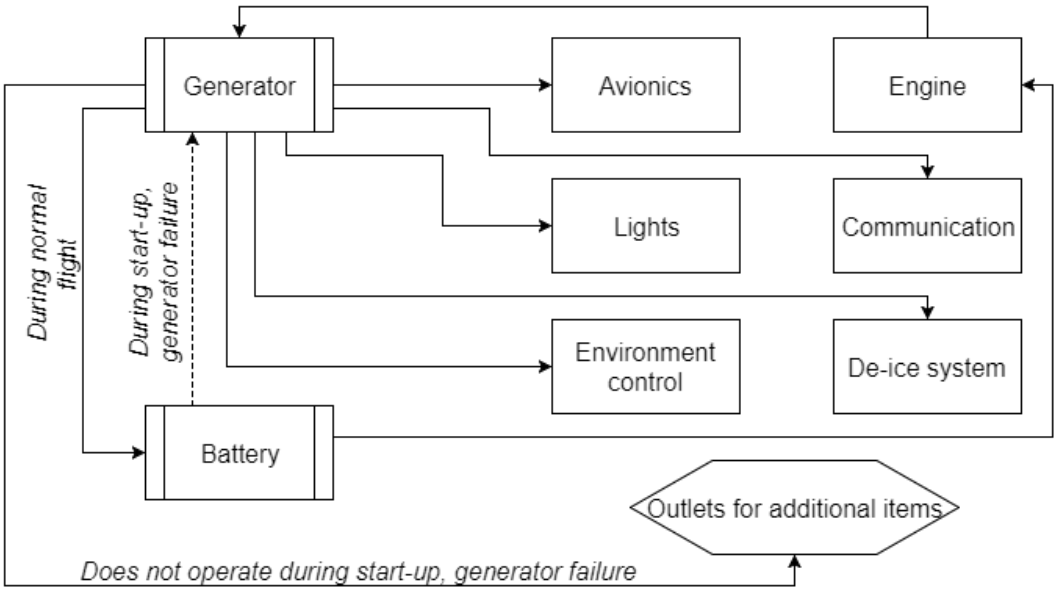

Figure 17.2: Electrical communication diagram

17.3. Avionics Hardware Diagram

The G1000 Flight Deck includes practically all avionics systems the aircraft needs to operate. As stated before, the unit consists of two 10.4 in displays which present all the flight information on a primary flight display (PFD) and a multi-functional display(MFD) and a so called Audio Panel which controls communications and marker beacon controls for ILS operations. All are connected to two Integrated Avionics Units which link the sensors to the displays and the audio panel. A detailed bock diagram is presented in Figure 17.3.

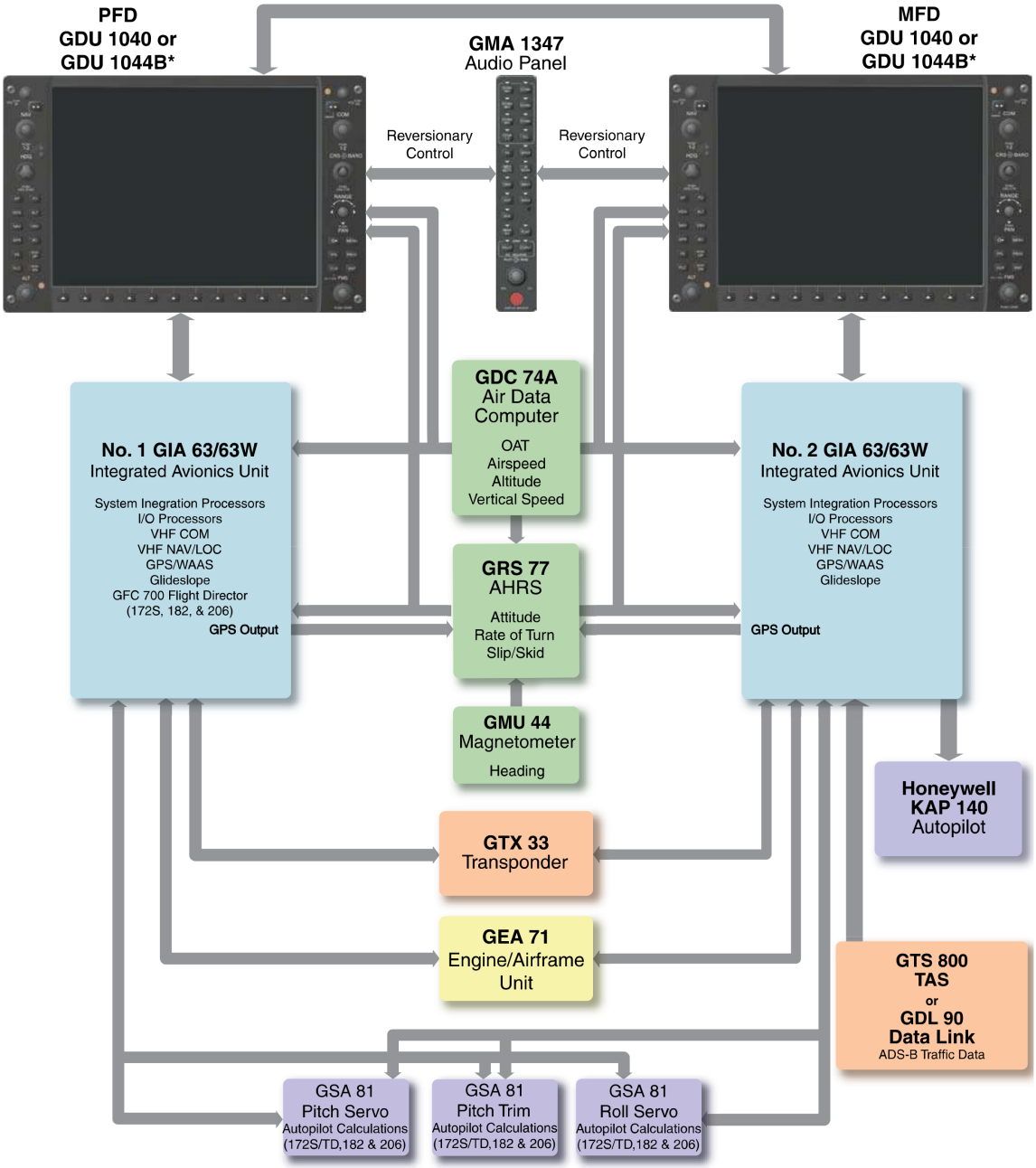

* The GDU 1040 is available in systems not using the GFC 700 Automatic Flight Control System.
The GDU 1044B is available in systems using the Garmin GFC 700 Automatic Flight Control System.

Figure 17.3: Hardware diagram for the Garmin G1000 Integrated Flight Deck [50]

18

Risk analysis

This chapter deals with analysing the risks that could be encountered during operation of the aircraft and proposes mitigation efforts. The identification of risks is presented in Section 18.1. For the unacceptable risks mitigation efforts are proposed in Section 18.2 and a risk map is presented. For all cases where inspection is required, for example after an incident, the inspection should be executed in a way that is suitable for the honeycomb composite material that is used, namely (ultra-)sonic inspection methods.

18.1. Risk identification

For the identification of the different operational risks a division of risk categories was devised and subsequently the risks within each category were determined:

- FO - Foreign objects
  - FO-1 - Small bird impact: a small bird, like a sparrow, striking the aircraft.
  - FO-2 - Big bird impact: a big bird, like a goose, striking the aircraft.
  - FO-3 - Stones and gravel impact: during take-off and landing stones can be swept up from the ground and hit the aircraft.
- WC - Weather conditions
  - WC-1 - Lightning strike: the current should be able to flow through the fuselage exterior easily to prevent damage due to excessive temperatures.
  - WC-2 - Hail impact: large hailstones can damage aircraft surfaces.
  - WC-3 - Excessive crosswind: excessive crosswinds can cause disaster during landing or take-off.
  - WC-4 - Icing: the build-up of ice on lifting surfaces or the propeller can hinder airflow and severely degrade the aerodynamic and propulsive properties.
  - WC-5 - Heavy turbulence: excessive turbulence can cause loading of the structure beyond the loading limits.
- System failure
  - SF-1 - Loss of fuel feed: during aerobatic manoeuvres and in particular during inverted flight the fuel feed could be impacted.
  - SF-2 - Loss of pressure: could be due to a decompression situation or failure of the pressurisation system. Lack of oxygen could incapacitate pilots and passengers if a safe altitude is not reached in time.
  - SF-3 - Control system failure: can lead to loss of control in different degrees.

  - SF-4 - Electrical system failure: will leave the avionics without power and therefore the pilot without instruments and possibly with limited controls.
  - SF-5 - Loss of communication: leaves the pilot unable to communicate with air traffic control (ATC).
  - SF-6 - Loss of navigation: leaves the pilot unable to navigate using the electronic systems.
  - SF-7 - Landing gear failure: either the landing gear cannot be extended or locked.
  - SF-8 - Engine failure: loss of engine power.
- Pilot failure
  - PF-1 - Tail strike: when the tail strikes the runway during rotation on take-off or during landing.
  - PF-2 - Mid-air collision: when the aircraft collides with another aircraft in mid-air.
  - PF-3 - Ground collision: when the aircraft collides with an object on the ground.
  - PF-4 - Wheelbarrowing: when the aircraft lands in such a way that excessive forces are placed on the nose wheel or when the propeller strikes the runway.
- Structural failure
  - ST-1 - Delamination: specific failure mode of composite panels where one or both sheets come loose from the core structure.
  - ST-2 - Crack propagation: growth of tiny cracks in the structure over time due to repetitive loading.
  - ST-3 - Propeller separation: where a crack in a propeller blade grows over time and eventually leads to loss of the propeller during operation.
  - ST-4 - Exceeding ultimate loading: where the aircraft is loaded such that the ultimate loading is exceeded.
- Miscellaneous
  - MS-1 - Fire: in-flight fire can lead to many subsequent failures and smoke can cause incapacitation of the pilot and passengers.

The risks are shown in Table 18.1, together with their probability of occurrence and the severity of the associated consequences. The probability of occurrence ranges from improbable and possible to probable and certain. The consequences range from:

- **Negligible**: Results in slight damage to the aircraft, but the mission can be continued and repair can wait until the next scheduled maintenance.
- **Minor**: Results in repairable damage to the aircraft that can possibly require abortion of the mission, also repair or patching should occur before another flight.
- **Moderate**: Results in damage to the aircraft, possible bodily harm and immediate abortion of the mission.
- **Major**: Results in major damage to the aircraft and considerable bodily harm.
- **Severe**: Results in loss of the aircraft and most likely also loss of life.

The above is a rough indication as the outcome of situations that can arise strongly depends on factors such as weather conditions, pilot experience, incident location and flight phase.
The last column of the table shows whether the risks are considered acceptable or whether they require mitigation efforts. The associated mitigation efforts are presented in Section 18.2, a pre-mitigation risk map is shown in Table 18.1.

Table 18.1: Unmitigated operational risk events

ID	Risk	Probability	Consequence	Acceptable risk
FO	**Foreign objects**			
FO-1	Small bird impact	Probable	Moderate	No
FO-2	Big bird impact	Possible	Major	No
FO-3	Stones and gravel impact	Probable	Negligible	Yes
WC	**Weather conditions**			
WC-1	Lightning strike	Probable	Major	No
WC-2	Hail impact	Probable	Moderate	No
WC-3	Excessive crosswind	Probable	Major	No
WC-4	Icing	Certain	Major	No
WC-5	Heavy turbulence	Probable	Moderate	No
SF	**System failure**			
SF-1	Loss of fuel feed	Probable	Moderate	No
SF-2	Loss of pressure	Improbable	Severe	No
SF-3	Control system failure	Possible	Major	No
SF-4	Electrical system failure	Possible	Major	No
SF-5	Loss of communication	Improbable	Negligible	Yes
SF-6	Loss of navigation	Improbable	Negligible	Yes
SF-7	Landing gear	Improbable	Major	Yes
SF-8	Engine failure	Improbable	Major	Yes
PF	**Pilot failure**			
PF-1	Tail strike	Possible	Moderate	No
PF-2	Mid-air collision	Improbable	Severe	Yes
PF-3	Ground collision	Improbable	Moderate	Yes
PF-4	Wheelbarrowing	Improbable	Major	Yes
ST	**Structural failure**			
ST-1	Delamination	Probable	Major	No
ST-2	Crack propagation	Probable	Major	No
ST-3	Propeller separation	Possible	Major	No
ST-4	Exceeding ultimate load	Improbable	Severe	Yes
MS	**Miscellaneous**			
MS-1	Fire	Possible	Severe	No

Probability / Impact	Negligible	Minor	Moderate	Major	Severe
Certain				WC-4	
Probable	FO-3	FO-1	WC-2, WC-5 SF-1	WC-1, WC-3 ST-1, ST-2	
Possible			PF-1	FO-2 SF-3, SF-4 ST-3	MS-1
Improbable	SF-5, SF-6		PF-3	SF-7, SF-8 PF-4	SF-2 PF -2 ST-4

Figure 18.1: Risk map before proposed mitigation efforts

18.2. Proposed mitigation efforts

For each risk that was determined to require mitigation a mitigation effort is proposed. Mitigation is done in thee ways, either by decreasing the probability, by decreasing the consequence or by doing both. The resulting list of mitigated risks is shown in Table 18.1. The risk events after the proposed mitigation efforts are presented visually in Figure 18.2.

- FO - Foreign objects
  - FO-1 - Small bird impact: the consequence is reduced to minor by ensuring that the structure or propeller can withstand the impact of a small bird without posing danger to the mission. The impacted area should be inspected thoroughly after the incident.
  - FO-2 - Big bird impact: the probability is expected to be reduced to improbable by implementation of an effective bird dispersal strategy by the airports, which is where bird strikes occur most often.
- WC - Weather conditions
  - WC-1 - Lightning strike: the probability is reduced to possible by avoiding flight through lightning storms. The consequence is reduced to minor by making the outside surface conductive using for example a metal mesh or conductive surface treatments. Extra attention will be paid to the most likely points of entry. The impacted area should be inspected thoroughly after the incident.
  - WC-2 - Hail impact: the probability is reduced to possible by avoiding flight through hail storms. The consequence is reduced to minor by ensuring that the structure or propeller can withstand the impact of hail without posing danger to the mission. The impacted area should be inspected thoroughly after the incident.
  - WC-3 - Excessive crosswind: the probability is reduced to possible by informing with ATC about local weather conditions beforehand and diverting when wind speeds exceed limits.
  - WC-4 - Icing: the probability is reduced to improbable by applying de-icing before take-off in freezing conditions and by installing an anti-icing system on vulnerable surfaces.
  - WC-5 - Heavy turbulence: the probability is reduced to possible by avoiding turbulent areas based on weather reports and info from other pilots.
- System failure
  - SF-1 - Loss of fuel feed: the probability is reduced to improbable by installing a small tank that supplies fuel specifically during inverted flight and the maximum time of inverted flight is mentioned in the flight manual.

  - SF-2 - Loss of pressure: the consequence is reduced to minor by providing small emergency oxygen tanks for each occupant, allowing the pilot to descend to a safe altitude.
  - SF-3 - Control system failure: the probability is reduced to improbable by implementing redundancies in the system.
  - SF-4 - Electrical system failure: the consequence is reduced to minor by installing a back-up system that provides power for vital flight instruments.

- Pilot failure
  - PF-1 - Tail strike: the consequence is reduced to minor by ensuring the structure can withstand the impact. The impacted area should be inspected thoroughly after the incident.

- Structural failure
  - ST-1 - Delamination: the probability is reduced to possible through regular visual inspections as well as extensive non-destructive inspections. The consequence is reduced to minor by designing the structure such that it is able to sustain ultimate loads with non-visible delamination present.
  - ST-2 - Crack propagation: the probability is reduced to possible through regular visual inspections as well as extensive non-destructive inspections. The consequence is reduced to minor by designing the structure such that it is able to sustain ultimate loads with non-visible cracks present.
  - ST-3 - Propeller separation: the probability is reduced to improbable through regular inspections and by prescribing clear life time limitations.

- Miscellaneous
  - MS-1 - Fire: the probability is reduced to improbable through usage of non-flammable materials wherever possible. The consequence is reduced to moderate by installing fire extinguishing systems and providing manual fire extinguishers to fight fire and by installing fire walls to isolate fire.

Probability \ Impact	Negligible	Minor	Moderate	Major	Severe
Certain					
Probable	FO-3	FO-1			
Possible		WC-1, WC-2 SF-4 PF-1 ST-1, ST-2	WC-5		
Improbable	SF-5, SF-6	SF-2	PF-3 SF-1 MS-1	WC-3, WC-4 PF-4 FO-2 SF-3, SF-7, SF-8 ST-3	PF-2 ST-4

Figure 18.2: Risk map after proposed mitigation efforts

Table 18.2: Mitigated operational risk events

ID	Risk	Probability	Consequence	Acceptable risk
FO	**Foreign objects**			
FO-1	Small bird impact	Probable	Minor	Yes
FO-2	Big bird impact	Improbable	Major	Yes
WC	**Weather conditions**			
WC-1	Lightning strike	Possible	Minor	Yes
WC-2	Hail impact	Possible	Minor	Yes
WC-3	Excessive crosswind	Improbable	Major	Yes
WC-4	Icing	Improbable	Major	Yes
WC-5	Heavy turbulence	Possible	Minor	Yes
SF	**System failure**			
SF-1	Loss of fuel feed	Improbable	Moderate	Yes
SF-2	Loss of pressurisation	Improbable	Minor	Yes
SF-3	Control system failure	Improbable	Major	Yes
SF-4	Electrical system failure	Possible	Minor	Yes
PF	**Pilot failure**			
PF-1	Tail strike	Possible	Minor	Yes
ST	**Structural**			
ST-1	Delamination	Possible	Minor	Yes
ST-2	Crack propagation	Possible	Minor	Yes
ST-3	Propeller separation	Improbable	Major	Yes
MS	**Miscellaneous**			
MS-1	Fire	Improbable	Moderate	Yes

19

Manufacturing, Assembly and Integration Plan

One of important considerations during the aircraft design is planning the manufacturing and assembly process. This needs to be done to make sure that the design is not only possible to be created, but also does not require too high costs to do so. This chapter presents the production plan related to the aircraft manufacturing and assembly. First, the material considerations are discussed in Section 19.1, then the manufacturing process is covered in Section 19.2, and finally the assembly process is explained in Section 19.3.

19.1. Material considerations

The material selected for the airframe structure is a composite sandwich with a Kevlar honeycomb core and carbon fibre facesheets. The consequence of this lightweight composite material is more complex manufacturing processes when compared to metal. The composite-specific considerations are discussed in this section.

First of all, the honeycomb composite is very stiff when shaped and fully cured. This means that forming the parts to obtain the correct shape with a high degree of precision is extremely important. Otherwise, the manufactured part simply will not be able to be matched to its neighbouring parts. Such a situation would most likely require remaking the part entirely from scratch.

Secondly, assembly of composite honeycomb parts requires adjusting the thickness of the connected surfaces for easier adhesive connectivity. This is not difficult to do at the edges of the details, however at non-edge locations such as spar locations this might be harder to achieve. This is compensated, however, by the fact that honeycomb wingbox does not require stiffeners to be strong enough in sustaining the loads. Thereby the amount of produced parts and connections is reduced.

For the sandwich composite production all elements (namely carbon fibre facesheets, the honeycomb core, the resin and the adhesive film) will have to be purchased from their respective suppliers. To put the elements together and produce the parts it is best to use an autoclave.The layers are going to be put together and placed in a chamber which provides the required pressure and temperature for successful curing. After the period of time required for the adhesive to cure properly has passed, the panel can be cooled down and then it is ready to be used in the assembly process. Two concerns related to this method are the required precision with respect to the shapes and dimensions of cured parts and making sure the layers of the sandwich are not damaged and preserve their mechanical properties.

To address the difficulties of composite sandwich manufacturing a carefully setup and executed quality control procedure is essential. Special focus must be payed to the dimension accuracy and the absence of damage to the part. For the shape and dimension quality control, visual inspection and measuring can be applied.

19.2. Manufacturing process

The proposed manufacturing process is presented in the Figure 19.1. In the figure rectangular shapes represent items which are going to be purchased from suppliers. The elliptical shapes represent items which will be manufactured at the production location.
For the airframe, the carbon fibre facesheets are manufactured using the purchased carbon fibres and resin at the production location because of the specific required shapes. These laminate sheets are then combined into the sandwich structure using the purchased adhesive and honeycomb.
Elements like windows, landing gear and control surface mechanics need to be tailored according to the needs of the design and are acquired from other companies. Systems like avionics and engine are purchased off-the-shelf.

19.3. Assembly

The primary assembly method for the aircraft components is going to be adhesive connection. Both film adhesives and pasta adhesives are suitable for the assembly, so the selection criteria for the adhesive are likely going to be the price, density, operating temperature and highest loading [3].
The assembly plan can also be seen in the Figure 19.1. Firstly, the main structural components are going to be completed separately: both wings, both horizontal tail sections, vertical tail and the fuselage. The fuselage does not necessarily need to be filled with all the items related to it, only major and non-moveable ones. Then the main components have to be carefully connected to each other. Finally, when the adhesives are properly cured, small electrical and furniture items can be installed.

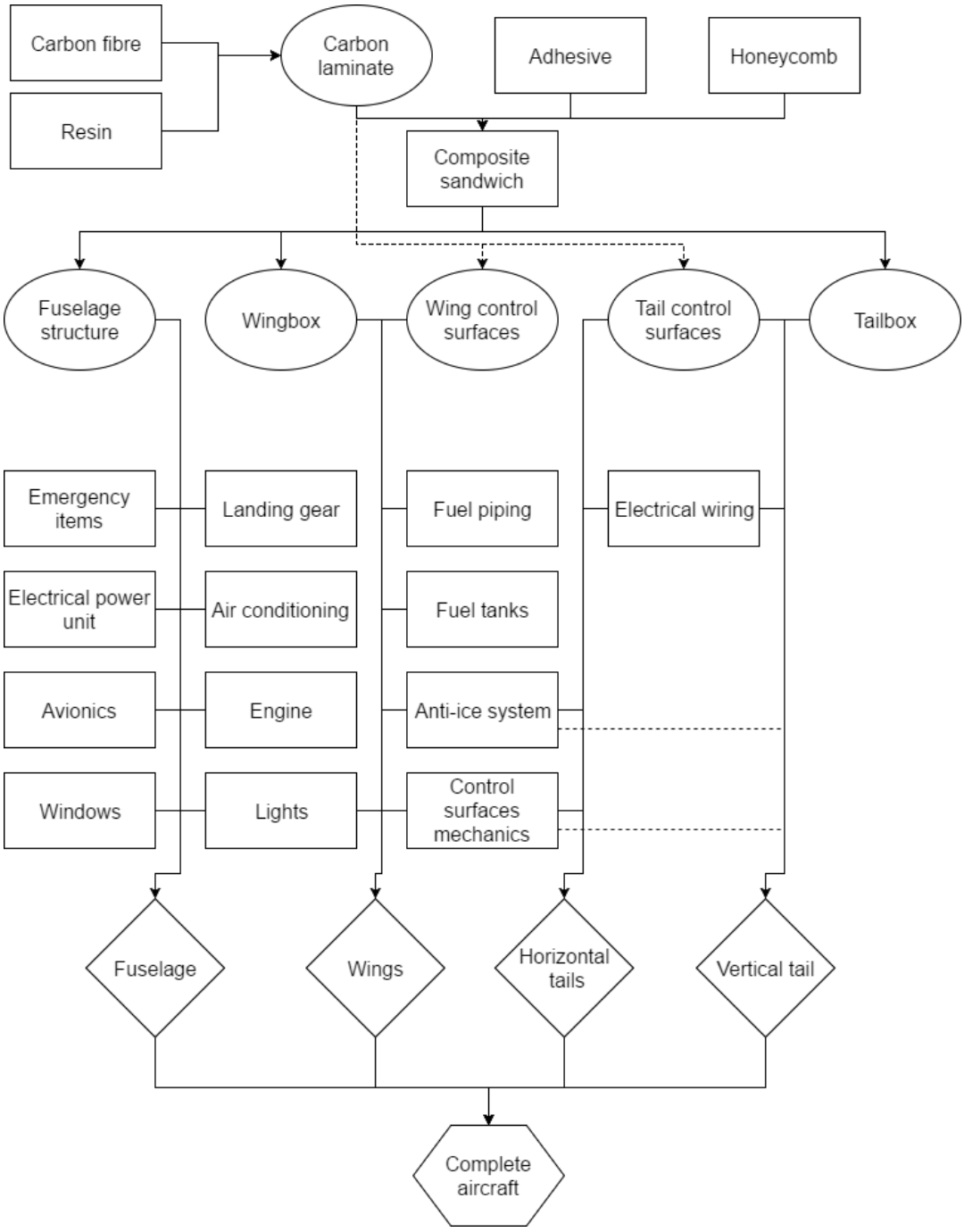

Figure 19.1: Manufacturing and assembly order related to the aircraft construction

20

Operations & logistics

The lifecylce of an aircraft does not consist only of the aircraft itself - it requires a variety of ground support items to ensure the efficiency of every aircraft stage of life. After the aircraft design is complete, the recurring activities together with required ground support are outlined in Figure 20.1. Elliptic blocks contain the stage of aircraft life, and rectangular blocks contain ground support elements which contribute to the respective stage.

Upon the design completion, the actual aircraft has to be built first. In order to manufacture the aircraft, the required *raw materials and parts* produced by outside companies have to be brought to the *manufacture and assembly site*. In order to know which parts and materials are needed and in which quantities, exact *part description* with all the dimensions is required as well. Finally, the aircraft has to be manufactures and quality controlled by the *assembly location personnel*.

The assembled aircraft has to be certified (in the case if it is not certified yet) and tested for quality. The certification is conducted by the *European Aviation Safety Agency* (EASA). First, they need to investigate the *documented design outcome* to know exactly the purpose of the aircraft and what it consists of. Secondly, they generate the *list of requirements* which need to be demonstrated to them in order to certify the aircraft. Then, the demonstration occurs, after which the certificate is given if all requirements are successfully met. If the design is certified, after each produced aircraft of this design a shorter version of certification can be done by the manufacturer to make sure that the aircraft is correctly assembled and is safe to fly.

After the design is certified and is ready to fly, it has to be sold to the customers to actually make profits. In fact, *advertising* the design can start even during the development stage, as more customers might be attracted and maybe even invest in the project. To support advertising, the *customer support* has to be available for a reasonable amount of time in order to answer the questions of interested in the design individuals. After the certification, every successfully attracted customer starts a new aircraft cycle, as it has to be manufactured and tested for that customer.

Finally, the aircraft is built, validated and sold to a customer, so he or she can actually use it. In order to do that however, the customer has to be trained to operate and support the aircraft in the provided *training facilities*. The customer should also have space to *store* the aircraft. In order to maintain safety and functionality of the aircraft, it has to go through regular maintenance program, done by dedicated *maintenance personnel*. Finally, in case of any questions, the customer should be able to contact the *customer support desk*.

When the aircraft reaches the end of operational life, it has to be properly disposed with the guidance of Aircraft Fleet Recycling Association. The aircraft has to be brought to the *dismantling facility*, where it can be properly recycled for items which still can be reused. These parts can then be used to manufacture and assemble a new aircraft, which benefits sustainability of the design a lot.

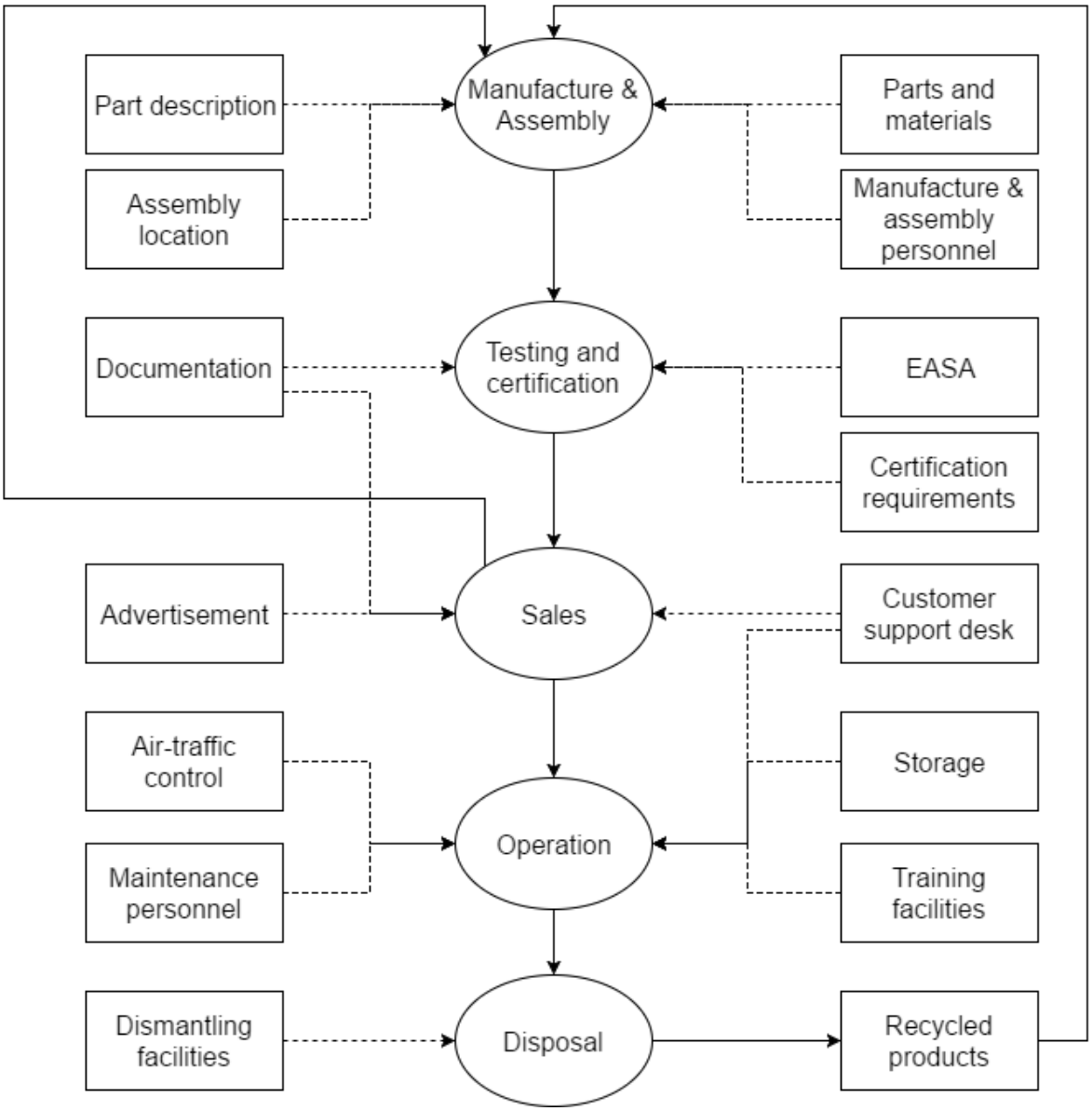

Figure 20.1: Operations Diagram

21

RAMS Analysis

The incorporation of the reliability, availability, maintainability and safety (RAMS) concepts in the design, production and operation of the aircraft, is required to ensure that the resultant product satisfies the customer needs. This chapter presents the RAMS analysis of the design and proposes future programmes to ensure that these concepts are maintained at an acceptable level throughout the life cycle of the product. First, the reliability of the design and the reliability programme are outlined in Section 21.1. Secondly, Section 21.2 addresses the maintainability of the aircraft. Section 21.3 discusses the relationship between reliability, maintainability and availability and provides a brief overview of the availability of the design. Finally, Section 21.4 details the methods for design for Safety. The procedures and methods employed in all analyses are presented in the System Engineering & Technical Management guide [56].

21.1. Reliability

Reliability can be defined as the probability that a system will perform in a satisfactory manner for a given period of time when used under specified operating conditions. The reliability of the system and its subsystem are modelled by the failure density function and the hazard function from which reliability factors, such as the the dispatch reliability and mean time between unscheduled removal, are derived. In general, each subsystem is divided to a basic component level, which is connected to other components in either series or parallel networks. In a series network all components must function properly, while in a parallel network all components must fail in order to cause system failure. Parallel networks generate redundancies in the design which increase the overall reliability of the system, thus they are desirable for the aircraft.

However, since the design is still currently in the preliminary stage not all subsystem parts and components have been selected or designed. Although the above mentioned tools will provide insight into the reliability of the aircraft, a large number of assumptions would have to be made in order to determine the system reliability. The estimates provided in the previous stage of the design, which are presented in Table 21.1, are still valid and are provided as target for the reliability of each subsystem. Reliability considerations in the design so far are evaluated for some of the subsystem, mainly in the ones with applied redundancies in them.

- **Cockpit Instrumentation**. The avionic system is a commercial available off the shelf component. Therefore it is assumed that it meets at least the regulation specifications on the number of redundancies necessary within the system.

- **Electrical**. A generator is attached to the engine in order to provide electrical power to the other subsystems. A battery, which is charged via the generator, is added into the design for redundancy. In case the generator fails, the battery should provide sufficient energy to power the primary instruments, the lighting and the electric distribution for 30 minutes as per CS-23 regulations[42].

Table 21.1: Reliability estimates for aircraft subsystems [77]

Subsystem	Reliability
Airframe	0.99940
Cockpit Instrumentation	0.976
Electrical	0.99997
Flight Control	0.98476
Ground Control	0.99589
Propulsion	0.99986
Interior, Environmental, Safety	0.9994

- **Ground Control**. The landing gear will use an actuation mechanism for retraction and deployment. In case this system fails an emergency actuation system which allows the pilot to manually deploy it is installed. This system was introduced purely to increase the reliability of the aircraft.
- **Propulsion**. No redundancies were added to the engine or the propeller in terms of thrust generation as the weight of the design would be severely increased. A parallel network was created for the fuel system in order to increase its reliability. Two fuel pumps are installed in the aircraft, an electrical driven pump operated by the battery and a mechanical driven pump operated via the engine. The engine driven pump will be used under nominal operations. In case the mechanical pump fails the electrical driven pump can take over its functions.
- **Interior,Environmental,Safety**. The main aspect considered is the pressurisation system. A parallel network was created by providing oxygen containers in the fuselage in case of cabin depressurisation. Both systems would have to fail before the entire system fails.

In order to provide customer support after purchase a reliability programme will be implemented by the design team. This programme will ensure periodic reevaluation of the aircraft components reliability, which will allow the design team to provide the consumer with updated maintenance programmes, impose corrective actions or to provide modifications in the design where necessary. The types of data to be collected should allow for assessments to be made as to whether any reaction, both to trends and to individual events, is necessary. The main sources of data will be: technical logs, maintenance worksheets, reports on technical delays and incidents. These will be gathered from as many models sold as possible to ensure a wide data set.

21.2. Maintainability

Maintainability pertains to the ease, accuracy, safety, and economy in the performance of maintenance actions. Maintainability is the ability of an item to be maintained, and like reliability, is an inherent characteristic of system design. Ideally, the aircraft should be maintained in the least amount of time possible, at the lowest possible cost and with the least amount of resources. However the system maintainability highly depends on the components and equipment used in the design.
Maintenance actions are split into preventative and corrective actions. Corrective actions are actions performed when a component has been damaged as a result of an incident and either has to be replaced or fixed. For instance, in case the sandwich composite is damaged it can be repaired by applying a patch to the damages places in cased the affected area is small, by using adhesive film, as it is shown in Figure 21.1. For components that need replacement, such as the engine, to increase the system reliability, easy access is ensured by cut outs such that the aircraft downtime can be minimised. Alterations and repairs must be performed by licensed personnel. The preventative measures can then be subdivided into periodic and condition dependent actions. In order to ensure the integrity of the system throughout its operational stage of the life cycle, regulations dictate that the aircraft must undergo a complete inspection every twelve months where airworthiness compliance checks must be performed by licensed personnel [43]. The preventative measures that are permitted by regulation agencies to performed by the aircraft owner on a periodic basis are specified by EASA[15, 24].
In addition to the above mentioned maintenance procedures, inspections by licensed personnel must be performed, when one of the incidents described in Section 18.1, on the airframe as damage to the

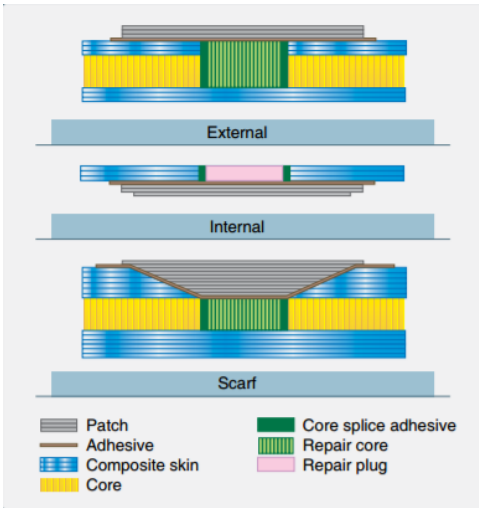

Figure 21.1: Patching the damaged sandwich [97]

composite cannot be identified visually. The following two methods can be used: sonic and ultrasonic inspection. Sonic inspection does not require dedicated equipment as it can be performed by using a coin or a small hammer. Ultrasonic inspection, on the contrary, requires dedicated ultrasonic equipment. However the latter inspection type is easier to perform and the results can be analysed faster. The ultrasonic method would be preferred due to its higher accuracy [97] and the reduction in system downtime that it provides.
Based on the reliability programme, the maintenance plan will be updated constantly based on the corrective actions and modifications implemented in the design.

21.3. Availability

Availability is often defined as the degree, percent, or probability that a system will be ready or available when required for use. Availability is the result of the reliability and maintainability. Three types of availability exist: inherent, achieved and operational. The operational availability of the aircraft is the most important aspect to be considered, as for example the customer using the airplane to reach a business meetings would not like to experience any delays due to maintenance operations.

21.4. Safety

Safety is defined as the freedom from hazards to humans and equipment. The main safety engineering issues are: the loss of life or injuries to humans, damage to the system or subsystem being designed and damage to the environment. Most concepts have been addressed by ensuring that the design complies with the airworthiness requirements CS-23 [42]. Technical risk which develop impose a threat on the personnel or equipment and are not addressed in the regulations are discussed and mitigated in Chapter 18. The footprint of the design on the environment is evaluated in Chapter 26.

22

Market analysis

This chapter presents an analysis of the current and future market and an evaluation of the design from a business case perspective. The current and future market are discussed in Sections 22.1 and 22.2 while the business case is evaluated in Section 22.3.

22.1. Current market

The general aviation market which peaked in 2007 suffered terribly as a result of the economic crisis of 2008. In the period 2007-2010 the global production of general aviation aircraft dropped by a total of 52.8%. Since then, the production of general aviation aircraft has been recovering slowly, with a total delivery of 2262 aircraft in 2016 compared to a total delivery of 2024 aircraft in 2010 [47]. The main reason for the incremental growth of the general aviation deliveries is that the price of a general aviation aircraft has almost doubled compared to 2007 [19]. As a result, revenues have not declined nearly as much, even though the number of deliveries is much lower when compared to the boom years leading up to 2007.

22.2. Market prediction

As can be seen in Table 22.1, the general aviation market is expected to increase by an average of 0.1% per year for the next 20 years in the United States. The turbine-powered market in particular is expected to increase by 1.9% each year, while the fixed wing piston aircraft segment is forecast to shrink by 0.8% yearly. This predicted trend was partly the motivation for the choice to design a turboprop aircraft as the business case would be stronger. This market gap is the gap that is aimed for by the design.

Table 22.1: FAA GA market prediction for the coming 20 years [45]

Segment	Change in fleet size	Change in hours flown
Overall GA market	+0.1%	+0.9%
Fixed wing piston aircraft	-0.8%	-0.8%
Turbine-powered aircraft	+1.9%	+2.4%
Light-sport aircraft	+4.1%	+4.6%

22.3. Evaluation

Table 22.2 shows the competitors in GA and the last row shows the Ultimate Personal Airplane design as developed in the project. It can be observed that within the GA market the design seems to fit in quite well as the listing price as established in Chapter 23 is competitive and the major aircraft characteristics are in line with the competition. It must be noted that the price prediction is preliminary and a price

growth due to increased development cost as is likely for a start-up without extensive experience in design & certification.
In the sense of aerobatic aircraft, for which the competition is shown in Table 22.3, the design is not up to the standards as established by the full-on aerobatic aircraft. However, as a design that aims for favourable flight characteristics as well as comfort, high cruising speed and long range it is thought that the aircraft can come along nicely.
The expected versatility of the design, the favourable flight characteristics and the low price are major selling points for the aircraft. It is expected that if these projected values are actually achieved the aircraft would be well positioned within the market and the chance that the aircraft would be a commercial success is present. The market gap that has been identified would be made use of in this respect. With the predicted yearly production rate of 48 aircraft the market share would end up being 2.1% of yearly global sales of general aviation aircraft, if total yearly sales figures for GA aircraft are 2237 using the 2016 sales figures and the FAA fleet growth prediction [45] [12]. With the worst case production rate of 24 aircraft per year the market share would be 1.05%. As the aircraft gains a positive reputation and the production rate is increased the market share can be increased possible up to the share of the top-selling Cirrus SR22T of 6.5% [12].

Table 22.2: GA aircraft overview

Aircraft	**Cost** [$]	**Range** [nm]	**Cruising speed** [kn]	**Number of occupants**	**Source**
Single piston engine					
Beech Bonanza	800 000	920	176	6	[27]
Cirrus SR22	520 000	810	183	4	[34]
Diamond DA40 XLT	420 000	830	137	4	[39]
Mooney M20V Acclaim Ultra	769 000	830	242	4	[73]
Cessna TTx	690 000	1270	235	4	[31]
Cessna 182	470 000	915	145	4	[30]
Robin DR401 (180LR)	350 000	763	139	4	[84]
Evolution Piston	995 000	1707	230	4	[44]
Twin piston engine					
Beech Baron	1 388 000	1480	202	6	[26]
Diamond DA42	522 750	1273	190	4	[38]
Piper Seminole	663 500	700	162	4	[81]
Single turboprop engine					
Piper M600	2 830 000	1484	274	6	[80]
Piper M500	2 250 000	1000	260	6	[79]
Socata TBM 850	3 367 000	1150	315	6	[93]
Evolution Turbine 750	1 392 000	1276	300	4	[44]
UPA	914 000	1422	250	4	N/A

Table 22.3: Aerobatic aircraft overview

Aircraft	**P/W** [kW/kg]	**G-limits** [g_0]	**RR** [deg/s]	**RoC** [m/s]	**price** [$]	**Source**
Mudry CAP 232	0.31	+10/-10	420	16	discontinued	[78] [83]
Zivko edge 540	0.31	+12/-12	420	19	450 000	[78] [72] [22]
Extra 300L	0.23	+10/-10	420	16	330 000	[78] [69] [22]
SU-29	0.32	+12/-10	340	16	340 000	[91] [22]
Yak-54	0.26	+9/-7	320	15	233 000	[18]
Cessna 152 Aerobat	0.11	+6/-3	unknown	3.6	discontinued	[90]
UPA	0.20	+6/-3	180	17.3	914 000	N/A

23

Cost breakdown

This chapter presents the cost estimation analysis and the resulting listing price and operational costs. First the theoretical model and the assumptions used for this model are presented in Section 23.1. Then an overview of the results is presented in Section 23.2.

23.1. Theory and assumptions

To determine the listing price and operational cost for the aircraft, a highly modified version of the DAPCA-IV model was used as presented in ”General Aviation aircraft design” [55]. To make effective use of this model, a number of assumptions had to be made. A list of assumptions including their explanation is provided below.

AS-COST-01 *Airframe weight is 412.5 kg*
The model requires an input of the airframe weight. This was estimated to be 412.5 kg for this aircraft and includes the structural mass of the wing, tail and fuselage, the control surfaces mass and the mass of the landing gears [5]. However, the exact definition of airframe weight is not specified. Therefore the weight input required here could be higher in reality, resulting in a higher price.

AS-COST-02 *The total amount of aircraft ever sold is estimated to be 802*
This numbers follows from an analysis of the total number of aircraft sold of four popular turboprop aircraft. The total amount of aircraft sold of the Pilatus PC-7 (>500) [76], Pilatus PC-12 (1400) [75], DAHER TBM series (822) [92] and Piper Meridian 500 (484) [47] was averaged and found to be 802. Since the aircraft differs quite significantly from these models besides the engine type it is hard to make an accurate estimation. However, it should be noted that this number represents the total number of aircraft that is ever going to be produced from this model, regardless of the amount of years it takes. Furthermore, it is not even close to the total amount that for example the Cirrus SR22T has sold (5194) [47][48] and similar to the amount of Diamond DA42 aircraft sold up until 2016 (815) [47], which has a similar MTOW and four seating capacity [38].

AS-COST-03 *The total amount of aircraft produced yearly is 48*
The aim is to produce four aircraft per month which amounts to a total of 48 aircraft in a year. An average yearly amount of produced aircraft was calculated based on shipment data from 2016 of the Cirrus SR22, Diamond DA42, Cessna CE-240 TTx, DAHER TBM 930 and Pilatus PC-12, which was found to be an average production of 67 aircraft per year [47]. Since the model will be unknown in the beginning but is predicted to be popular in the end an average yearly production of 48 is reasonable and still conservative with respect to existing manufacturers. A lower monthly production will result in a longer time to break-even.

AS-COST-04 *The labour rates, storage rate and fuel price are established*
To estimate the cost of labour, storage and fuel, assumptions had to be made regarding

the labour and storage rates. Furthermore, the fuel price (Jet-A1) of today (26-6-2017) was used for the calculations. Since these rates are dependent on many variables and the fuel price changes daily, it is hard to accurately estimate these values. A table of the assumptions for these rates is provided to use as a reference. The labour and storage rates were based on values provided in ”General Aviation aircraft design” [55].

Table 23.1: Wages and prices used for the cost estimation.

Parameter	Value	Unit
Engineering rate	92	$/hr
Tooling rate	61	$/hr
Manufacturing rate	53	$/hr
A&P Mechanic rate	67	$/hr
Storage rate	875	$/month
Fuel price	1.697	$/L

AS-COST-05 *A profit margin of 15% is used*
Based on the minimal selling price (0% profit margin) and the market analysis, a profit margin of 15% was found to be feasible. The resulting price, as presented in Section 23.2, is still competitive with other aircraft in the market. At the same time the 15% margin allows for a reasonable predicted break-even time, as presented in Chapter 24. In case the sales are disappointing, a lower profit margin can be adapted, this can result in a more attractive pricing but elongates the break-even time.

The model uses a set of equations that estimates the cost for several phases of the aircraft manufacturing, necessary tooling and parts like the avionics and propulsion system. The equations are set-up based on statistical data. The original DAPCA-IV model, which was based on military aircraft and established in 1986, was updated and tailored to General Aviation aircraft[55]. Using the assumptions and the aircraft characteristics the costs and price were estimated, the results are presented in Section 23.2.

23.2. Results

The relevant resulting prices that followed from the cost model are presented in Table 23.2.

Table 23.2: Cost model results per aircraft

Parameter	Value
Certification cost	$ 39700
Minimum selling price (0% profit)	$ 794405
Selling price	$ 914000
Operational cost	229.3 $/hr

23.3. Cost Break-down Structure

The cost break-down structure is a tool that gives a clear and structured overview of all the costs of the total system, in this case the aircraft. It is structures as an AND tree, which means the subdivisions add up and together make up the higher class block. The cost break-down structure for the aircraft system is shown in Figure 23.1.

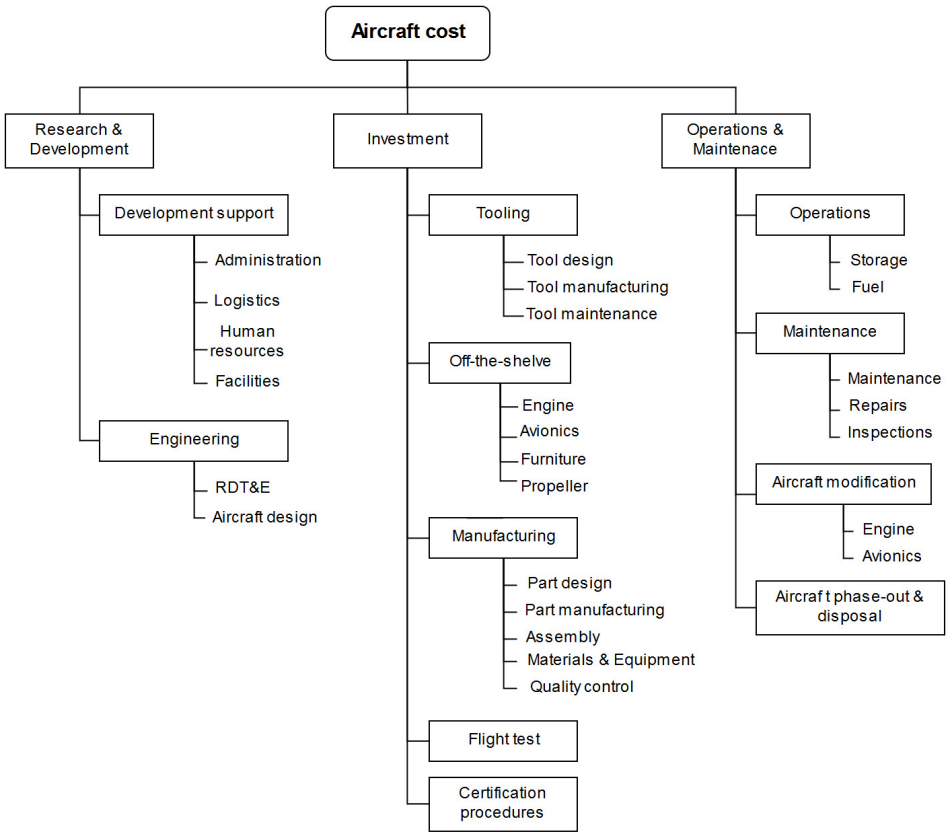

Figure 23.1: Cost break-down structure of the aircraft.

24

Return on investment

This chapter presents the predicted return on investment. This includes a break-even analysis for several prices and a worst-case scenario analysis. The data used for this chapter is taken from Chapter 23 and Chapter 22.

Break-even analysis A break-even analysis is used to determine how many units must be produced before the total revenue equals the total cost. The amount of units that need to be sold to break-even can be calculated with Equation (24.1).

$$N_{BE} = \frac{\text{total fixed cost}}{\text{unit sales price} - \text{unit variable cost}} \tag{24.1}$$

In which the total fixed cost is the combined predicted certification cost of all the aircraft that are going to be produced, which is estimated to be 802 aircraft as was specified in Chapter 23. The unit variable cost is the extra cost needed for one unit. The unit sales price was established by multiplying the minimum selling price by a certain profit margin. The total amount of aircraft produced yearly was set to be 48 aircraft for reasons specified in Chapter 23. Using these data the amount of units to break-even could be calculated as well as the break-even time based on the predicted average yearly sales. To illustrate the effect of changing the profit margin on the break-even time, the break even-time has been calculated for a few different profit margins as shown in Table 24.1. A profit margin of 15% was found to be feasible for this design because it allows for competitive pricing but still results in a reasonable break-even time of 70.5 months (close to 6 years).

Table 24.1: Break-even analysis for several profit margins

Profit margin [%]	Selling price [$]	Break-even units [-]	Break-even time [months]
5	834000	352	88
10	874000	313	78.25
15	914000	282	70.5
20	953000	256	64
25	993000	235	58.75

In a worst-case scenario, the total amount of aircraft sold and the amount of aircraft sold per month was taken to be 50% of the predicted values (scenario 1). Furthermore, a situation was analysed in which all the rates as specified in Chapter 23 requirement **AS-COST-04** turn out to be 150% of that which they are now (scenario 2). Lastly, a situation was analysed in which everything stays constant but the amount of aircraft sold yearly turns out to be 30 instead of 48 (scenario 3). The profit margin was kept constant throughout both scenarios. The results can be seen in Table 24.2.

Table 24.2: Worst-case scenario analysis results

Scenario	Selling price [$]	Break-even units [-]	Break-even time [months]
1	1320000	149	74.5
2	1250000	289	72.25
3	910000	229	112.4

As can be seen in every worst case scenario the selling price stays below 1.5 million dollars, complying to requirement **REQ-MIS-17**. Furthermore, if the sales are disappointing like in scenario 3, it will significantly increase the break-even time. This could be mitigated by either increasing the profit margin, betting on low sales but more profit per sold aircraft, or lowering the profit margin to try and ramp up the sales numbers. Once the popularity of the aircraft is growing, the profit margin could be scaled up again. In conclusion it can be seen that the aircraft business case is still feasible in very bad scenarios as long as appropriate measures are taken.

25

Compliance & sensitivity

This chapter discusses the compliance of the design with the mission requirements and addresses the sturdiness of the design through a sensitivity analysis. Section 25.1 shows the compliance matrix, while Section 25.2 presents the sensitivity analysis.

25.1. Compliance matrix

To verify if all requirements are met by the resulting design a compliance matrix is constructed, as can be seen in Table 25.1. The compliance matrix shows the requirement code and the requirement type, whether it is a key and/or driving requirement, in the first and second column. The associated required value and current value are shown in the third and fourth column. The last two columns show whether the requirement has been met and where the explanation for the current value can be found.
The only requirement that is not directly proven is the aerobatic capabilities of the aircraft, this is due to the fact that simulating aerobatic manoeuvres is beyond the scope of this design stage. Since it is proven that the requirements on roll rate, climb rate and structural loads are met, it is deemed as enough prove of aerobatic capabilities for this stage. The compliance matrix shows that all requirements have been met at this stage, this means that the design is feasible and can continue into later stages of development.

25.2. Sensitivity analysis

Because the models have not been integrated into a single model that describes the entire aircraft, a sensitivity analysis of the parameters on the entire aircraft was impossible. Instead a sensitivity analysis on the model level has been made. By varying major input parameters and recording the different outputs of the models the sensitivity to these input parameters could be determined.

25.2.1. Aerodynamic model

For the aerodynamic model the 2 major inputs were determined to be the aspect ratio of the main wing and the dihedral of the main wing. The design values for these are 7.35 and 8 degrees respectively By taking the chosen design parameters for both these parameters and adding 1 to the aspect ratio and 1 degree to the dihedral. the most interesting output parameters for the aerodynamic models are the oswald efficiency factor e, the lift over drag ratio, zero lift drag coefficient, downwash factor and the Lift slope. The results of this can be seen in Table 25.2.
Out of the results in Table 25.2 the more interesting result is that the aspect ratio not only increases the lift over drag ratio directly, but also decreases the downwash on the tail. This could possibly allow for a smaller tail which also reduces drag and therefore increases the lift over drag ratio.

25.2.2. Structural model

For the structural model, the two most important parameters to alter for the sensitivity analysis are the MTOW and the ultimate load factor, Nz. These two parameters are interesting because the MTOW and Nz have a direct and clear impact on the weight of the structure because the higher these values, the

Table 25.1: Compliance matrix

Requirement code	Type	Requirement value	Current value	Compliance	Reference
Mission requirement					
REQ-MIS-01	D	<2000	1651	v	Chapter 16
REQ-MIS-02	D	4+	4	v	Chapter 15
REQ-MIS-03	K, D	-	-	v	Chapter 13
REQ-MIS-04		444	444	v	Chapter 15
REQ-MIS-05	K	1400+	1400	v	Chapter 13
REQ-MIS-06	K	-	-	v	Chapter 13
~~**REQ-MIS-07**~~		-	N/A	N/A	N/A
REQ-MIS-08	K	<500	373	v	Chapter 13
REQ-MIS-09	K	<500	497	v	Chapter 13
REQ-MIS-10		-	-	?	Chapter 13
REQ-MIS-11		-	-	?	Chapter 13
REQ-MIS-12		180+	250	v	Chapter 13
REQ-MIS-13		18000+	25000	v	Chapter 13
REQ-MIS-14		-	-	v	Chapter 14
REQ-MIS-15		<1.500.000	914.000	v	Chapter 23
REQ-MIS-16	D	<400	229	v	Chapter 23
REQ-MIS-17		<0.387	0.325	v	Chapter 13
REQ-MIS-18		40+	40+	v	Chapter 21
REQ-MIS-19	D	-	-	v	Chapter 20
System requirement					
REQ-SYS-01		<-3	-3	v	Chapter 11
REQ-SYS-02		>+6	+6	v	Chapter 11
REQ-SYS-03		180+	180	v	Chapter 12
REQ-SYS-04		15+	17	v	Chapter 13
REQ-SYS-05	D	-	-	v	N/A
REQ-SYS-06		-	-	v	Chapter 14

stronger the structure must be, so the more material is used. For the wing and tail (both vertical and horizontal), the skin thickness was adjusted to 0.71 and 0.36 mm respectively so that it can just hold the bending tensile stresses (but this does not account for compressive stressed, see Section 11.1). This sensitivity analysis is based only on tensile stresses.

From the analysis, it can be concluded that increasing the MTOW and Nz directly impacts the final mass of the structure. There is a total of 20.27 kg for the change in MTOW and a total of 19.26 kg for an increase of Nz by 1. It should be noted, that the tail critical loads are not $+6g$ loads, but dive and turn loads instead, so those loads were multiplied by $\frac{13}{12}$ to bring it in line with other structural parts load sensitivity by scaling the tail load by the same factor that wing and fuselage loads use. This is of course an approximation, because to conduct exact load change a lot of tail-related parameters have to be recalculated using all the other models.

25.2.3. Stability model

A sensitivity analysis of the most important output parameters was conducted on the stability and control model. The results are listed in Table 25.4.

The change in the horizontal tail surface area over main wing area ratio was analysed for an increase in OEW and in downwash. Increasing the OEW will slightly decrease the required tail surface since the centre of gravity range is more limited. The effect of a small change in the downwash is negligible. Yet, it must be noted downwash reduces the effectiveness of the tail; hence more downwash leads to a bigger tail.

Table 25.2: Aerodynamic model sensitivity

	Aspect ratio +1 [-]	Dihedral angle +1 [deg]	Unit
e	+0.00680	-0.00233	[-]
$\frac{L}{D}$	+1.188	-0.0306	[-]
C_{D0}	-2.427e-6	+8.60e-6	[-]
$\frac{d\epsilon}{d\alpha}$	-0.01755	+0.00103	[-]
C_{L_α}	+0.2402	+0.005741	$[rad^{-1}]$

Table 25.3: Structural model sensitivity

	MTOW +10%	Nz +1	Fuselage Length -	Unit
Wing mass	+4.97	+4.26	-	[kg]
Tail mass	+1.704	+1.396	-	[kg]
Fuselage mass	+13.6	+13.6	+82	[kg]
Total	+20.27	+19.26	+82	[kg]

Table 25.4: Stability & Control model sensitivity

	OEW +1%	$\frac{d\epsilon}{d\alpha}$ +1 %	C_e/C_h +1 %	Unit
S_h/S	-0.002	0.0002	-	[-]
X_{nfix}	-	-0.0004	-	[m]
$C_{m_{\delta_e}}$	-	-	0.0002	[-]

25.2.4. Performance model

For the performance model a sensitivity analysis was conducted only on the outputs that are bounded by the requirements. For the performance model, a change in MTOW or $\frac{L}{D}$ was found to have the largest impact on the results. The results of the sensitivity analysis are presented in Table 25.5.

Table 25.5: Performance model sensitivity

	MTOW +1%	$\frac{L}{D}$ -1 %	Unit
Take-off distance	+1.22	+0.36	[m]
Climb rate	-0.26	-0.03	[m/s]
Landing distance	+1.69	-0.73	[m]
Range at 250 kn	-12.4	-15.3	[km]

Of special interest are the increase in landing distance as a result of increasing MTOW. The landing distance at this moment is estimated to be 496.8 m, very close to the requirement of maximum 500 meter (**REQ-MIS-09**). Since the difference is just 3.2 m the 500 m boundary will be passed quickly if the MTOW is going to increase a lot. This could possible be mitigated by installing speed brakes or spoilers on the wing, although this would add extra weight as well. This is therefore something to look into for further development.

The range of the aircraft is quite dependent on the weight of the aircraft. Increasing the MTOW with 1% while assuming this increase originates from the OEW so the fuel weight is kept constant, results in a decrease of the range of 12.4 km. Since the aircraft complies with the range requirement, **REQ-MIS-05**, with a margin of only 22 km, this should be carefully monitored. It is a similar story for the impact of the aerodynamic performance on the range, as decreasing the lift-drag polar with 1% results in a decrease in range of 15.3 km. A solution would be carrying more fuel. The tanks are about 1.5 times the size as is required at the moment, so that is not a problem. It will however also increase the MTOW, for which the plane will have to be specified.

26

Sustainability

This chapter presents the sustainability strategy applied throughout the project and present the elements incorporated in the design to meet the sustainability requirements. Section 26.1 presents the sustainability strategy, while Section 26.3 displays the results.

26.1. Strategy

Climate change and pollution pose a grave threat to Earth, nature and people. Therefore, in any design process nowadays sustainability should be addressed. In the aviation industry even more so, as in general this industry is a major source of pollutants. At the same time, efficiency is beneficial for the product commercially as it lowers operating costs. Sustainability for this project is considered from three points, environmental, economical and social. A visualisation is presented in Figure 26.1.

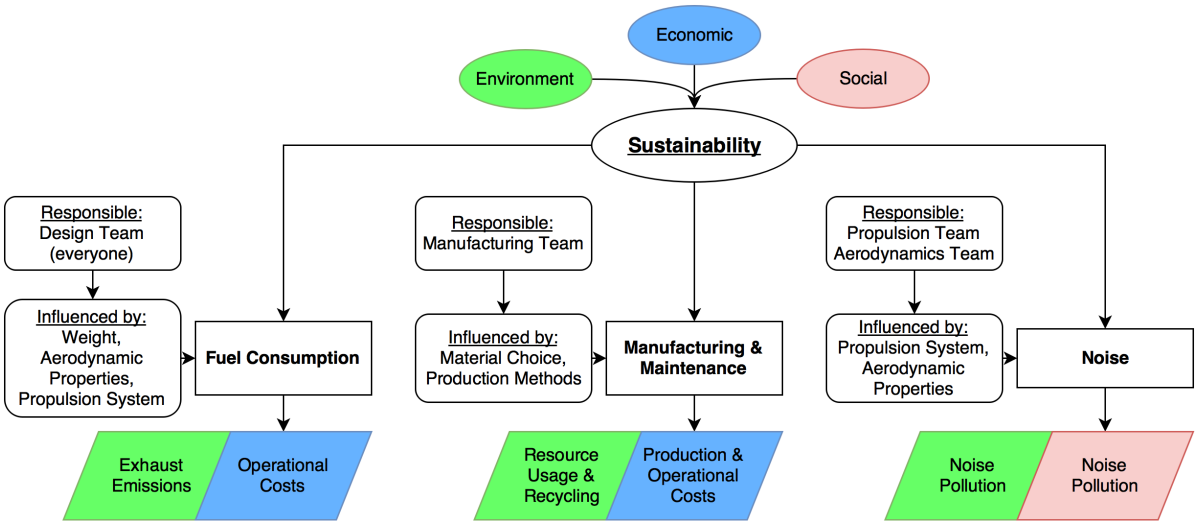

Figure 26.1: Sustainability strategy visualisation

From these fields the following areas of importance are identified: fuel consumption, manufacturing & maintenance and noise. Decreased fuel consumption limits the aircraft's emission of pollutants and lowers operational costs. As the **REQ-MIS-17** requirement is met, it could be stated that the aircraft is 16% more efficient in fuel consumption than the Lancair Evolution aircraft and that it will therefore be the most efficient four seat-er turboprop aircraft on the market. The manufacturing & maintenance procedures however, which are established with sustainability in mind, have the effect of decreasing production & operational costs as well as limiting resource usage and facilitating recycling practises. Limiting the noise emissions of the aircraft has a benefit both environmentally and socially.

26.2. Noise

The efforts regarding the limitation of noise emissions focus on two fields: engine noise and aerodynamic noise. Engine noise itself is difficult to directly reduce, but its impact on the airport's surroundings can be limited due to the relatively high climb rate. The impacted area is limited by climbing out fast. Aerodynamic noise is limited through the aerodynamically efficient design, which has been a major focal point during the design process. All these design features combined ensured that the current design is regarded as relatively sustainable while still fulfilling the requirements. However, it is still of importance to determine whether the aircraft complies with the maximum noise levels stated by the ICAO Annex 16 (also for FAA and ESEA certification)[74].

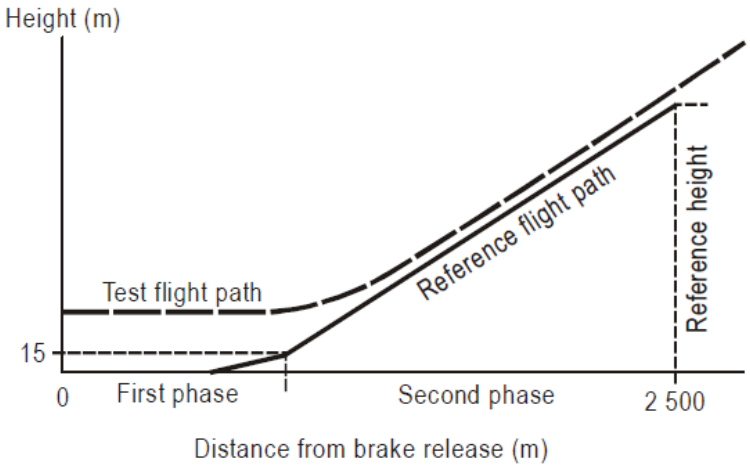

Figure 26.2: ICAO take-off noise certification point [74]

According to the ICAO noise regulation, a aircraft with a MTOW of 1658 kg, for which the application for the Type Certificate was submitted after 4 November 1999, a maximum noise limit of 85 dB(A) is defined [74]. The aircraft should not exceed this noise level at the take-of reference noise measurement point indicated in Figure 26.2. Since aircraft noise is clearly not directly related to aircraft size or engine type [23] it has therefore been chosen to determine the noise characteristics by performing the test flights as presented in Figure 26.2.

26.3. Evaluation of design

While establishing the current design care was taken to limit its fuel consumption while still being able to fulfil the requirements. Since the design features a turboprop engine it will be able to run on Jet-A1 fuel, which is significantly less polluting than Avgas. During the conceptual design a hybrid option was investigated, but this would drive the design to an unacceptable extent with the current state of technology. It is expected that the aircraft's emissions will be on par with aircraft of similar size and configuration. A field where a large leap can be made is the manufacturing and maintenance process. If the project is continued, the detailed design of the parts will be performed with recyclability in mind to ensure that the larger part of the aircraft can be recycled at end-of-life. To achieve this, the guidelines from the Aircraft Fleet Recycling Association (AFRA) will be adhered to and if feasible the company will apply for accreditation with this organisation.

27

Project design & development logic

The design of the aircraft can be further expanded after the time allocated for the Design Synthesis Exercise. In this chapter a framework for further development is presented. A general overview is given in Section 27.1 while the model specific planning is shown in Section 27.2.

27.1. General project plan

The typical design process for a GA aircraft is shown in Figure 27.1, according to [54]. Figure 27.2 shows the more specific activities that would follow the design process of this project [54]. The project start and the conceptual phase, as executed earlier in this project, have not been included in the diagram. The concurrent aspect of the process is clearly indicated in the first figure. The text below discusses the five design & development phases that remain to be executed as well as the marketing phase:

Preliminary design phase The concept that has resulted from the conceptual design phase is investigated further in the preliminary design phase. Part of this phase has already been executed during the project, these activities are coloured green in the diagram. The other activities still remain to be done. The outcome of this phase would be evaluated in a preliminary design evaluation and if the verdict is positive the project would continue, if negative the programme is altered severely or even cancelled.

Detailed design phase Using the outcomes of the preliminary phase a detailed design is performed of the systems and elements of the aircraft and the exact specifications of the parts are established. This phase would be initiated rather soon as part of the results from the preliminary design phase are already at hand. The outcome of this phase is the outside mold line and the internal structure. The outside mold line defines the exact outer surface of the aircraft.

Prototype & testing phase Using the exact specifications as obtained in the detailed design phase the first prototype is constructed. Also, the parts and structures are tested when necessary. Important elements of this phase are also the preparations for bringing the aircraft to the market by taking the first steps towards type certification (TC) and preparing the tooling for production. The maiden flight and the associated tests are the final steps of this phase.

Development phase This phase consists of establishing the flight procedures and planning the flight tests. The focus is on ensuring the flight tests can be executed safely. Outcome consists of the aircraft operating limitations (AOL), the pilot's operating handbook (POH) and master flight test schedule (MFTS). Once this phase is completed the aircraft should be ready for certification.

Post-development phase During this phase the very last steps are taken before the first aircraft are delivered. This includes executing the certification process with the applicable authorities and starting the production line in order to be able to deliver the aircraft as soon as the TC has been acquired.

Marketing In order to make the aircraft a commercial success a solid marketing plan should be formulated and executed. This is a process that is executed concurrently with the design & development phases. The target would be to have orders for the aircraft already before the development phase is completed.

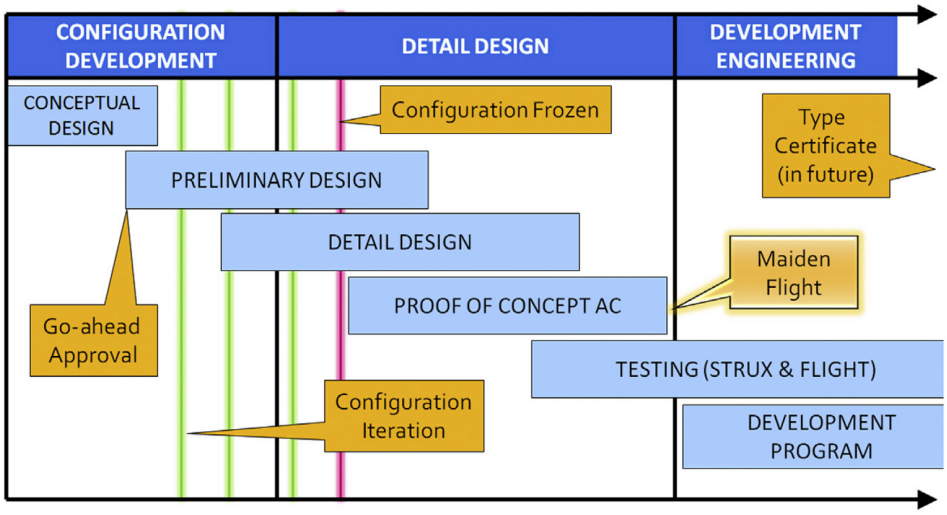

Figure 27.1: Aircraft design for a typical GA aircraft [54]

27.2. Model-specific planning

This section outlines the areas that require special attention for further optimisation of the design. At this point in time these improvements have not been implemented due to lack of time or the complexity of the subject.

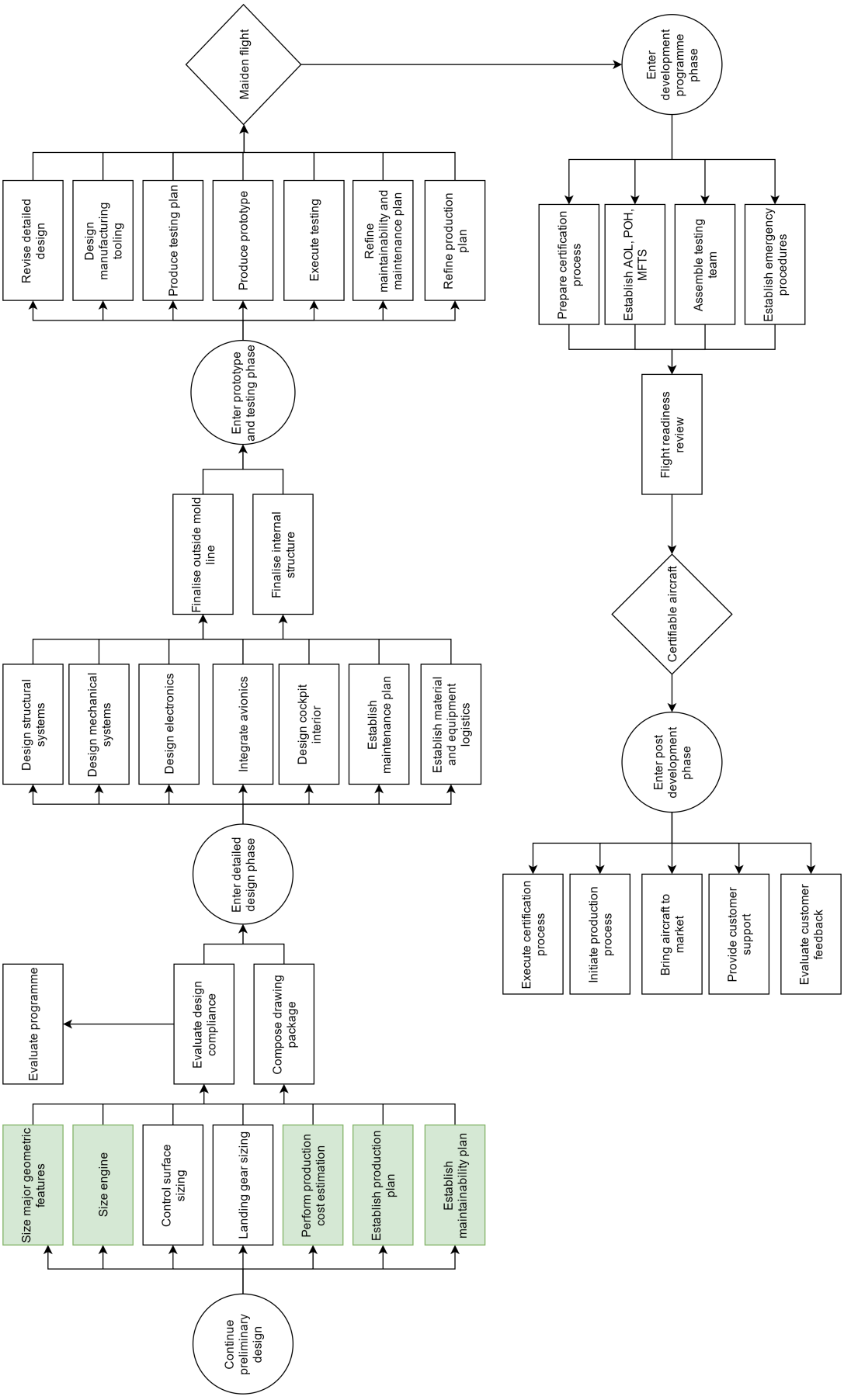

Figure 27.2: Project design & development flowchart

27.2.1. Aerodynamics Model

- The **Fuselage** was not implemented at this stage due to weird results, this is am area where a lot of improvements can be made.

- The **stability derivatives** were not accurate enough to be used, fixing the calculations done by the model in this area will result in accurate stability derivatives, and thus improve the model.

27.2.2. Structural Model

- **Buckling** of the composite sandwich plate is a complex phenomena, and also is one of major failure mods for the composite. However, it requires exact composite properties, for both honeycomb and laminate, and therefore it was not accounted for at the current development stage. The outcome of buckling analysis might *increase* or *decrease* structural mass, depending upon whether the current sandwich is overdesigned or underdesigned for buckling.

- Exact **rib placement** is one of the outcomes of the buckling analysis. At the moment, there are only three ribs in each wingbox, which is expected to be not enough to deal with the buckling of the material. Therefore, the structural mass is expected to *increase* from rib placement investigation.

- Obtaining the required **honeycomb thickness** is another outcome of the buckling analysis, as the honeycomb significantly increases buckling resistance as the replacement of stiffeners. Another requirement for the honeycomb is to withstand the load that are experienced during composite manufacturing (for example during curing process). Considering currently assumed honeycomb thickness, the structural mass can either *increase* or *decrease*, however taking into consideration very low density of the honeycomb, [82] the change is not expected to be very significant.

- **Isotropity** has been assumed for the entire aircraft for now to simplify calculations. In a further stage of the design, a thorough investigation shall be done on isotropic properties of the composite so that mass can be saved as we may not need to be isotropic in some parts of the aircraft. This can *reduce* both mass of the structure and cost.

- **Thickness** has been assumed to be constant throughout the structural airframe. This is not an optimised design and results in a heavier wingbox, tailbox and fuselage. In future developments, when buckling and shear failure have been properly investigated, it might be possible to reduce sandwich thickness in the locations where stress is not very high. The only severe restriction for this optimisation type is manufacturing problems that might arise. Overall, the mass and cost of the structure is expected to be *reduced*.

- Adding **extra layers and their properties** in the sandwich is going to be important for the mission success. First of all, because of using carbon composite, the nose of the aircraft has to be made from different fiber such as aramid, because of carbon electrical properties. Secondly, because of the same reason, electrical insulation has to be applied in the form of either adding an aluminium powder layer or adding metal rods on the structure to avoid lightning strike damage. Other sandwich layers can include acoustic insulation in the fuselage, anti-impact or anti-vibration layers. The necessity and properties of these options have to be carefully considered. Any additional layer is expected to *increase* both cost and mass of the airframe structure.

- **Exact shear stress** calculation is a complex procedure, which has to account for a variety of sandwich properties, such as honeycomb cell dimensions and orientation, exact fibre placement angles. Considering other possible changes which still can be done to the sandwich, listed in this chapter, this is unlikely to be done at the current development stage. The mass of the structure can either *increase* or *decrease* as an outcome of shear analysis.

- **The mounts, cutouts and local reinforcements** still need to be designed. Cut-out such as the door and windows which require local reinforcement need to be analysed. For the further development it is advised to use a finite element model for the composite structure.

  used.

27.2.3. Stability & Control Model

- **Stick free neutral point** As mentioned in **AS-STAB-01** the stick free neutral point should be located more in front than the stick fixed neutral point. The determination of the elevator hinge moment coefficients should reveal whether this condition could be satisfied. Since this determination relies on windtunnel experiments which are behind are resources, the specification of the stick free stability characteristics can only be defined in a later design stage.

- **Control surface** Although the dimensions of the control surfaces are defined, it is obvious that it is necessary to redesign several them several times since it is expected that the design will change in the future. Also flight tests should clarify whether the control surfaces are placed and sized such that the manoeuvrability and controllability requirements are met. From these tests it becomes clear if it is necessary to install for example control horns to improve the handling qualities.

- **Dynamic stability** As also stated in the previous item, it is necessary to reconsider the dynamic stability since design changes can effect the stability of the aircraft significantly. As described in Section 8.2.4 a specification on the dynamic stability characteristics mainly relies on experimental tests and more detailed computational fluid dynamics model. Based on these methods, a determination on whether additional taillets and stabilons or stakes are required can be made. .

27.2.4. Performance Model

- **Take-off and landing performance with crosswinds** could not accurately be estimated as was outlined in Section 13.3.3. To make a more accurate estimation of the performance in crosswinds a more in-depth analysis should be performed on the rudder authority and rudder sizing in general should be more detailed. However, only by flight test the real crosswind limits can be tested. It is expected that the aircraft will be *able to withstand* the crosswind limits of 25 kn during both flight phases as required by requirements **REQ-MIS-10** & **REQ-MIS-11**.

- **Landing distance performance** is very close to its maximum of 500 metre (**REQ-MIS-08**). With its current estimated 496.8 metre it will easily pass the 500 metre mark if for example the aircraft mass will turn out a to be a little higher. To improve the landing performance, a form of speedbrakes or spoilers could be included or the brake system could be improved. Also the high-lift devices could be redesigned if absolutely necessary. It is expected that if these measures are taken into consideration the landing performance will improve which will result in a *decrease* of the currently estimated landing distance. Or at the very least ensure that the requirement of 500 metre will be met.

- **Range** was analysed using the Breguet range and endurance equations (9.36 and 9.37). Though very convenient, this is not the most accurate approach. To get a better estimation, a model should be set up which simulates the aircraft flying the entire mission. Accurate fuel consumption data should be available for this to work. To acquire this, the turboprop engine should be tested extensively.

- **Propulsion** was analysed using blade element theory, but the model did not produce credible results. A better BEM (Blade Element Momentum) model should be developed, or even a CFD analysis. A connection with the fuel consumption could be made and hereby improve the range model.

27.2.5. Optimisation Model

- At first the goal was to make one **integrated model** out of the four models that exist currently. This integrated model would then be optimised by use of the particle swarm optimisation method. Since the integration of the four models could not be done in time, this is a first step to a better optimisation.

- An **Optimisation** can be performed on the integrated model by using the particle swarm optimisation method. This method will run thousands of iterations to find the most optimum input data, which gives the best output data.

28

Project Gantt chart

The proposed Gantt chart for continued development of the aircraft up to the delivery of the first aircraft is shown in Figure 28.1.

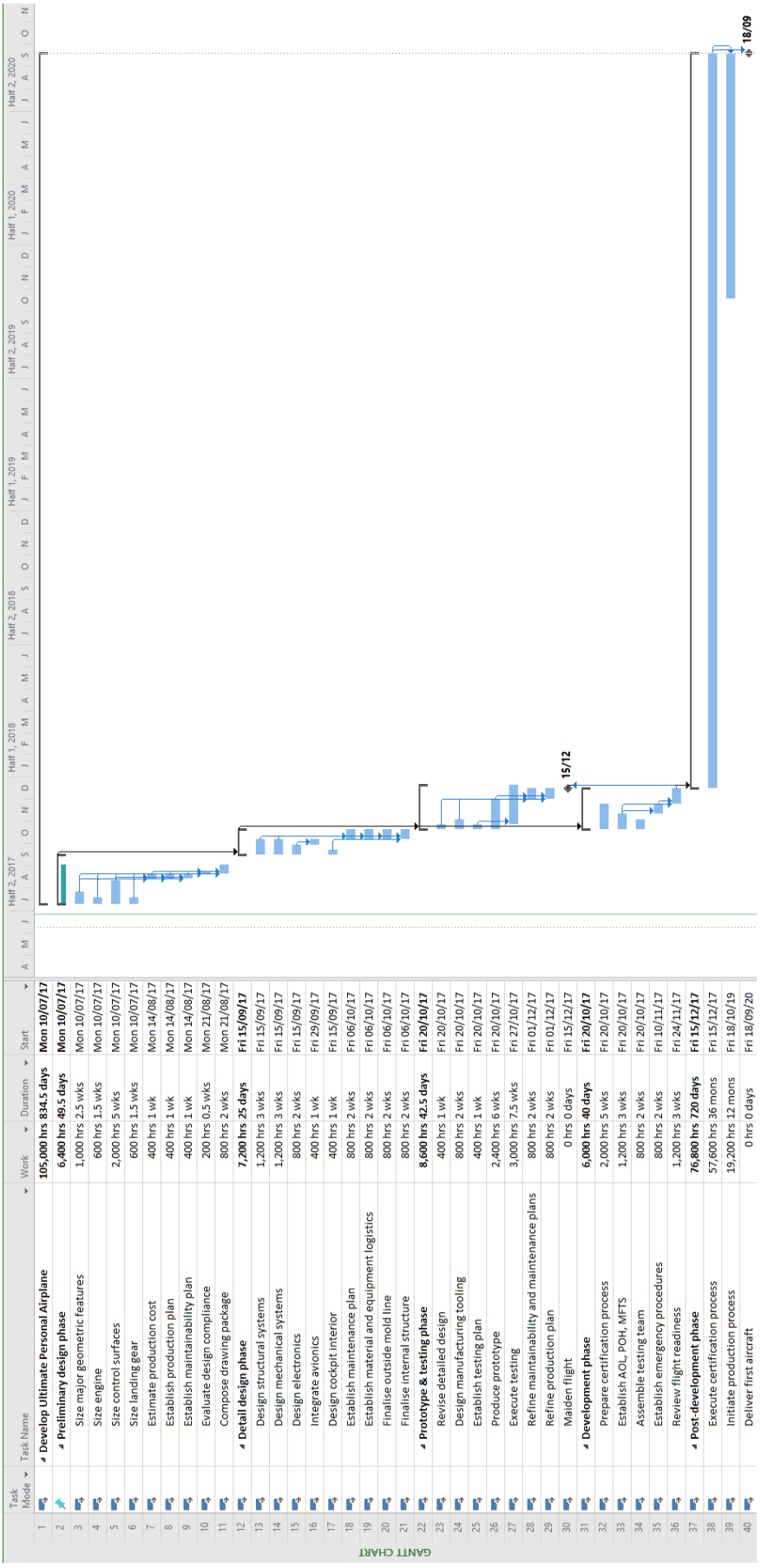

	Task Mode	Task Name	Work	Duration	Start
1		**Develop Ultimate Personal Airplane**	**105,000 hrs**	**834.5 days**	**Mon 10/07/17**
2		**Preliminary design phase**	**6,400 hrs**	**49.5 days**	**Mon 10/07/17**
3		Size major geometric features	1,000 hrs	2.5 wks	Mon 10/07/17
4		Size engine	600 hrs	1.5 wks	Mon 10/07/17
5		Size control surfaces	2,000 hrs	5 wks	Mon 10/07/17
6		Size landing gear	600 hrs	1.5 wks	Mon 10/07/17
7		Estimate production cost	400 hrs	1 wk	Mon 14/08/17
8		Establish production plan	400 hrs	1 wk	Mon 14/08/17
9		Establish maintainability plan	400 hrs	1 wk	Mon 14/08/17
10		Evaluate design compliance	200 hrs	0.5 wks	Mon 21/08/17
11		Compose drawing package	800 hrs	2 wks	Mon 21/08/17
12		**Detail design phase**	**7,200 hrs**	**25 days**	**Fri 15/09/17**
13		Design structural systems	1,200 hrs	3 wks	Fri 15/09/17
14		Design mechanical systems	1,200 hrs	3 wks	Fri 15/09/17
15		Design electronics	800 hrs	2 wks	Fri 15/09/17
16		Integrate avionics	400 hrs	1 wk	Fri 29/09/17
17		Design cockpit interior	400 hrs	1 wk	Fri 15/09/17
18		Establish maintenance plan	800 hrs	2 wks	Fri 06/10/17
19		Establish material and equipment logistics	800 hrs	2 wks	Fri 06/10/17
20		Finalise outside mold line	800 hrs	2 wks	Fri 06/10/17
21		Finalise internal structure	800 hrs	2 wks	Fri 06/10/17
22		**Prototype & testing phase**	**8,600 hrs**	**42.5 days**	**Fri 20/10/17**
23		Revise detailed design	400 hrs	1 wk	Fri 20/10/17
24		Design manufacturing tooling	800 hrs	2 wks	Fri 20/10/17
25		Establish testing plan	400 hrs	1 wk	Fri 20/10/17
26		Produce prototype	2,400 hrs	6 wks	Fri 20/10/17
27		Execute testing	3,000 hrs	7.5 wks	Fri 27/10/17
28		Refine maintainability and maintenance plans	800 hrs	2 wks	Fri 01/12/17
29		Refine production plan	800 hrs	2 wks	Fri 01/12/17
30		Maiden flight	0 hrs	0 days	Fri 15/12/17
31		**Development phase**	**6,000 hrs**	**40 days**	**Fri 20/10/17**
32		Prepare certification process	2,000 hrs	5 wks	Fri 20/10/17
33		Establish AOL, POH, MFTS	1,200 hrs	3 wks	Fri 20/10/17
34		Assemble testing team	800 hrs	2 wks	Fri 20/10/17
35		Establish emergency procedures	800 hrs	2 wks	Fri 10/11/17
36		Review flight readiness	1,200 hrs	3 wks	Fri 24/11/17
37		**Post-development phase**	**76,800 hrs**	**720 days**	**Fri 15/12/17**
38		Execute certification process	57,600 hrs	36 mons	Fri 15/12/17
39		Initiate production process	19,200 hrs	12 mons	Fri 18/10/19
40		Deliver first aircraft	0 hrs	0 days	Fri 18/09/20

Figure 28.1: Proposed Gantt chart for continued development

29

Conclusion

The aim of the Ultimate Personal Aircraft was to create an aircraft design which is capable of performing the majority of aerobatic manoeuvres and have a decent cruise performance. Such an airplane is expected to sell really well to those customers that do not want to limit themselves to a certain single-purpose aircraft, and want their vehicle to be as universal as possible.

So far, the airplane in question has the following main features:

- To achieve multifunctionality, a **conventional configuration** was chosen because of the many customisation possibilities, so it can be easily tailored according to the needs of the project.
- A **turboprop engine** is safe and can easily provide the high amounts of power, which are needed for various manoeuvres the aircraft is expected to perform.
- The primary material for the aircraft structure is **carbon composite sandwich structure**, as it is sufficient to withstand the expected load of -3/+6g with the composite safety factor of 2, while also being lightweight and removing the necessity of stiffeners.
- For the wing, a **custom airfoil** was generated to provide the optimal lift curve for the variety of missions that aircraft is expected to perform.
- For the design as it is right now, the **stability, control and performance characteristics satisfy the requirements**, which is a great success, considering that the biggest challenge of the project was fulfilling conflicting requirements. Some of the characteristics which outperform the requirements by a significant margin are take-off distance of 422.3 m and climb rate of 17.3 $\mathrm{m\,s^{-1}}$
- **Bladder fuel tanks** supported by the **fuel pumps** are a simple and reliable fuel system, which maintains good operation during aerobatics
- **Cabin pressurisation** allows for the highest comfort when it comes to environment control inside the cabin, making the design more appealing, albeit slightly heavier.
- **Retractable landing gear** contributes to the drag reduction, which is highly beneficial for extended cruise performance. Besides, there is enough space in the fuselage to house retractable mechanism, which makes higher complexity the only downside.
- **Electro-thermal de-ice system** is a very smooth system, which does not disrupt the laminar flow over leading edges of wings and tails, and is also very light. Besides, such a system can also be operated as anti-ice system, preventing the formation of ice. The only downside is electrical consumption of this system, which however can be seen as benefit considering the flexibility of operation.
- **Side stick** is the most comfortable choice of control system available for this aircraft, as steering wheel would be difficult to operate at higher loads, and middle stick is not comfortable for long cruise.

- A turboprop engine is very reliable comparing to a piston engine, however for the customers that want an even safer aircraft, a ballistic recovery system in the form of a **parachute** can be installed for additional safety. It features extra weight and is not really needed, this is why it is made optional.

At this stage of the design, the aircraft looks very promising. The majority of potential risks is already mitigated, and those which are not mitigated yet have a proposed course of action to be dealt with. The estimated selling price of the aircraft is $920,000, which is a good price comparing to other single turboprop aircraft, making it a decent market competitor. Finally, it does not create significant problems with respect to sustainability, as the fuel used is Jet-A1, which is more environment-friendly than the alternative Avgas.

The design has progressed far over these several weeks, however the models still have to undergo significant improvement to yield more representative results. Aerodynamics model has to include fuselage in the derivative calculations, which in turn can likely fix the stability derivative results which are unrealistic. Structural model has to focus on the properties of composites, as those are much more complex comparing to more commonly used metals, which in turn might make the structure even lighter and cheaper than it is now. Performance model requires accurate flying simulation in order to produce more accurate results, as current model is based upon statistical relationships like Breguet equations. Stability & control model has to keep a careful track of all the changes made, as any changes affect the sizing of the control surfaces and therefore stability characteristics. Finally, all the models can be connected into one big model, which can react to any changes made to design parameters and produce the analysis of aircraft from the point of view of all aforementioned models.

Bibliography

[1] Aerodynamics of 3d lifting surfaces through vortex lattice methods. URL http://www.dept.aoe.vt.edu/~mason/Mason_f/CAtxtChap6.pdf. Accessed: 2017-06-22.

[2] Mazda wankel rotary engines for aircraft. http://www.rotaryeng.net/. Accessed: 2017-06-27.

[3] Application of adhesives in aircraft. URL http://www.argosyinternational.com/products/adhesives. Accessed: 2017-06-23.

[4] Airbus 320. http://www.aircraft.airbus.com/aircraftfamilies/passengeraircraft/a320family, . Accessed: 2017-06-27.

[5] Aircraft structures, . URL https://www.faa.gov/regulations_policies/handbooks_manuals/aircraft/amt_airframe_handbook/media/ama_ch01.pdf. Accessed: 2017-06-26.

[6] 20 things you never know about your airplane (or someone else's). URL http://www.planeandpilotmag.com/article/20-things-you-never-knew-about-your-airplane-or-someone-elses/#.WVIT0cZ7Gu4. Accessed: 2017-06-27.

[7] Cessna 172. https://en.wikipedia.org/wiki/Cessna_172. Accessed: 2017-06-27.

[8] Carbon fabrics. URL http://www.corecomposites.com/products/reinforcements/carbon-fabrics.html. Accessed: 2017-06-23.

[9] Da-20 katana. http://www.diamondaircraft.com/aircraft/da20/. Accessed: 2017-06-27.

[10] Aircraft fuel system. URL https://www.faa.gov/regulations_policies/handbooks_manuals/aircraft/amt_airframe_handbook/media/ama_ch14.pdf. Accessed: 2017-06-26.

[11] How do airplanes manage to stay straight on the runway during takeoff? URL https://www.quora.com/How-do-airplanes-manage-to-stay-straight-on-the-runway-during-takeoff. Accessed: 2017-06-27.

[12] General aviation market data. URL http://www.fi-aeroweb.com/General-Aviation.html. Accessed: 2017-06-27.

[13] Controls on moving controls? URL https://ux.stackexchange.com/questions/34682/controls-on-moving-controls. Accessed: 2017-06-27.

[14] Atr: The optimum choice for a friendly environment. *Avions de Transport Regional*, 2001.

[15] Pilot owner maintenance. Technical report, EASA, May 2006.

[16] CES Edupack 2009. Epoxy/hs carbon fiber, ud composite, quasi-isotropic laminate. URL https://www.scribd.com/document/76975806/Carbon-Fiber-Quasi-Isotropic-Laminate. Accessed: 2017-06-19.

[17] ISO/TC 20/SC 6. Standard atmosphere. Standard, International Organization for Standardization, 1975.

[18] aeroconcept. aero-concpet yak 54 data. http://www.aero-concept.com/fiches/54.html, 2017. Accessed: 2017-04-26.

[19] Aeroweb. General aviation market data. http://www.fi-aeroweb.com/General-Aviation.html, 2017. Accessed: 2017-04-26.

[20] AI-450C. AI-450C turboprop gas turbine aero engine. http://ivchenko-progress.com/wp-content/uploads/pdf/ai450s.pdf, 2016. Accessed: 2017-05-08.

[21] Diamond Aircraft. *Airplane Flight Manual DA 40 NG*, 2010.

[22] aircraftcompare. aicraftcompare data. https://www.aircraftcompare.com/subcategory/Aerobatic/18, 2017. Accessed: 2017-04-26.

[23] Oxford Airport. Aircraft noise comparison the factss. http://www.oxfordairport.co.uk/home/noise_comparison.pdf, 2006.

[24] AOPA. Aopa's guide to preventive maintenance. URL https://www.aopa.org/training-and-safety/pic-archive/aircraft-ownership/preventive-maintenance. Accessed: 2017-06-30.

[25] E.J.Biss A.T. Nettles. Low temperature mechanical testing of carbon-fiber/epoxy resin composite materials. Technical report, NASA, 1996.

[26] beechbar. Beechcraft Baron web page. http://beechcraft.txtav.com/en/baron-g58, 2016. Accessed: 2017-04-26.

[27] beechbon. Beechcraft Bonanza web page. http://beechcraft.txtav.com/en/bonanza-g36, 2016. Accessed: 2017-04-26.

[28] BoH. Blade element angles. URL https://commons.wikimedia.org/wiki/File:Blade_element.svg.

[29] Dr. Angelo Cervone and Dr. Ali Elham. Aerospace design and systems engineering elements ii - lecture slides, 2017.

[30] cessna182. Cessna 182 Skylane web page. http://cessna.txtav.com/en/piston/cessna-skylane, 2016. Accessed: 2017-04-26.

[31] cessnaTTx. Cessna TTx web page. http://cessna.txtav.com/en/piston/cessna-ttx, 2016. Accessed: 2017-04-26.

[32] Cirrus. Guide to caps, 2017. URL https://cirrusaircraft.com/wp-content/uploads/2014/12/CAPS_Guide.pdf.

[33] cirrus-manual. Airplane information manual for the cirrus design sr22. http://www.aeroprague.com/cz/download/Cirrus_SR22_Handbook_and_Manual.pdf, 2011. Accessed: 2017-06-26.

[34] cirrussr22. Cirus SR22 international pricelist. https://cirrusaircraft.com/wp-content/uploads/2017/01/2017-SR22-International-Pricelist.pdf, 2016. Accessed: 2017-04-26.

[35] C.Kassapoglou. Structural analysis and design - lecture slides, 2015.

[36] Falls Church VA C.N. Adkins, Consulting Engineer and Long Beach CA R.H. Liebeck, Douglas Aircraft Co. Design of optimum propellers. *American Institute of Aeronautics and Astronautics*, January 1983. DOI: 10.2514/6.1983-190.

[37] Jack Cowell. Shockwave - electric anti-icing technology comes to homebuilts—and none too soon. *KITPLANES*, May 2009. URL http://www.kitplanes.com/magazine/miscellaneous/Shockwave_0409.php.

[38] diamondda 42. Diamond DA42 web page. http://www.diamondaircraft.com/aircraft/da42/, 2016. Accessed: 2017-04-26.

[39] diamondda40. Diamond DA40 XLT web page. http://www.diamondaircraft.com/aircraft/da40-xlt/, 2016. Accessed: 2017-04-26.

[40] Vijgent P.M.H.W Holmes B.J. Dodbele S.S, van Dam C.P. Shaping of airplane fuselages for minimum drag. *AIAA Journal of Aircraft*, 24(5), May 1987.

[41] Raymer D.P. and American Institute of Aeronautics and Astronautics. *Aircraft design: a conceptual approach*. Educ Series. American Institute of Aeronautics and Astronautics, 1989. ISBN 9780930403515. URL https://books.google.nl/books?id=Q9QeAQAAIAAJ.

[42] EASA. Cs-23 normal, utility, aerobatic and commuter aeroplanes, 2017.

[43] EASA. Acceptable means of compliance, 2017.

[44] evolutionpist. Evolution Aircraft comparison web page. http://www.evolutionaircraft.com/compare/, 2016. Accessed: 2017-04-26.

[45] FAA. Faa aerospace forecast 2017-2037. https://www.faa.gov/data_research/aviation/aerospace_forecasts/media/FY2017-37_FAA_Aerospace_Forecast.pdf, 2016. Accessed: 2017-04-26.

[46] freevalve. Freevalve web page. http://www.freevalve.com/, 2017. Accessed: 2017-05-15.

[47] GAMA. 2016 general aviation statistical databook & industry outlook. https://gama.aero/wp-content/uploads/2016-GAMA-Databook_forWeb.pdf, 2016. Accessed: 2017-04-26.

[48] GAMA-old. 2007 general aviation statistical databook & industry outlook. https://gama.aero/wp-content/uploads/2007gamadatabookoutlook_pdf_498c889640.pdf, 2007. Accessed: 2017-06-26.

[49] Garmin. G1000™ integrated avionics system. http://www.safeflightintl.com/downloads/g1000specsheet.pdf, 2003. Accessed: 2017-05-15.

[50] Garmin. G1000™ integrated flight deck, pilot's guide. https://static.garmincdn.com/pumac/190-00498-07_0A_Web.pdf, 2011.

[51] O.H. Gerlach. Lecture notes on airplane stability and control part i. Technical report, TU Delft, May 1983.

[52] W.H. Gray and Nicholas Mastrocola. Representative operating charts of propellers tested in the naca 20-foot propeller-research tunnel. Technical report, NACA, September 1943. URL www.dtic.mil/dtic/tr/fulltext/u2/a801230.pdf.

[53] Rayner Groh. Fancy a sandwich? URL http://aerospaceengineeringblog.com/sandwich-panel/. Accessed: 2017-06-19.

[54] Snorri Gudmundsson. *General Aviation Aircraft design, Applied Methods and Procedures*. 1st Edition. Butterworth-Heinemann, 2013. ISBN 9780123973085. URL https://books.google.nl/books/about/General_Aviation_Aircraft_Design.html?id=XtU4HVnWeZIC&redir_esc=y.

[55] Snorri Gudmundsson. *General Aviation Aircraft design, Applied Methods and Procedures*. 1st Edition. Butterworth-Heinemann, 2013. ISBN 9780123973085. URL https://books.google.nl/books/about/General_Aviation_Aircraft_Design.html?id=XtU4HVnWeZIC&redir_esc=y.

[56] R. J. Hamann and M. J .L. van Tooren. *Lecture Notes on Systems Engineering & Technical Management Techniques*, 2006.

[57] John B Hege. *The Wankel rotary engine: A history*. McFarland, 2006.

[58] Martinh Hepperle. Design of a propeller, 2003. URL http://www.mh-aerotools.de/airfoils/jp_propeller_design.htm. Accessed 03/07/2017.

[59] ICAO. Pans ops/611 doc 8186, 2006. URL http://www.chcheli.com/sites/default/files/icao_doc_8168_vol_1.pdf.

[60] Legal Information Institute. 14 cfr 23.73 - reference landing approach speed., . URL https://www.law.cornell.edu/cfr/text/14/23.73. Accessed: 2017-06-21.

[61] Legal Information Institute. 14 cfr 23.841 - pressurized cabins., . URL https://www.law.cornell.edu/cfr/text/14/23.841. Accessed: 2017-06-20.

[62] J.A. Mulder and W.H.J.J. van Staveren and J.C. van der Vaart and E. de Weerdt and C.C. de Visser and A.C. in 't Veld and E. Mooij. *Flight Dynamics Lecture Notes*. TU Delft, 2013.

[63] Anil K. Thayamballib Gyu Sung Kima Jeom Kee Paika, *. The strength characteristics of aluminum honeycomb sandwich panels. *Elsevier*, 1999.

[64] John D, Anderson Jr. *Aircraft Performance and Design*. Tata McGraw-Hill, 2012.

[65] Coşku Kasnakoğlu. Investigation of multi-input multi-output robust control methods to handle parametric uncertainties in autopilot design. *PloS one*, 11(10):e0165017, 2016.

[66] Dennis L. Kasper, Anthony S. Fauci, Stephen L. Hauser, Dan L. Longo, J. Larry Jameson, Joseph Loscalzo, and Tinsley Randolph Harrison. *Harrison's principles of internal medicine*. McGraw Hill Education, 19th edition, 2015.

[67] Lancair. Evolution evot-550 specifications. URL http://www.evolutionaircraft.com/aircraft/evolution-turbine/. Accessed: 2017-06-15.

[68] Andrew Lewis. T-visual approach slope indicator system (t-vasis) versus precision approach path indicator (papi) – the debate revisited. URL http://muir.massey.ac.nz/bitstream/handle/10179/3712/AERP2011-020%20Lewis.pdf?sequence=1. Accessed: 2017-06-20.

[69] markjefferie. mark jefferie extra 300l data. http://markjefferiesairdisplays.com/mark-jefferies-extra-330sc-aerobatic-air-display-aircraft/, 2017. Accessed: 2017-04-26.

[70] Cytec Engineered Materials. Fm® 73 epoxy film adhesive. URL http://www.argosyinternational.com/sites/default/files/datasheet/FM_73_081111.pdf. Accessed: 2017-06-19.

[71] T.H.G. Megson. *Aircraft Structures for Engineering Students*. 5st Edition. Butterworth-Heinemann, 2012. ISBN 9780080969053.

[72] mikegoulian. mike goulian edge 540 data. http://mikegoulian.com/aircraft/edge-540, 2017. Accessed: 2017-04-26.

[73] mooneym20v. Mooney M20V Acclaim Ultra web page. http://www.mooney.com/en/acclaim-ultra.html#top-header, 2016. Accessed: 2017-04-26.

[74] International Civil Aviation Organization. Envrionmental protection, annex 16, volume i, aircraft noise. Cr-2001-210647, International Civil Aviation Organization, 2011.

[75] PC12. Pilatus delivers 1400th pc-12 and achieves major flight time milestone. http://www.pilatus-aircraft.com/#68, 2016. Accessed: 2017-06-26.

[76] PC7. Pilatus pc-7. http://www.pilatus-aircraft.com/#45, 2017. Accessed: 2017-06-26.

[77] Duane Pettit and Andrew Turnbull. General aviation aircraft reliability study. Cr-2001-210647, NASA, February 2001.

[78] pilotfriend. pilot friend preformance data. http://www.pilotfriend.com/aircraft%20performance/aero.htm, 2017. Accessed: 2017-04-26.

[79] piperm500. Piper M600 web page. http://http://www.piper.com/aircraft/m-class/m500/, 2017. Accessed: 2017-05-03.

[80] piperm600. Piper M600 web page. http://www.piper.com/aircraft/m-class/m600/, 2017. Accessed: 2017-05-03.

[81] pipersem. Piper Seminole web page. http://www.piper.com/aircraft/trainer-class/seminole/, 2016. Accessed: 2017-04-26.

[82] Plascore. Pk2 kevlar® n636 para-aramid fiber honeycomb. URL https://www.plascore.com/download/datasheets/honeycomb_data_sheets/Plascore_PK2.pdf. Accessed: 2017-06-19.

[83] revolvy. revolvy cap 232 data. https://www.revolvy.com/main/index.php?s=CAP%20Aviation%20CAP-232&item_type=topic, 2017. Accessed: 2017-04-26.

[84] robindr401. Robin DR401 comparative performance grid. http://www.robin-aircraft.com/wp-content/uploads/2017/04/PERFORMANCES-DR401-Robin-Aircraft-Perfo-ENG.pdf, 2016. Accessed: 2017-04-26.

[85] Dr.ir. Gianfranco La Rocca. System engineering and aerospace design lecture slides, 2017.

[86] J. Roskam. *Airplane Design*. Number dl. 5 in Airplane Design. DARcorporation, 1999. ISBN 9781884885501. URL https://books.google.nl/books?id=mMU47Ld7yQkC.

[87] Ger J.J. Ruijgrok. *Elements of Airplane Performance*. Delft Academic Press, 2013. ISBN 978-90-6562-203-7.

[88] Mohammad H. Sadraey. *Aircraft Design: A Systems Engineering Approach*. 1st Edition. Wiley Publications, 2012. ISBN 978-1-119-95340-1. URL http://www.aero.us.es/adesign/Slides/Extra/Stability/Design_Control_Surface/Chapter%2012.%20Desig%20of%20Control%20Surfaces%20(Rudder).pdf.

[89] Eddie Sez. Reduced vertical separation minimums (rvsm), normal procedures: Airspace. URL http://code7700.com/airspace_rvsm.htm. Accessed: 2017-06-15.

[90] skytamer. skytamer 152 aerobat data. http://www.skytamer.com/Cessna_152.html, 2017. Accessed: 2017-04-26.

[91] sukhoi. sukhoi su-29 data. http://www.sukhoi.org/eng/planes/civil/su-26/characteristic/, 2017. Accessed: 2017-04-26.

[92] TBM. Daher delivers 54 tbm aircraft in 2016 and prepares a new integrated flight deck for the tbm 900 version. http://www.tbm.aero/daher-delivers-54-tbm-aircraft-in-2016-and-prepares-a-new-integrated-flight-deck-for 2017. Accessed: 2017-06-26.

[93] tbm850. Aopa pilot magazine. http://www.tbm.aero/wp-content/uploads/2016/07/2012-01-AOPA-Pilot.pdf, 2012. Accessed: 2017-05-03.

[94] Dunlop Aircraft Tyres. Tire specifications. URL http://www.dunlopaircrafttyres.co.uk/. Accessed: 2017-06-23.

[95] T. L. Tzu. A reliability-based safety factor for aircraft composite structures. *Computers & Structures*, 48(4), aug 1993.

[96] CAA UK. Cap 698 caa jar-fcl examinations. https://publicapps.caa.co.uk/docs/33/CAP698.pdf, 2006.

[97] United States Department of Transportation. *Aviation Maintenance Technician Handbook - Airframe*. United States Department of Transportation, Federal Aviation Administration, Airman Testing Standards Branch, 2012.

[98] Wouter van der Wal. Simulation, verification and validation - lecture slides, 2017.

[99] M.J.L. Van Tooren. Sandwich fuselage designs. Technical report, TU Delft, 12 1998.

[100] R. Vos, J. A. Melkert, and B. T. C. Zandbergen. Aerospace design and systems engineering elements - lecture slides, 2017.

[101] Tjalling J. Ypma. Historical development of the Newton-Raphson method. *SIAM Review*, 37(4): 531–551, December 1995.